PRESSURE-INDUCED EFFECTS IN INHOMOGENEOUS SPECTRA OF DOPED SOLIDS

KRISTJAN LEIGER

PRESSURE-INDUCED EFFECTS IN INHOMOGENEOUS SPECTRA OF DOPED SOLIDS

KRISTJAN LEIGER

The study was carried out at the Institute of Physics of the University of Tartu.

The dissertation was admitted on January 15, 2002, in partial fulfilment of the requirements for the degree of Doctor of Philosophy in physics (solid state physics), and allowed for defence by the Council of the Department of Physics, University of Tartu.

Supervisor: Prof. Jaak Kikas, Institute of Material Sciences, University of Tartu

Opponents: Dr. Lothar Kador, Bayreuther Institut für Makromolekül-forschung, University of Bayreuth, Germany

Dr. Raivo Jaaniso, Institute of Physics, University of Tartu

Defence: March 22, 2002 at the University of Tartu, Estonia

CONTENTS

LIST OF PUBLICATIONS

I   J. Kikas, K. Leiger, "Diaelastic pressure-induced effects on spectral holes in crystals", J. Chem. Phys. **104**, 5384–5390 (1996).

II J. Friebel, J. Friedrich, A. Suisalu, J. Kikas, An. Kuznetsov, A. Laisaar, K. Leiger, "Pressure-induced dynamics in solid n-alkanes as probed by optical spectroscopy", J. Chem. Phys. **108**, 1830–1835 (1998).

III J. Kikas, K. Leiger, "Pressure-Induced Broadening of Spectral Holes in Glasses as a Measure of Disorder", [Proc. of] the 6th meeting "Disorder in Molecular Solids" (DISMOS-6), May 31 – June 6, 1999, Garchy, France, pp. 49–52, 1999.

IV V. Zazubovitch, A. Suisalu, K. Leiger, A. Laisaar, An. Kuznetsov, J. Kikas, "Pressure effects on the spectra of dye molecules in incommensurate and commensurate phases of biphenyl", Chem. Phys. (submitted).

V K. Leiger, J. Kikas, A. Suisalu, "Diaelastic pressure-induced broadening of spectral holes in molecular crystals", J. Lum. (accepted)

The following paper is not directly related to the subject of this thesis:

VI J. Kikas, K. Leiger, "Effect of geometry on storage density in spectral hole burning memories", Opt. Commun. **94**, 557–560 (1992).

1. INTRODUCTION

Inhomogeneous broadening of spectra is a common phenomenon in spectroscopy of doped solids. Due to different surroundings the spectra of a transition originating from different probe molecules (atoms, ions, etc.) are shifted and in the overall picture the original (homogeneous) transition line is convoluted with an often many orders of magnitude wider inhomogeneous distribution of frequencies. In disordered (amorphous) solids the situation can be naturally understood as arising from disorder in the local neighborhood, while in ordered solids, such as crystals, defects of various kind are considered as sources of inhomogeneity. There are also systems that fall in between these extremes, e.g. incommensurate systems where the modulation of the periodicity of a crystal contributes remarkably to the inhomogeneous distribution.

Depending on the problem, inhomogeneity can turn out to be useful (e.g. creating spectral hole burning memories [1–3]) or troublesome (when trying to determine the homogeneous linewidth). It also presents considerable interest in itself as far as it carries information about the structure of the solid (type and density of defects etc.). Hence, the understanding and description of the exact mechanisms of the effect is essential.

It appears that spectral hole burning [4–6], more used as a means of eliminating inhomogeneity, can also successfully be used to explore the same when combined with external fields like pressure. The so-called pressure tuning technique [7–22] – applying a moderate hydrostatic pressure on a burnt-in hole and monitoring the changes in hole parameters – can reveal a lot of information concerning probe-host interactions. The method is rather sensitive; pressure values typical for this kind of experiments are in order of 10–100 bar, which can be viewed upon as a small perturbation for the system and is easily reached with simple devices.

Another, but less sensitive, method of using pressure is measuring the pressure-induced changes of the inhomogeneous spectrum as a whole. However, the pressures one needs to use in this case are orders of magnitude greater (in kbars) and this may cause technical as well as physical problems (perturbation is no longer small).

For correct interpretation of the experimental results also the underlying models are needed. There has been some activity in developing the pressure models of impurity spectra previously (e.g. [7, 15]). The goal of the current thesis is, firstly, to review the existing knowledge, and, secondly, propose and analyze some further models for the cases not covered before. We also present some experimental results.

The layout of this work is as follows. In chapter 2 we will outline the results essential for deriving further concepts and evaluating some experimental data in following chapters. These are the results concerning inhomogeneous effects in doped solids, including incommensurately modulated systems, elements of elasticity theory and an elementary treatment of the spectral hole burning.

Chapter 3 is devoted to using the pressure-induced spectral effects to explore the inhomogeneity. A general classification of the corresponding models into two broader classes, dispersive and diffusive, is presented. Main features of either of them are discussed. The existing models are systematized according to this classification. Original results include a proposed new diaelastic model for crystalline matrices, also studied experimentally, and a model analysis for the diffusive case. Also, a novel technique is proposed to distinguish between the two pressure mechanisms.

In chapter 4 we will extend the results obtained in the previous chapter to the incommensurately modulated systems. We discuss experimental data on spectral inhomogeneity of chlorin-doped biphenyl. Interesting results are obtained both in hole tuning spectra and fluorescence spectra at higher pressures, where phase transition from incommensurate to commensurate structure is observable.

2. BASIC CONCEPTS

2.1. Statistical theory of inhomogeneous broadening in defective solids

In this section we will review a rather general statistical method for calculating the inhomogeneous broadening of electronic transition lines of impurity spectra. Though probably proposed earlier, the method was developed in its final form by Stoneham [23]. It describes the situation where impurities (probes) within a matrix (host) structure are exposed to some field f due to a set of inhomogeneity sources, such as defects or disorder in positions of host particles. In what follows, we will use the terms "defect" and "defective solid" as general references to such inhomogeneity sources and solids where this kind of inhomogeneity is prevalent (note that in practice, though, no solid is completely free from defects). Assuming a large number of probe impurities and homogeneity of the host material at the macroscopic level, the probability distribution of the probe transition frequency should well represent the actual observable inhomogeneous distribution function (IDF).

The theory is based on three main assumptions:

(i) The defect-created internal field causes a shift E of the impurity frequency ω that is linear in field components f_i:

$$\omega = \omega_0 + E(Z) = \omega_0 + \sum_i c_i f_i \, .\qquad (2.1)$$

Here ω_0 is the unperturbed frequency and Z incorporates the coordinate set of all defects under consideration. If ω_0 represents the vacuum frequency of the active transition, $E(Z)$ is often referred to as the "solvent shift". The (unity-normalized) IDF is now generally given by

$$\rho_{ih}(\omega) = \int P_1(Z)\delta(\omega - \omega_0 - E(Z))dZ \, ,\qquad (2.2)$$

where $P_1(Z)$ is the unity-normalized probability density of occurrence of a particular configuration of parameters Z.

(ii) The frequency shifts caused by different defects are linearly superimposed:

$$E(Z) = \sum_{i=1}^{N} \varepsilon(z^i) \, ,\qquad (2.3)$$

where $\varepsilon(z^i)$ is the single-defect contribution to the overall shift. We assume here that the coordinate set Z consists of N similar subsets corresponding to N defects, denoted by upper indices: $Z = (z^1, z^2, ..., z^N)$. Each of the subsets z^i can in turn consist of many, say n, coordinates which we will denote by lower indices: $z^i = (z^i_1, z^i_2, ..., z^i_n)$. The space element in (2.2) is thus given by $dZ = dz^1 dz^2 ... dz^N = dz^1_1 dz^1_2 ... dz^1_n ... dz^N_n$. When arguing on a single-defect level, upper indices can be omitted.

(iii) There is no correlation in the distribution of various defects in the coordinate space z^i:

$$P_1(Z) = \prod_{i=1}^{N} p_1(z^i). \tag{2.4}$$

Here p_1 is the single-defect distribution density, normalized to unity. This lack of correlation requires the defect density to be low. In following calculations it is more convenient to introduce the density p_N normalized to the number of defects N:

$$p_N(z) = N p_1(z). \tag{2.5}$$

$p_N(z)$ expresses the spatial density of defects in the coordinate space. Now the IDF is given, by (2.2):

$$\rho_{ih}(\omega) = \frac{1}{N^N} \int dz^1 p_N(z_1) ... \int dz^N p_N(z_N) \delta(\omega - \omega_0 - E(Z)) \tag{2.6}$$

Using the Fourier representation of δ-function:

$$\delta(y) = \frac{1}{2\pi} \int \exp(ixy) dx \tag{2.7}$$

and expanding $E(Z)$ according to (2.3), we have

$$\rho_{ih}(\omega) = \frac{1}{2\pi} \int dx \exp[ix(\omega - \omega_0)] \left[\frac{1}{N} \int dz p_N(z) \exp(-ix\varepsilon(z)) \right]^N . \tag{2.8}$$

Now we introduce a new function, $J(x)$, so that

$$\frac{1}{N} \int p_N(z) \exp(-ix\varepsilon(z)) dz = 1 - \frac{J(x)}{N}, \tag{2.9}$$

which implies that

$$J(x) = \int p_N(z)[1 - \exp(-ix\varepsilon(z))] dz. \tag{2.10}$$

With N becoming infinitely large and using the well-known relation

$$\lim_{N \to \infty} \left(1 - \frac{A}{N}\right)^N = \exp(-A), \tag{2.11}$$

we get

$$\rho_{ih}(\omega) = \frac{1}{2\pi} \int \exp[ix(\omega - \omega_0) - J(x)] dx. \tag{2.12}$$

In calculations it is also often convenient to shift the frequency coordinate so that ω_0 will coincide with zero.

To examine the correlation between the frequencies of different transitions due to the same sources of inhomogeneity, the theory can be easily generalized to many frequency coordinates [24]. This approach enables one to describe many situations regarding techniques like fluorescence line narrowing and spectral hole burning.

Calculation of the joint distribution $\rho_{ih}(\omega_1, \omega_2)$ is quite similar to the above deduction. All the assumptions made previously remain valid and the calculations are very similar, only two Fourier variables appear because instead of one δ-function, as in (2.2), we now have the product of two δ-functions, one for each frequency:

$$\rho_{ih}(\omega_1, \omega_2) = \int P_1(Z)\delta(\omega_1 - \omega_{01} - E_1(Z))\delta(\omega_2 - \omega_{02} - E_2(Z)) dZ, \tag{2.13}$$

where ω_{01} and ω_{02} are the respective unperturbed frequencies. Analogously to (2.12), one gets

$$\rho_{ih}(\omega_1, \omega_2) = \frac{1}{(2\pi)^2} \int\int \exp[i(\omega_1 - \omega_{01})x_1 + i(\omega_2 - \omega_{02})x_2 - J(x_1, x_2)] dx_1 dx_2, \tag{2.14}$$

where J is defined as

11

$$J(x_1, x_2) = \int p_N(z)[1 - \exp(-i x_1 \varepsilon_1(z) - i x_2 \varepsilon_2(z))]dz, \qquad (2.15)$$

where $\varepsilon_1(z)$ and $\varepsilon_2(z)$ are the frequency shifts caused by a defect for the first and second transition frequency, respectively. If ω_1 and ω_2 refer to spectra taken under different conditions, there may be other parameters (pressure, for example) that $\varepsilon_1(z)$ and $\varepsilon_2(z)$ depend on.

An extension to more coordinates is straightforward and easily made upon necessity.

2.2. Continuum theory of lattice defects

A rather suitable phenomenological way of describing lattice defects in a crystal is the so-called continuum approach [25]. The idea is to view the (regular part of the) crystal as a continuous, homogeneous and isotropic medium that is generally in a state of stress due to the defects. The situation can thus be described by the theory of elasticity. Depending on the defect type, various ways of modeling them can be figured out. In subsection 3.2.4 we will use the misfitting sphere model for a point defect [26], which we will extend to enable for an external pressure exerted on the crystal.

As long as we are viewing pressures and strains that cause only small relative deformations (much less than unity), we are going to use the linear approximation of the general elasticity theory. In the linear elasticity theory (LET), the displacement vector is defined with:

$$\vec{u}(\vec{r}_0, t) = \vec{r}(\vec{r}_0, t) - \vec{r}_0, \qquad (2.16)$$

where $\vec{r}_0 = (x_1^0, x_2^0, x_3^0)$ is the position of some point within an elastic body at an initial moment, $\vec{r}(\vec{r}_0, t) = (x_1, x_2, x_3)$ is the position of the same point at some other moment t.

The symmetric tensor of infinitely small displacements e is defined:

$$e_{km} = \frac{1}{2}\left(\frac{\partial u_k}{\partial x_m^0} + \frac{\partial u_m}{\partial x_k^0}\right), \qquad (2.17)$$

which, under the assumptions of LET, may also be rewritten as

$$e_{km} = \frac{1}{2}\left(\frac{\partial u_k}{\partial x_m} + \frac{\partial u_m}{\partial x_k}\right). \tag{2.17'}$$

Physically, the diagonal components of the E tensor express the relative stretches of vectors originally parallel to the coordinate axes, while non-diagonal ones give half of the angle change between the vectors.

The stress tensor is generally defined as an entity describing the interaction forces between different parts of the body. Namely, if S is any surface within the body and $\vec{f}(P)$ is the interaction force at a point P on the surface S, the stress tensor σ is defined with the expression:

$$\vec{f}(P) = \sigma\vec{n}, \tag{2.18}$$

where $\vec{n}$ is the normal unit vector of the surface S at the point P.

Within LET, σ and e tensors are related by the general Hooke's law:

$$\sigma_{kl} = c_{klmn}e_{mn}, \tag{2.19}$$

where c is the 4th-order symmetric elastic constant tensor. For isotropic bodies it has only two independent components and (2.19) may be rewritten:

$$\sigma_{kl} = \lambda\delta_{kl}e_{mm} + 2\mu e_{kl} \tag{2.20}$$

where λ and μ are the Lamé constants (μ being the shear modulus and $\kappa = (\lambda + 2\mu/3)^{-1}$, the volume compressibility). We will use (2.20) later to derive an expression for defect-impurity interaction based on our model of a point defect.

2.3. Inhomogeneity in incommensurate systems

Incommensurate systems constitute a rather intriguing class of solids. In these systems, some property of crystal elements (atoms, molecules) is modulated along one or more spatial dimensions with a period that is incommensurate with the period of the reference lattice (i.e. their ratio is irrational). Such a property may be atomic position or molecular orientation in structurally incommensurate systems, spin magnetization, electron charge density, etc. This way, an incommensurately modulated solid lacks the translational symmetry, since no

13

lattice translation will map the lattice exactly onto itself. Rigorously speaking, such a solid is not a crystal.

Such a spatial modulation gives rise to specific features in the spectra of probe impurities in incommensurate solids. The resulting inhomogeneous broadening is basically different from the effects considered in the section 2.1. Blinc in [27] has developed the theory of incommensuracy for nuclear magnetic resonance. It also provides the guidelines for our treatment.

The arising of incommensurate modulation can be viewed as a result of freezing of a soft frequency mode of the system on the change of its thermodynamical parameters. Denoting the modulated quantity by u, the modulation in one-dimensional case is given by

$$u = A \cos \varphi(x) \tag{2.21}$$

with the phase in the simplest case:

$$\varphi(x) = \frac{2\pi}{\lambda} x + \varphi_0, \quad \varphi_0 = const., \tag{2.22}$$

where λ is the wavelength of the frozen-in mode, incommensurate with the lattice period. However, often minimization of the free energy of the system upon phase transition requires higher harmonics of the modulated wave to appear, so that $\varphi(x)$ will not take the simple linear form (2.22) but a more complicated one governed by the sine-Gordon equation [27]:

$$\frac{d^2\varphi}{dx^2} - \alpha^2 \sin p\varphi = 0. \tag{2.23}$$

The resulting shape of $\varphi(x)$ is staircase-like, i.e. consisting of relatively constant-phase regions separated by a regular array of domain walls ("phase solitons") where the phase changes rapidly (Fig. 1(c)). Following [27] we will call this type of modulation the "multi-soliton limit" and the case of linear φ the "plane wave limit".

Now let us introduce the probe molecules into an incommensurately modulated lattice and let us try to derive the IDF due to incommensuracy. For now, let us assume that:
(i) the probe molecules are distributed spatially uniformly along the modulation wave, i.e. they do not prefer any particular phase value in their spatial position,
(ii) the value of the probe transition frequency v depends linearly on the local u value. This yields:

$$v = v_0 + v_1 \cos \varphi(x). \qquad (2.24)$$

We will first deal with the one-dimensional case. Since $u(x)$ is periodic with the period λ, i.e. $u(x) = u(x + n\lambda)$, where n is an integer, we may view only the x values $[0 .. \lambda]$ and project the probe sites from $n\lambda \leq x < (n+1)\lambda$ onto the first range $0 \leq x < \lambda$ with a transition $x \rightarrow x - n\lambda$, since they give the same phase value. The lattice being incommensurate with λ, we thus fill the range $[0 .. \lambda]$ quasi-continuously and also uniformly, by assumption (i). We now introduce the phase density $f(\varphi)$ and the density of spectral lines $\rho_{ih}(v)$ by

$$\rho_{ih}(v)dv = f(\varphi)d\varphi = Cdx, \qquad (2.25)$$

where C is a constant which can be determined from normalizing conditions. In
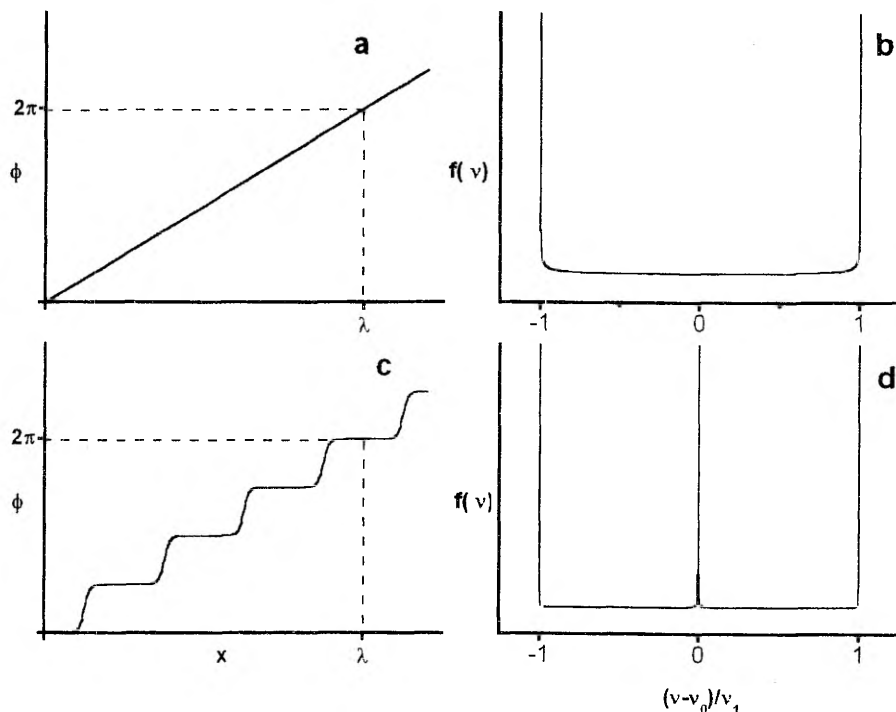
Figure 1. The phase as a function of spatial coordinate (a, c) and the resulting inhomogeneous distribution functions (b, d) in a doped 1D incommensurately modulated system. The plane wave limit (a, b) and multi-soliton limit with the number of solitons $p = 4$ (c, d) are viewed separately. While (c) has only edge singularities, in (d) 4 new singularities appear, two of which coincide with edge singularities and two with one another at v_0.

15

case of the plane wave limit also $f(\varphi) = const$ and, normalizing the area of $\rho_{ih}(v)$ to unity, we get from (2.24), (2.25):

$$\rho_{ih}(v) = \frac{1}{2\pi\left|\dfrac{dv}{d\varphi}\right|} = \frac{1}{2\pi v_1 |\sin\varphi|} = \frac{1}{2\pi v_1 \sqrt{1 - \left(\dfrac{v - v_0}{v_1}\right)^2}} . \qquad (2.26)$$

The IDF has thus two edge singularities at

$$v_{a,b} = v_0 \pm v_1 \qquad (2.27)$$

(see Fig. 1(c)). In [27] also the case with a quadratic term in (2.24) was considered. Adding a term $0.5 v_2 \cos^2\varphi(x)$ to (2.24), we get the result that the edge singularities in (2.27) are shifted by an amount v_2 towards higher frequencies and if $|v_1| \leq |v_2|$, a third singularity appears at

$$v_c = v_0 - \frac{v_1^2}{2v_2} . \qquad (2.28)$$

Hence the violation of the assumption (ii) can cause additional structure of the IDF only in case when the perturbation to the active probe transition is rather strongly non-linear in terms of u. This, however, does not seem likely in most cases, especially if the modulation wave amplitude is not very large.

Considering of two- or three-dimensional modulations requires numerical calculations. The main result is that two maxima persist, but no longer as infinite singularities [27].

For the multi-soliton limit (2.25) gives for one-dimensional modulation

$$\rho_{ih}(v) = \frac{C}{\left|\dfrac{dv}{dx}\right|} = \frac{C}{v_1 \left|\sin\varphi \dfrac{d\varphi}{dx}\right|} , \qquad (2.29)$$

which may have additional singularities between the edge ones in places where the derivative $d\varphi/dx$ turns to zero. If we have p phase solitons in the x range $[0 .. \lambda]$, we also have the same number of flat parts on the $\varphi(x)$ graph. In these places the derivative is zero or very small. Thus generally p new maxima appear in the IDF, not all of which may be distinguishable as they may coincide with edge singularities or with one another (Fig. 1(d)). It is easily seen that if p is even, the placement of singularities must be symmetrical with respect to v_0.

Another reason that can cause structure in the IDF of incommensurate systems is the so-called pinning of the modulation wave by probe molecules. In an ideal crystal it takes zero energy to shift the incommensurate modulation wave along the modulation axis since the regions whose energy is increasing as a result of this motion are always balanced by the regions whose energy is decreasing. Thus in the presence of slightest thermal excitation the modulation waves would be in constant movement. In a real crystal, however, defects act as obstacles to such movement and if the thermal energy is not high enough, the wave is stopped, or *pinned*. Probes act likewise as defects and as far as the probe-host interaction energy depends on *u*, the phase distribution at the probe location may not be uniform, but is weighed by the respective Boltzmann factor. Such a possibility is discussed in [28] for EPR experiments. Hence, our above assumption (i) becomes invalid and additional peaks may appear in the IDF at lower temperatures.

2.4. General theory of spectral hole burning

The zero-phonon part of an absorption or emission spectrum of an ensemble of probe impurities in a solid is actually determined by a convolution of the homogeneous (single-impurity) zero-phonon line κ with the IDF ρ_{ih}:

$$I(\nu) = \int \kappa(\nu - \omega)\rho_{ih}(\omega)d\omega. \qquad (2.30)$$

This way, the real shape of the homogeneous spectrum is obscured. To reveal it, one can use selective spectroscopic methods like spectral hole burning (SHB) [4–6].

The idea of SHB is to irradiate the sample monochromatically so that the probes in resonance with the irradiation are transferred from their initial (educt) state into a second (photoproduct) one, which is more or less stable. This prohibits these centers from contributing to the envelope (2.30), leaving a "hole" in respective spectral position.

Let us briefly review the modeling of the kinetics of the SHB process, given in more detail in [29]. The simplest model includes a number of assumptions:

- relatively weak excitation;
- low impurity concentration;
- small optical thickness of sample;
- single-dimensional inhomogeneity (only by ω);
- one-photon mechanism of photochemistry;
- stability of photoproducts;

- large educt → product photochromic shift.

The SHB process can be considered as a modification of the IDF, which, in this case, is time-dependent ($\rho_{ih} = \rho_{ih}(\omega, t)$). Under the assumptions made above, the kinetics of SHB is described by a simple equation

$$\dot{\rho}_{ih}(\omega, t) = -I_0 \sigma \eta \kappa (v_0 - \omega) \rho_{ih}(\omega, t), \tag{2.31}$$

where I_0 and v_0 are the intensity and frequency of the monochromatic irradiation, respectively; σ is the absorption cross-section and η is the quantum yield of the SHB process. (2.31) gives:

$$\rho_{ih}(\omega, Q) = \rho_{ih}(\omega, 0) f_{hb}(\omega, v_0, Q), \tag{2.32}$$

where $Q = I_0 t$ is the irradiation dose and

$$f_{hb}(\omega, v_0, Q) = \exp(-Q\sigma\eta\kappa(v_0 - \omega)) \tag{2.33}$$

is a function we will call the SHB exposure function.

Let us now further assume that

(i) the inhomogeneous band is broad as compared to the homogeneous width, i.e. we may take $\rho_{ih}(\omega, 0) = const\ (= 1)$;

(ii) the homogeneous line is of Lorentzian shape of width (FWHM) 2Γ;

(iii) the burning position is at the origin, $v_0 = 0$.

Then (2.30), (2.32) and (2.33) combine to

$$I(v) = \frac{1}{\pi} \int \frac{\Gamma}{\Gamma^2 + (v - \omega)^2} \exp\left(-Q\eta\sigma \frac{\Gamma^2}{\Gamma^2 + \omega^2}\right) d\omega, \tag{2.34}$$

with $I(v)$ normalized to unity at $Q = 0$. The exponent in (2.34) describes saturation effects. In the low dose limit, (2.34) reduces to

$$I(v) \approx 1 - Q\eta\sigma \frac{(2\Gamma)}{(2\Gamma)^2 + v^2}, \tag{2.35}$$

which means that a low-dose hole has twice the homogeneous width and its depth depends linearly on the dose.

Note that here and in what follows we have assumed that the burning source is fully monochromatic, i.e. has a zero spectral width. Otherwise, a second convolution with the spectrum of the burning light must be carried out in (2.32).

3. INHOMOGENEOUS PRESSURE-INDUCED SPECTRAL EFFECTS IN DEFECTIVE SOLIDS

3.1. General remarks

A productive way to study local interactions and inhomogeneous effects in doped solids is by means of applied external fields. Hydrostatic pressure is a good example of such a field. Its scalar nature makes the physical situation simpler as compared to effects in electric and magnetic (vector) fields. However, to get a detectable change of the inhomogeneous band as a whole, often very high pressures (several kbars) are needed. With high-pressure equipment constantly evolving, technical problems arising from this fact may be solved, but the question still remains whether such a high pressure can be regarded as a small perturbation of the impurity-host system.

At the same time, pressure effects on spectral holes can be observable at much lower pressure values. The reason is, generally speaking, spectrally selective approach and smaller spectral scale under consideration. Thus the ratio of pressures needed to obtain a comparable effect on the whole inhomogeneous band and on a spectral hole is of the order of inhomogeneous to homogeneous width ratio. The main method here is the pressure tuning [7-13] – measuring spectral holes at pressures different from the burning one and examining the dependence of their parameters on the pressure change. This technique has been used in a number of works [7-22] in order to study local interactions and elastic properties of solids.

When burning a hole into the inhomogeneously broadened band and then applying pressure one observes both hole shift and broadening. The pressure shift of the holes is explained by a change of the average interaction between the probe and host molecules with compression of the sample. At the same time, the mechanisms of hole broadening are not always quite as clear. The broadening must obviously stem from inhomogeneity since the effect of pressure on the homogeneous linewidth is negligible in this low pressure range. An especially large broadening has been detected in disordered solids such as glasses, where its magnitude is comparable to that of the pressure-induced shift [7-13]. Relatively large broadening of holes with pressure has also been observed in "soft" crystals of n-alkanes (Shpol'skii systems) [13,14]. In some cases, it can even exceed the values typical for glasses [22]. However, even in "hard" molecular crystals such as durene [13] and bensophenone [11] a minor broadening of holes is readily observable.

In this chapter we are going to introduce two principal mechanisms of inhomogeneous spectral pressure behavior: the dispersive and diffusive

mechanisms. Their basic properties and some special cases will be discussed and a technique to distinguish between the mechanisms will be proposed.

3.2. The dispersive mechanism

3.2.1. Definition of the dispersive mechanism

Let us return to the statistical theory given in section 2.1 and consider the effect of pressure on the IDF. Applying pressure to the system, all the coordinates Z undergo a variation. It is noteworthy that in pressure tuning experiments with spectral holes, the hole position always turns out to be linear with pressure. Indeed, in the pressure range where hole is still detectable (not too broadened), to our knowledge, no significant deviation from linearity has ever been reported. Thus it is natural to assume that every single homogeneous line also moves linearly with pressure, being governed by the first term of expansion into series:

$$E(Z, \Delta p) = E(Z, 0) + \left(\frac{\partial E}{\partial p} + \sum_{i,j} \frac{\partial E}{\partial z'_j} \frac{\partial z'_j}{\partial p} \right)_{p=0} \Delta p = E(Z, 0) + A(Z) \Delta p, \ (3.1)$$

where Δp is the pressure change, $A(Z)$, as defined by (3.1), is the integral pressure coefficient depending on all the defects (their internal and external coordinates). With (2.3) we get on the single-defect level:

$$\varepsilon(z, \Delta p) = \varepsilon(z, 0) + \left(\frac{\partial \varepsilon}{\partial p} + \sum_i \frac{\partial \varepsilon}{\partial z_i} \frac{\partial z_i}{\partial p} \right)_{p=0} \Delta p = \varepsilon(z, 0) + \alpha(z) \Delta p, \ (3.2)$$

where $\alpha(z)$ is the single-defect pressure coefficient. For this expansion to become possible and meaningful, following three assumptions must be made:

(i) The solvent shift function $\varepsilon(z)$ is continuous in terms of $p, z_1, z_2, ..., z_n$. This is not a very critical assumption though $\varepsilon(z)$ can contain a singularity at the origin.

(ii) The parameters $z_1, z_2, ..., z_n$ depend continuously on the applied pressure. This assumption is probably the most suspicious one since pressure can induce structural flips and discontinuous relaxations of any kind. However, for a material with well-defined structure and little void volume it may still be appropriate.

21

(iii) The pressure remains low enough to cause only small variations of $\varepsilon(z)$. This is rather reasonable, since also hole shifts observed in a typical pressure tuning experiment are very small compared to the whole solvent shift.

These assumptions specify the mechanism of pressure behavior of probe spectra that we refer to as the dispersive mechanism. In other words, within the dispersive mechanism, the whole zero-phonon spectrum of the active transition can be viewed upon as a spectral distribution of homogeneous (single-impurity) spectra each of which shifts linearly with pressure. Most of the existing pressure models of probe spectra actually rely on this mechanism.

From (3.1) and (3.2) we can see that, similarly to (2.3), additivity holds for the pressure coefficient:

$$A(Z) = \sum_{i=1}^{N} \alpha(z^i). \tag{3.3}$$

To calculate the pressure-dependent IDF for a model belonging to this category, it is sufficient to substitute the function ε from (3.2) into (2.10), (2.12). However, for effects related to the spectral holes, such as pressure tuning, it is more suitable to use the joint distribution function of two frequencies (2.13) with pressure change as an extra parameter. For simplicity, we will consider in the following $\omega_0 = \omega_{01} = \omega_{02} = 0$, thus disregarding the pressure shift of the unperturbed frequency (we will make a remark if there may be any). We get:

$$\rho(\omega_1, \omega_2, \Delta p) = \int P_1(Z)\, \delta(\omega_1 - E(Z,0))\delta(\omega_2 - E(Z,\Delta p))dZ. \tag{3.4}$$

It gives us the probability for a homogeneous line to be peaked at ω_1 before and at ω_2 after the application of pressure. Another way is to use the joint distribution function of frequencies and pressure coefficients:

$$\rho_\alpha(\omega, \alpha) = \int P_1(Z)\delta(\omega - E(Z,0))\delta(\alpha - A(Z))dZ \tag{3.5}$$

which assigns a distribution of pressure coefficients to every point of the inhomogeneous structure. (3.4), (3.5) are also referred to as the pressure kernel functions. In the narrower sense, we will use the term "pressure kernel (at a frequency)" also to denote the distribution of the pressure coefficients α or final frequencies ω_2 at a given initial frequency ω (ω_1). To obtain the IDF, (3.4) and (3.5) need to be integrated over ω_2 and α accordingly, as seen from definitions. The distributions are related as follows:

$$\rho(\omega_1, \omega_2, \Delta p) = \frac{1}{|\Delta p|} \rho_\alpha\left(\omega_1, \frac{\Delta\omega}{\Delta p}\right), \tag{3.6}$$

$$\rho_\alpha(\omega, \alpha) = |\Delta p|\, \rho(\omega, \omega + \alpha\, \Delta p, \Delta p), \tag{3.7}$$

where $\Delta\omega = \omega_2 - \omega_1$. On a pressure change Δp_0 (3.4) and (3.5) transform as follows:

$$\rho(\omega_1, \omega_2, \Delta p) \rightarrow$$

$$\rho'(\omega_1, \omega_2, \Delta p) = \rho\left(\omega_1 - \Delta\omega\, \frac{\Delta p}{\Delta p_0}, \omega_2 - \Delta\omega\, \frac{\Delta p}{\Delta p_0}, \Delta p\right); \tag{3.8}$$

$$\rho_\alpha(\omega, \alpha) \rightarrow \rho'_\alpha(\omega, \alpha) = \rho_\alpha(\omega - \alpha\, \Delta p_0, \alpha). \tag{3.9}$$

The influence of SHB on (3.4) and (3.5) can be described by multiplication with the exposure function (2.33) (with $\omega = \omega_1$ for (3.4)). The modification of the IDF on pressure tuning is then given by

$$\rho'_{ih}(\omega_2) = \int f_{hb}(\omega_1, v_0, Q)\rho(\omega_1, \omega_2, \Delta p)d\omega_1, \tag{3.10}$$

$$\rho'_{ih}(\omega) = \int f_{hb}(\omega - \alpha\, \Delta p, v_0, Q)\rho_\alpha(\omega - \alpha\, \Delta p, \alpha)d\alpha. \tag{3.11}$$

Let us now calculate (3.4) using the results (2.14), (2.15). Together with (3.2) they can be rewritten for the dispersive models as follows:

$$\rho(\omega_1, \omega_2, \Delta p) = \frac{1}{(2\pi)^2} \iint \exp[i\omega_1 x_1 + i\Delta\omega x_2 - J'(x_1, x_2, \Delta p)]dx_1 dx_2, \tag{3.12}$$

where J' is defined:

$$J'(x_1, x_2, \Delta p) = \int p_N(z)[1 - \exp(-i\varepsilon(z)x_1 - i\alpha(z)\Delta p x_2)]dz. \tag{3.13}$$

Quite similarly, one gets for (3.5):

$$\rho_\alpha(\omega,\alpha) = \frac{1}{(2\pi)^2} \iint \exp\left[i\omega x_1 + i\alpha x_2 - J''(x_1,x_2)\right] dx_1 dx_2, \quad (3.14)$$

$$J''(x_1,x_2) = \int p_N(z)\left[1 - \exp\left(-i\varepsilon(z)x_1 - i\alpha(z)x_2\right)\right] dz. \quad (3.15)$$

For further evaluation of (3.4) and (3.5) some more detailed assumptions must be made. In the following we will discuss a few examples.

3.2.2. The simple isotropic model

In the simplest case we may assume [7] that the defect-probe mutual distance r is the only pressure-dependent coordinate and the interaction is governed by the r^{-n} – law (e.g. $n = 6$ for van der Waals forces). Then the single-defect solvent shift can be expressed:

$$\varepsilon(r) = Ar^{-n}, \quad (3.16)$$

where A is a constant that describes the host-probe coupling. We can obtain a general result for the pressure coefficient function for the case when r is the only pressure-dependent coordinate in ε:

$$\alpha(r) = \frac{\partial \varepsilon(r)}{\partial r}\frac{\partial r}{\partial p} = -\frac{r}{3}\kappa\frac{\partial \varepsilon(r)}{\partial r}. \quad (3.17)$$

Here κ is the local volume compressibility of the host:

$$\kappa = -\frac{1}{V}\left(\frac{\partial V}{\partial p}\right)_T. \quad (3.18)$$

Its value may differ from the bulk one depending on how much the host structure is disturbed around the probe molecule. With (3.16) the value of $\alpha(r)$ is given by

$$\alpha(r) = \kappa\frac{n}{3}\varepsilon(r). \quad (3.19)$$

The distribution (3.5) becomes with (3.16), (3.19):

$$\rho_\alpha(\omega,\alpha) = \rho_{ih}(\omega)\delta\left[\alpha - \kappa\frac{n}{3}\omega\right]. \tag{3.20}$$

We see that, due to the scaling of $\alpha(r)$ with $\varepsilon(r)$, only one α value corresponds to every point of the IDF. (3.4) reads:

$$\rho(\omega_1,\omega_2,\Delta p) = \rho_{ih}(\omega_1)\delta\left[\omega_2 - \omega_1 - \kappa\frac{n}{3}\omega_1\Delta p\right]. \tag{3.21}$$

The effect of pressure on the IDF is thus simply linear remapping of the frequency coordinate:

$$\rho_{ih}(\omega) \to \rho'_{ih}(\omega) = \frac{1}{\left(1+\kappa\frac{n}{3}\Delta p\right)}\rho_{ih}\left(\frac{\omega}{1+\kappa\frac{n}{3}\Delta p}\right). \tag{3.22}$$

For a spectral hole with a minimum position ω_m and width Γ we can calculate pressure shift and broadening as follows:

$$\frac{d\omega_m}{d(\Delta p)} = \kappa\frac{n}{3}\omega_m, \tag{3.23}$$

$$\frac{d\Gamma}{d(\Delta p)} = \kappa\frac{n}{3}\Gamma. \tag{3.24}$$

Actually, the same relations apply for any substructure of the IDF with a defined width Γ and a chosen point ω_m (such as maximum or minimum, for example), including the whole distribution itself. We see that the pressure coefficient varies linearly from point to point within the inhomogeneous distribution. This phenomenon (often called the "color effect") is well observed experimentally ([10]). Note also that the coefficient is predicted to be of the same sign as the overall solvent shift.

The reason why this simple approach remains insufficient is the fact that the pressure broadening observed in experiments exceeds the value given by (3.24) by several orders of magnitude for any reasonable choice of n. However, for treating hole shifts it may still be applicable. Sesselmann *et al.* [7,8] have

calculated volume compressibilities for some polymers from hole shift data assuming $n = 6$ (dispersive dipole-dipole interactions) and have arrived at results very well coinciding with data retrieved from mechanical measurements. The problem may be that if the initial hole width is very small compared to the solvent shift ($\Gamma << \omega_m$), the effect of broadening (3.24) is also correspondingly smaller and more easily overrun by other effects while the shift remains to be tractable within this scheme.

3.2.3. The Gaussian approximation

As an extension to the previous model and in order to explain its shortcomings, Laird and Skinner [15] have developed their model for pressure behaviour of spectral holes. While the foregoing model is of rather general nature in terms of the host structure, the work of Laird and Skinner is clearly directed towards disordered systems such as glasses and polymers.

Firstly, they use the so-called Gaussian approximation to calculate the IDF and joint distribution function $\rho(\omega_1, \omega_2, \Delta p)$. In strongly disordered systems the nearby host molecules can be viewed as the prevailing inhomogeneity sources for the probe molecules. In this case the shape of (2.12) is determined mostly by small $J(x)$ values. Therefore we can expand $J(x)$ (2.10) into Taylor series about $x = 0$ and use only the first two terms. Let us still assume only the mutual distance of host-probe pairs, r, to be a pressure-dependent coordinate. The whole coordinate set z still contains all the spatial coordinates, i.e. in spherical representation $z = (r, \theta, \varphi)$. Using the pressure-dependent solvent shift function (3.2), $J(x)$ becomes

$$J(x) = i\left(v_G + A\Delta p\right)x + \frac{\sigma_G^2(\Delta p)}{2}x^2,\tag{3.25}$$

where v_G, A and σ_G are defined as

$$v_G = \int p_N(z)\varepsilon(r)dz,\tag{3.26}$$

$$\sigma_G(\Delta p) = \sqrt{B\Delta p^2 + 2C\Delta p + \sigma_{G0}^2},\tag{3.27}$$

$$\sigma_{G0}^2 = \int p_N(z)\varepsilon^2(r)dz.\tag{3.28}$$

$$A = \int p_N(z)\alpha(r)dz,\tag{3.29}$$

26

$$B = \int p_N(z)\alpha^2(r)dz, \tag{3.30}$$

$$C = \int p_N(z)\alpha(r)\varepsilon(r)dz. \tag{3.31}$$

Here for $\alpha(r)$ the result (3.17) from the previous subsection holds. Substituting (3.25) into (2.12) gives us the Gaussian line shape:

$$\rho_{ih}(\omega, \Delta p) = \frac{1}{\sqrt{2\pi}\sigma_G(\Delta p)} \exp\left(-\frac{(\omega - (\nu_G + A\Delta p))^2}{2\sigma_G^{\ 2}(\Delta p)}\right). \tag{3.32}$$

At the zero pressure, its center is displaced from the unperturbed frequency by ν_G and its standard deviation equals σ_{G0} (full-width at half-maximum (FWHM) $\Gamma_{G0} = 2\sigma_{G0}\sqrt{2\ln 2}$).

The pressure-dependent two-frequency joint distribution function can be calculated in the same manner from (3.12), (3.13), giving

$$\rho(\omega_1, \omega_2, \Delta p) = \frac{\rho_{ih}(\omega_1)}{2\pi\gamma_G|\Delta p|} \exp\left(-\frac{(\omega_2 - \omega_1 - \beta_G(\omega_1)\Delta p)^2}{2(\gamma_G\Delta p)^2}\right), \tag{3.33}$$

where

$$\beta_G(\omega) = A + \frac{C}{\sigma_{G0}^2}(\omega - \nu_G), \tag{3.34}$$

$$\gamma_G = \sqrt{B - \frac{C^2}{\sigma_{G0}^2}}, \tag{3.35}$$

The pressure coefficient distribution function (3.5) becomes:

$$\rho_\alpha(\omega, \alpha) = \frac{\rho_{ih}(\omega)}{\sqrt{2\pi}\gamma_G} \exp\left(-\frac{(\alpha - \beta_G(\omega))^2}{2\gamma_G^{\ 2}}\right). \tag{3.36}$$

We see that the pressure kernel is of a Gaussian shape, too. The shift of a spectral hole is linear, with a coefficient given by $\beta_G(\omega_m)$. The dependence of the coefficient on the burning wavelength indicates the presence of the color effect. The broadening of a narrow hole is hence Gaussian in shape and proportional to the absolute value of the pressure change. The broadening

27

coefficient is γ_G and does not depend on the frequency ω. For wide holes, though, there should also appear a small contribution to the broadening due to the color effect.

The IDF moves linearly with pressure and the shifting coefficient (shift per unit pressure) is the same as for a hole burnt in the IDF maximum. The broadening, however, is non-linear because there are two different factors that cause it: the broadening due to dispersion of pressure coefficients at any point within the IDF and the so-called color effect broadening. Linearizing (3.27) for small pressure values yields:

$$\left.\frac{d\sigma_{ih}}{d(\Delta p)}\right|_{\Delta p=0} = \frac{C}{\sigma_{G0}}. \tag{3.37}$$

Note that using the interactions of type r^{-n} here would give $\gamma_G = 0$ and bring us back to the situation described in previous subsection. Here Laird and Skinner make their second major assumption pointing out that the interaction potential for a probe with its nearby host molecule should also include a short-range repulsive term. They suggest using the familiar Lennard-Jones (LJ) potential, which is shifted radially by an amount r_0 to account for the circumstance that in polymers the effective radius of a single monomer unit is typically much smaller than that of the probe molecule:

$$\varepsilon(r) = \begin{cases} 4\varepsilon\left[\left(\dfrac{\sigma}{r-r_0}\right)^{12} - \left(\dfrac{\sigma}{r-r_0}\right)^{6}\right], & r > r_0 \\ \infty, & r \leq r_0 \end{cases} \tag{3.38}$$

Here ε and σ are parameters adjusting the energy and length scales, correspondingly. They use a simple uniform spatial distribution of host molecules around the probe, which is made zero at small r values that are physically unreachable:

$$p_N(z) = \begin{cases} \rho, & r \geq r_c + r_0 \\ 0, & r < r_c + r_0 \end{cases} \tag{3.39}$$

Here ρ is proportional to the molar density of the host, r_c is some cutoff value for the radial coordinate. The homogeneous pressure coefficient is then given by:

$$\alpha(r) = \begin{cases} \dfrac{8\varepsilon\kappa r}{r-r_0}\left[2\left(\dfrac{\sigma}{r-r_0}\right)^{12} - \left(\dfrac{\sigma}{r-r_0}\right)^6\right], & r > r_0 \\ \infty, & r \le r_0 \end{cases} \qquad (3.40)$$

Thus the scaling of $\alpha(r)$ with $\varepsilon(r)$ is removed and, generally, γ_G is not zero.

Noting that the difference of shifts of two spectral holes burnt at $(v_G + \sigma_{G0}/2)$ and $(v_G - \sigma_{G0}/2)$ has the pressure coefficient C/σ_{G0}, we can conclude that (3.37) represents the pure color effect contribution to the broadening, as the difference mentioned is caused by this effect only. This illustrates the fact that while the broadening of spectral holes is determined by short-range repulsive interactions, the broadening of the IDF as a whole remains governed by the long-range attractive ones. And so does the hole shift. Thus in this approach, the appearing of short-range repulsive forces plays the role of the superimposing factor that causes the hole broadening but does not affect their shift.

In their article, Laird and Skinner compare their calculations to experimental data and find them to be satisfactory in the case of polymers. Kador and coworkers have taken the theory further to either take into account the third-order terms in the expansion (3.25) [18] or to bypass it completely [19, 30]. Though analytical results are then difficult to achieve, they have shown by calculations that, under these conditions, the pressure kernel width can acquire frequency dependence, increasing from blue to red side of the IDF. Furthermore, its shape can become asymmetric, especially at the blue side of the IDF. They also ask a natural question [20, 21] about the contradiction between the assumption of the high density of perturbers required for the Gaussian approximation and that of the low density made in the initial layout (see (2.4) in section 2.1) and find that the spatial correlations within the matrix must be taken into account, otherwise the results may be (at least quantitatively) incorrect.

3.2.4. The diaelastic model

Let us next turn to another class of materials, the crystals. In a perfect crystal for a single site (way of fitting of the impurity center into the matrix structure) one expects no inhomogeneous broadening to take place. Yet in real crystals it is present and also a moderate pressure broadening of spectral holes is observable [11, 13].

The inhomogeneous effects here are attributed to defects within the crystal structure. At the same time, the concentration of the defects is generally rather low and their interaction with the impurities is prevalently of long-range type.

Therefore we can here rely on neither of the main assumptions of the Laird and Skinner theory.

In [16] we have made an attempt to describe the situation in crystals using the same statistical theory. We restrict ourselves to the point defects and consider the so-called diaelastic effect [26] as a possible mechanism of defect-impurity interaction. The diaelastic effect is an analog of the diamagnetic effect, where an additional magnetic moment is induced in a molecule by an external magnetic field. Based on the continuum theory of lattice defects, we can view point defects as regions with compressibility different from the bulk one. Such regions create a spatially inhomogeneous strain field inside the crystal that is modified by the applied external pressure.
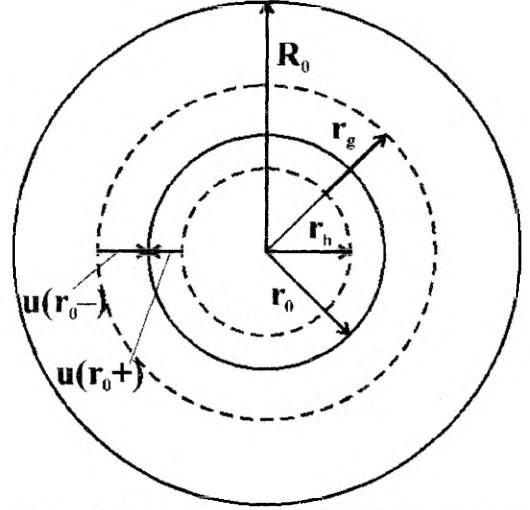

Figure 2. Model of a point defect. A spherical elastic inclusion of the initial radius r_g (larger dashed-line circle) is forced into a spherical cavity of the initial radius r_h (smaller dashed-line circle) formed in a homogeneous isotropic elastic sample of the radius $R_0 \gg r_g$, r_h (large solid-line circle). The radius of the inclusion after the strain relaxation (small solid-line circle) is r_0. Such relaxation is accompanied by changes of the initial dimensions of the cavity and the inclusion, by $u(r_0+)$ and $u(r_0-)$, respectively.

We consider the following model for a point defect [26]. From a spherical cavity of the radius r_h and the volume $V_h = (4\pi/3)r_h^3$ at zero external pressure the host material is removed. It is replaced by a sphere of the initial radius r_g and the volume $V_g = (4\pi/3)r_g^3$ made of a material with the Lamé constants λ_g and μ_g (and compressibility κ_g) in general differing from those of the host material, λ_h and μ_h (and κ_h). Let us call it the guest sphere. Assuming for the sample a spherical shape concentric with the cavity and of the radius $R_0 \gg r_g$, r_h, the spherical symmetry is preserved in the course of strain relaxation. In spherical coordinates the displacement vector has only a radial non-zero component, generally given by [17; 26, Eq. (21.5)]:

$$u_r(r) = Cr^{-2} + \overline{C}r. \tag{3.41}$$

Eq. (3.41) describes the displacement field inside as well as outside the inclusion. The constants C and $\overline{C}$ (different for the interior and the exterior of the inclusion) can be expressed via the elastic constants κ_g, μ_g, κ_h, μ_h and the

geometrical characteristics r_g, r_h. First we note that $C_g \equiv C(inside) = 0$ due to the absence of singularity at the origin, i.e.

$$u_r(r) = \begin{cases} \overline{C}_g r, & r < r_0 \\ Cr^{-2} + \overline{C}_h r, & r > r_0 \end{cases},$$

(3.42)

where r_0 is the final radius of the inclusion after strain relaxation (see Fig. 2).

In spherical coordinates only the diagonal components of the stress tensor have nonzero values. The σ_{rr} component is given by

$$\sigma_{rr}(r) = \begin{cases} 3\overline{C}_g \kappa_g^{-1}, & r < r_0 \\ -4\mu_h Cr^{-3} + 3\overline{C}_h \kappa_h^{-1}, & r > r_0 \end{cases}.$$

(3.43)

For determination of the (pressure-dependent) coefficients C, $\overline{C}_h$, $\overline{C}_g$ we have the following equations:
(i) for the change of the radius of the inclusion

$$r_0 - r_g = u_r(r \to r_0 -),$$

(3.44)

(ii) for the change of the cavity radius

$$r_0 - r_h = u_r(r \to r_0 +),$$

(3.45)

(iii) from continuity of the stress at the guest-host interface

$$\sigma_{rr}(r \to r_0 -) = \sigma_{rr}(r \to r_0 +),$$

(3.46)

(iv) and from the equilibrium of the sample surface (strain counterbalanced by the external pressure p)

$$\sigma_{rr}(r \to \infty) + p = 0.$$

(3.47)

Eqs. (3.42)–(3.47) yield

$$C = \frac{\left(r_g + \frac{4}{3}\mu_h\kappa_g r_h\right)^2\left[\left(r_g - r_h\right)+\left(\kappa_h r_g - \kappa_g r_h\right)\frac{p}{3}\right]}{\left[\left(1+\frac{4}{3}\mu_h\kappa_g\right)+\left(1+\frac{4}{3}\mu_h\kappa_h\right)\frac{\kappa_g p}{3}\right]^3}, \qquad (3.48)$$

$$\overline{C}_h = -\frac{\kappa_h}{3}p, \qquad (3.49)$$

$$\overline{C}_g = -\frac{\frac{4}{3}\mu_h\kappa_g\left(r_g - r_h\right)+\left(1+\frac{4}{3}\mu_h\kappa_h\right)r_g\frac{\kappa_g p}{3}}{r_g + \frac{4}{3}\mu_h\kappa_g r_h}, \qquad (3.50)$$

and

$$r_0 = \frac{r_g + \frac{4}{3}\mu_h\kappa_g r_h}{\left(1+\frac{4}{3}\mu_h\kappa_g\right)+\left(1+\frac{4}{3}\mu_h\kappa_h\right)\frac{\kappa_g p}{3}}. \qquad (3.51)$$

Outside the cavity the stress tensor is given by

$$\sigma_{rr} = -\frac{4\mu_h C}{r^3} - p, \qquad (3.52)$$

$$\sigma_{\theta\theta} = \sigma_{\varphi\varphi} = \frac{2\mu_h C}{r^3} - p, \qquad (3.53)$$

or in Cartesian coordinates ([26]):

$$\sigma_{kl} = -p\delta_{kl} + \frac{2\mu_h C}{r^3}\left(\delta_{kl} - \frac{3x_k x_l}{r^2}\right), \quad k, l = 1, 2, 3 \qquad (3.54)$$

The single-defect solvent shift function is now expressed as a linear combination of the stress components (see (2.1)). We will omit in (3.54) the

hydrostatic term $-p\delta_{kl}$, yielding a uniform pressure shift independent of defects. Then $\varepsilon(z)$ can be expressed in polar coordinates:

$$\varepsilon(z) = 2\mu_h C \frac{\Phi(\theta,\varphi)}{r^3}, \tag{3.55}$$

where the function Φ depends only on the symmetry of the states involved in the actual transition and their coupling to the stress field and *does not* depend on the defects. The spherical angles θ and φ give the direction of the impurity (or defect, if one takes the impurity location for the origin).

The parameter C in (3.55) can actually be viewed as an internal coordinate of the defect; we may call it the defect strength. The full set of coordinates z characterizing a defect thus includes beside the spatial coordinates r, θ, φ its strength C as well. For the expansion (3.2) we need its zero-pressure value $C_0 \equiv C(p = 0)$ which, by (3.48), equals:

$$C_0 = \frac{2\mu_h\left(r_g + \frac{4}{3}\mu_h\kappa_g r_h\right)^2 \left(r_g - r_h\right)}{\left(1 + \frac{4}{3}\mu_h\kappa_g\right)^3}. \tag{3.56}$$

Note that here we also included the factor $2\mu_h$ from (3.54).

Since C has volume dimensionality, we can define a quantity κ_C analogously to the volume compressibility:

$$\kappa_C = \left(\frac{1}{C}\frac{\partial C}{\partial p}\right)_{p=0}. \tag{3.57}$$

By analogy with the compressibility, we could call κ_C the *amplificability* (mechanical polarizability) of the defect as it shows how easily the external pressure changes its influence on the surrounding probes. With (3.48) κ_C is expressed as follows:

$$\kappa_C = \left(\frac{r_g}{3(r_g - r_h)}\right)\kappa_h - \left(\frac{r_h}{3(r_g - r_h)} + \frac{3 + 4\mu_h\kappa_h}{3 + 4\mu_h\kappa_g}\right)\kappa_g. \tag{3.58}$$

The pressure coefficient function becomes

$$\alpha(z) = \left(\frac{\partial \varepsilon}{\partial r} \frac{\partial r}{\partial p} + \frac{\partial \varepsilon}{\partial C} \frac{\partial C}{\partial p} \right)_{p=0} = \varepsilon(z)(\kappa_h + \kappa_C). \qquad (3.59)$$

We define ΔV to express the volume change of the host cavity due to the defect substitution ("volume defect"): $\Delta V = 4\pi(r_0^3 - r_h^3)/3$. Let us view the case when ΔV is small, i.e. $\Delta V \ll V_g$, V_h. Then C_0 and κ_C can be approximated as

$$C_0 \approx \frac{\mu_h}{2\pi} \Delta V \qquad (3.60)$$

and

$$\kappa_C \approx \frac{\kappa_h - \kappa_g}{\left(1 + \frac{4}{3} \kappa_g \mu_h \right)} \frac{V_h}{\Delta V}. \qquad (3.61)$$

These estimations hold with a precision of an order of magnitude at least within limits given by $|\Delta V/V_h| \le 1$, which every physically reasonable point defect should satisfy. They also express the following important points:

(i) the amplificability κ_C depends not only on the bulk parameters (κ_h, μ_h) but on the local ones ($V_h/\Delta V$, κ_g) as well, i.e. for the same host material defect-dependent variations of κ_C are possible and thus it may be treated as an internal coordinate of the defect;

(ii) depending on the signs of ΔV and $\kappa_h - \kappa_g$, C_0 and κ_C can acquire both positive and negative values;

(iii) the variations of C_0 and κ_C (arising from the variations of V_h and ΔV) need not be absolutely correlated.

It is clear that if all defects have equal amplificabilities then the situation reduces to that viewed in subsection 3.2.2, i.e. no pressure broadening is expected for narrow spectral holes. To explain the broadening, we must assume that there exists some distribution of values for κ_C (and possibly for C_0 as well). Guided by (3.59), we include κ_h in the definition of the amplificability and denote the quantity by $\kappa = \kappa_h + \kappa_C$. Note that the remarks made above for κ_C generally hold for κ, too. Let us assume a spatially uniform distribution of defects with a density ρ. The distribution function $p_N(z)$ is then

$$p_N(z) = \rho \, p_1(C_0, \kappa), \qquad (3.62)$$

34

where $p_1(C_0, \kappa)$ is the unity-normalized joint distribution function for C_0 and κ. If these quantities are uncorrelated, $p_1(C_0, \kappa)$ factorizes into a product of two distributions.

Let us now calculate the pressure-dependent shape of the IDF. Substituting ε from (3.55) (with pressure dependence added) into (2.10) and integrating over r, (see [23], app. III for the details of this integration) one obtains for $J(x)$:

$$J(x) = i(v_D + \alpha_D \Delta p)x + \Gamma_D(\Delta p)|x|, \qquad (3.63)$$

where

$$v_D = a_I \rho \iint p_1(C_0, \kappa) C_0 dC_0 d\kappa, \qquad (3.64)$$

$$\alpha_D = a_I \rho \iint p_1(C_0, \kappa) C_0 \kappa \, dC_0 d\kappa, \qquad (3.65)$$

$$\Gamma_D(\Delta p) = a_R \rho \iint p_1(C_0, \kappa) C_0 |1 + \kappa \Delta p| dC_0 d\kappa, \qquad (3.66)$$

$$a_R = \frac{\pi}{6} \int_0^{2\pi}\int_0^{\pi} |\Phi| \sin\theta d\theta d\varphi, \qquad (3.67)$$

$$a_I = -\frac{1}{3} \int_0^{2\pi}\int_0^{\pi} \Phi \ln|\Phi| \sin\theta d\theta d\varphi. \qquad (3.68)$$

With $J(x)$ as given by (3.63), integral (2.12) can be calculated. It gives for the IDF a Lorentzian shape centered at $v_D + \alpha_D \Delta p$ and of a width $2\Gamma_D$:

$$\rho_{ih}(\omega) = \frac{1}{\pi} \frac{\Gamma_D(\Delta p)}{\Gamma_D^{\,2}(\Delta p) + (\omega - (v_D + \alpha_D \Delta p))^2}. \qquad (3.69)$$

Since in (3.66) the distribution of defect strengths plays only a role of a weighting factor for the amplificability distribution, let us define instead an effective amplificability distribution as follows:

$$p_1^{eff}(\kappa) = \frac{\int p_1(C_0, \kappa)|C_0| dC_0}{\iint p_1(C_0, \kappa)|C_0| dC_0 d\kappa} . \qquad (3.70)$$

If the distributions for zero-pressure strength and amplificability are not correlated, the effective amplificability distribution coincides with the actual one. Now $\Gamma_D(\Delta p)$ can be expressed via $p_1^{eff}(\kappa)$ as

$$\Gamma_D(\Delta p) = \Gamma_0 \int p_1^{eff}(\kappa)|1 + \kappa \Delta p| d\kappa , \qquad (3.71)$$

where $\Gamma_0 \equiv \Gamma_D(0)$ is the zero-pressure width (FWHM/2) of the IDF. At sufficiently low pressures always $\kappa \Delta p > -1$ and the absolute value signs may be dropped. Thus the broadening coefficient near the zero pressure is

$$\left. \frac{d\Gamma_D}{d(\Delta p)} \right|_{\Delta p = 0} = \Gamma_0 \bar{\kappa}_{eff} \qquad (3.72)$$

Depending on the sign of the average effective amplificability value, a pressure-induced broadening as well as a pressure-induced narrowing of the IDF is possible. For rigid (incompressible) defects the former case corresponds to $r_g > r_h$ and the latter one to $r_g < r_h$. It is also possible that a counterbalance between the defects of both positive and negative amplificability values can result in rather a weak pressure broadening of the IDF even in crystals with high concentration of defects.

Next we will turn to evaluation of the joint distribution function $\rho_\alpha(\omega, \alpha)$ for the diaelastic model, to analyze the pressure effects on spectral holes. In this section we will limit ourselves to this distribution; the two-frequency distribution function $\rho(\omega_1, \omega_2, \Delta p)$ is always available from the transformation (3.6). Note that the shift and broadening of narrow holes at any point ω within the IDF is given correspondingly by the center position and width of the α-distribution (pressure kernel) at ω.

In order to simplify the following consideration, we exclude all the factors that shift the whole IDF uniformly with pressure:

- The pressure dependence of the unperturbed frequency ω_0. In case of crystals ω_0 is to be understood as the transition frequency in a perfect crystal. However, this frequency is pressure dependent because of compression of the surrounding crystal cage with pressure.

- Due to surface effects at finite defect densities there is another homogeneous contribution to the frequency shift, the so-called Eshelby term [25].
- The hydrostatic term $-p\delta_{kl}$ in (3.54) mentioned earlier.
- The factor α_D in (3.69).

In this purpose it is most convenient to express the joint distribution $\rho_\alpha(\omega, \alpha)$ in coordinates shifted so that the origin coincides with the IDF maximum. We will also use Γ_0 as a measure for both ω (to give a dimensionless quantity) and α (which will obtain the dimensionality of κ). Let us denote the new coordinates by ω', α':

$$\begin{cases} \omega' = (\omega - \nu_D)/\Gamma_0 \\ \alpha' = (\alpha - \alpha_D)/\Gamma_0 \end{cases}. \tag{3.73}$$

Then we get from (3.14), (3.15):

$$\rho_\alpha(\omega', \alpha') = \frac{1}{(2\pi\Gamma_0)^2} \iint \exp(i\omega' x_1 + i\alpha' x_2 - K(x_1, x_2)) dx_1 dx_2, \tag{3.74}$$

$$K(x_1, x_2) = \int p_1^{eff}(\kappa)|x_1 + \kappa x_2| d\kappa. \tag{3.75}$$

We see that $p_1^{eff}(\kappa)$ is in fact the maximum of information that pressure tuning experiments can ultimately yield.

3.2.5. Calculations on the diaelastic model

Let us now analyze the general properties of (3.74), (3.75). A few things here can be said without any particular specification of $p_1^{eff}(\kappa)$.

Firstly, we note that, due to obvious relation $K(x_1, x_2) = K(-x_1, -x_2)$, always $\rho_\alpha(\omega', \alpha') = \rho_\alpha(-\omega', -\alpha')$, from which in the case $\omega' = 0$ we get that the pressure kernel in the center is always symmetrical with respect to the origin $\alpha' = 0$, regardless of the shape of the amplificability distribution. It is also easy to verify that the central distribution always has a maximum at the origin, which, at least for all studied cases, appears to be the only maximum this distribution has.

Further, as shown in Appendix I, the first two statistical moments of $p_1^{eff}(\kappa)$ and the pressure kernel (i.e. the α'-distribution in $\rho_\alpha(\omega', \alpha')$ depending on ω') are linked by simple relations as follows:

$$\overline{\alpha}'(\omega') = \overline{\kappa}_{\mathit{eff}}\,\omega', \qquad (3.76)$$

$$\sigma_\alpha(\omega') = \sigma_\kappa \sqrt{1 + \omega'^2}, \qquad (3.77)$$

where $\overline{\alpha}'$ and $\overline{\kappa}_{\mathit{eff}}$ are the mean values and σ_α, σ_κ the standard deviations of the pressure kernel and the effective amplificability distribution, correspondingly. (3.76) and (3.77) are valuable relations connecting the mean value and width of the pressure kernel with the respective values for the amplificability distribution and including the color effects for both hole shifting and broadening. The only assumption for these relations to hold is that the mean value and standard deviation can be calculated for $p_1^{\mathit{eff}}(\kappa)$. Note that, as seen from (3.76), (3.72), the pressure broadening of the IDF is, like in previous models, in the first approximation driven by the color effect.

For further analysis a specification of the amplificability distribution is required. A simple choice for $p_1^{\mathit{eff}}(\kappa)$ that can be handled analytically is the two-point distribution, i.e. when there are two subsets of defects in the crystal with different amplificabilities [16, 17]:

$$p_1^{\mathit{eff}}(\kappa) = n_1\delta(\kappa - \kappa_1) + n_2\delta(\kappa - \kappa_2), \qquad (3.78)$$

where n_1 and n_2 are the relative concentrations of the corresponding defect type, $n_1 + n_2 = 1$. The distribution $\rho_\alpha(\omega', \alpha')$ is then a product of two shifted Lorentzians:

$$\rho_\alpha(\omega',\alpha') = \frac{|\Delta\kappa|}{\pi^2\Gamma_0^2} \frac{n_1\Delta\kappa}{n_1^2\Delta\kappa^2 + (\omega'\kappa_2 - \alpha')^2} \frac{n_2\Delta\kappa}{n_2^2\Delta\kappa^2 + (\omega'\kappa_1 - \alpha')^2}, \quad (3.79)$$

where $\Delta\kappa = \kappa_2 - \kappa_1$.

We first examine the pressure kernel in the center of the IDF (i.e. $\omega' = 0$). It can be written down in a general form:

$$\rho_\alpha^0(\alpha') = \frac{n_{b\sigma}(b,\sigma_{\alpha 0})}{\pi} \frac{1}{\sigma_{\alpha 0}^4 + b\sigma_{\alpha 0}^2\alpha'^2 + \alpha'^4}, \qquad (3.80)$$

where

$$\sigma_{\alpha 0} = \sigma_\alpha(0) = \sigma_\kappa = \Delta\kappa\sqrt{n_1 n_2} \qquad (3.81)$$

38

is the standard deviation of the distribution,

$$b = \frac{n_1}{n_2} + \frac{n_2}{n_1}$$

(3.82)

is a second parameter and $n_{b\sigma}(b, \sigma_{\alpha 0})$ is a normalizing function

$$n_{b\sigma}(b, \sigma_{\alpha 0}) = \sigma_{\alpha 0}^3 \left(\frac{\sqrt{\sqrt{b^2 - 4} + b}}{\sqrt{2}} + \frac{\sqrt{2}}{\sqrt{\sqrt{b^2 - 4} + b}} \right).$$

(3.83)

In the symmetrical case, when $n_1 = n_2 = 1/2$, the distribution obtains the form of a squared Lorentzian.

The mean value and width of the off-center pressure kernel follow the general laws (3.76) and (3.77) with

$$\overline{\kappa}_{eff} = n_1 \kappa_1 + n_2 \kappa_2$$

(3.84)

and σ_κ given by (3.81). Let us study the shape of the kernel in the symmetrical
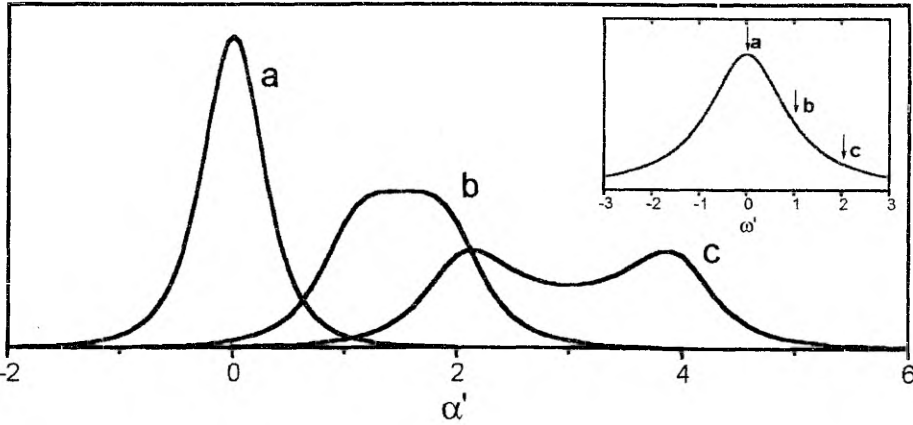
Figure 3. The shapes of the pressure coefficient distributions in the joint distribution $\rho_\alpha(\omega', \alpha')$ for the symmetrical two-point effective amplificability distribution with $\kappa_1 = 1$, $\kappa_2 = 2$ ($\overline{\kappa}_{eff} = 1.5$, $\Delta\kappa = 1$). The insert shows the positions on the IDF where the distributions are taken: $\omega' = 0$ (a), $\omega' = 1$ (b), $\omega' = 2$ (c). The distributions are divided by the IDF value at the given position to normalize them to the same area.

39

case (Fig. 3). It appears that, starting from $|\omega'| = 1$, it obtains two maxima. Indeed, one finds three possible extreme value points for (3.79) with $n_1 = n_2 = 1/2$:

$$\begin{cases} \alpha'_{1m} = \overline{\kappa}_{\mathit{eff}}\,\omega' \\ \alpha'_{2,3m} = \overline{\kappa}_{\mathit{eff}}\,\omega' \pm \dfrac{\Delta\kappa}{2}\sqrt{\omega'^2 - 1} \end{cases}. \qquad (3.85)$$

The maxima diagram is depicted in Fig. 4. Up to $|\omega'| = 1$, the pressure kernel has one central maximum at α'_{1m}. From there towards the wings splitting sets in and α'_{1m} becomes an intermediate minimum between two maxima α'_{2m} and α'_{3m}.

At large ω' values the two maxima approach the lines $\alpha' = \kappa_1\omega'$ and $\alpha' = \kappa_2\omega'$, correspondingly. Note that these are the lines that the maximum of the pressure kernel would follow if only the defects of either type were present independently (the kernel would then be given by a δ-function). This is a manifestation of a more general assimilation effect lying in the circumstance that the pressure kernel becomes increasingly similar in shape to the stretched effective amplificability distribution $p_{\mathit{eff}}(\kappa = \alpha'/\omega')$ when moving from the IDF center towards the wings. The reason is that the probes that contribute to the IDF far on the wings are basically influenced by a single nearby defect (let us call such an approach the single defect limit) and the whole multitude of such probes copy in the α'-dimension quite well the existing amplificability distribution. The stretching comes from the fact that for a single defect-probe pair holds $\alpha(r) = \kappa\,\varepsilon(r)$ and $\varepsilon(r)$ here represents the detuning from the IDF center ω'.
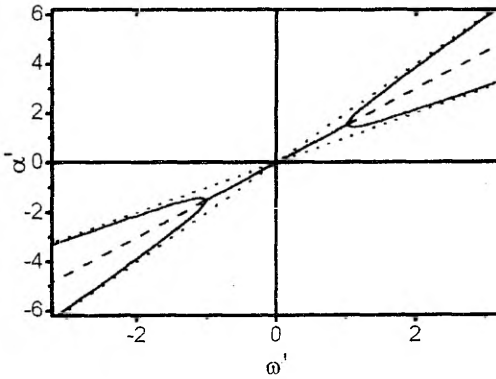
Fig. 5 depicts the evolution of the pressure kernel along the frequency coordinate in case of an asymmetrical $(n_1 \neq n_2)$ two-point distribution where the assimilation effect gives asymmetrical distribution shapes on the wings of the IDF. In the center of the IDF, where the probes receive a more or less equal contribution from a number of defects, the kernel still stays symmetrical.

Although (3.77) sets a clear relation between the standard

Figure 4. The maxima diagram of the joint distribution $\rho_\alpha(\omega', \alpha')$ for the symmetrical two-point effective amplificability distribution with $\kappa_1 = 1$, $\kappa_2 = 2$. The solid line shows the position of maximum(s), the dashed line the position of the intermediate minimum at $|\omega'| > 1$. The dotted lines are $\alpha' = \kappa_1\omega'$ and $\alpha' = \kappa_2\omega'$, the asymptotic positions of the maxima at large ω' values.
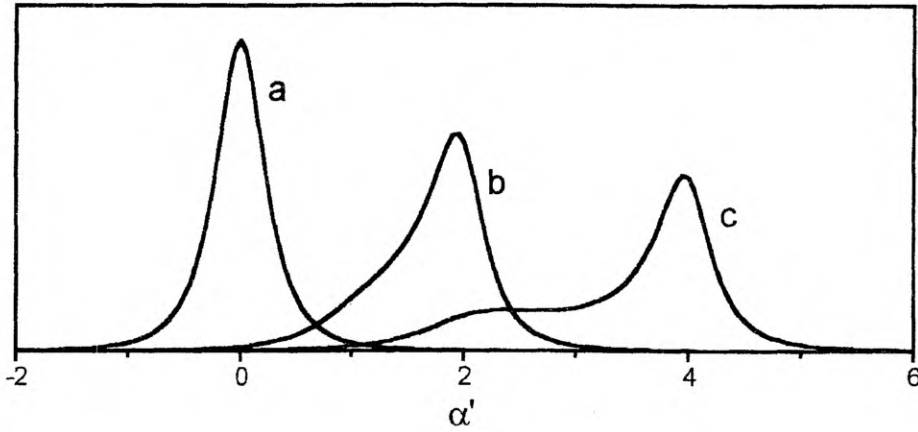
Figure 5. The same as Fig. 3 for an asymmetrical two-point effective amplificability distribution ($n_1 = 0.3$, $n_2 = 0.7$, everything else is unchanged). Note that the distribution (a) taken at the centre of the IDF remains symmetrical in shape but is narrower.

deviations of the pressure kernel and the amplificability distribution, one could also want to know another measure for the hole broadening, the FWHM of the pressure kernel, which is often more useful for interpreting experimental results. However, FWHM and standard deviation are not fully equivalent as characteristics for the width of a distribution. It is easy to see that, with distribution type and other parameters fixed, the FWHM to standard deviation ratio is generally constant for any distribution where the very concept of FWHM has any conceivable meaning. This follows from the fact that both quantities are linear in distribution rescaling with fixed normalization. The value of this ratio (denote it by γ) is the greater the steeper the falloff of the distribution on the wings since variance (square of the standard deviation) weighs everything on the wings with the distance from the distribution center squared. This way, γ could even be regarded as a kind of characteristic value within a certain group of distributions (with definite FWHM). In practice, γ ranges from zero (e.g. Lorentzian shape where the variance integral diverges) to a few units for the uniform distribution ($\gamma = 2\sqrt{3} = 3.454$) as a limiting case. For a Gaussian shape one gets $\gamma = 2\sqrt{2 \ln 2} = 2.355$. The central pressure kernel in case of the two-point amplificability distribution (3.80) is expressed as

$$\gamma = \sqrt{2}\sqrt{\sqrt{b^2 + 4} - b} \qquad (3.86)$$

and can, depending on n_1/n_2, have γ from 0 to $2\sqrt{\sqrt{2} - 1} = 1.287$, the former value corresponding to the one-point distribution and the latter to the

symmetrical case. Moving away from the IDF center, γ of the kernel obtains frequency dependence and approaches, as demanded by the assimilation effect, γ of the effective amplificability distribution in the process $\omega' \to \infty$.

For the symmetrical two-point distribution the frequency-dependent γ of the pressure kernel is given as follows:

$$
\gamma_\alpha(\omega') = \begin{cases} 2\sqrt{\sqrt{2\left(1 - 2\left(\dfrac{\omega'}{1+\omega'^2}\right)^2\right)} + 2\dfrac{\omega'^2}{1+\omega'^2} - 1}, & |\omega'| < 1 \\ 2\sqrt{1 + 2\dfrac{|\omega'| - 1}{\omega'^2 + 1}}, & |\omega'| > 1 \end{cases} \tag{3.87}
$$

(see Fig. 8(a)). Note that its value approaches 2 in the high ω' limit, which is the γ value for the symmetrical two-point distribution.

In addition to the two-point case, some numerical calculations with other effective amplificability distribution shapes were performed. One case of interest was the uniform distribution:

$$
p_1^{eff}(\kappa) = \frac{1}{\Delta\kappa} Y(\kappa - \kappa_1) Y(\kappa_2 - \kappa), \tag{3.88}
$$

where $Y(\kappa)$ is the unit step function. Here we assume $\kappa_1 < \kappa_2$. The standard deviation of (3.88) is $\sigma_\kappa = \Delta\kappa / 2\sqrt{3}$. This case could be treated in part analytically, but we used numerical integration in the final stage to obtain $\rho_\alpha(\omega', \alpha')$. Another distribution that was calculated was the Gaussian:

$$
p_1^{eff}(\kappa) = \frac{1}{\sigma_\kappa \sqrt{2\pi}} \exp\left(-\frac{(\kappa - \bar{\kappa}_{eff})^2}{2\sigma_\kappa^2}\right), \tag{3.89}
$$

which required a fully numerical approach.

The central kernel calculated using these distributions is in many aspects very close to that obtained with the two-point amplificability distribution. Though it obviously cannot be exactly expressed in the general form (3.80), the difference is in both cases rather minor (Fig. 6). The asymptotic form $\rho_\alpha(0, \alpha') \sim \alpha'^{-4}$ is clearly observable and also the numerically obtained FWHM to standard deviation ratio, $\gamma = 1.235$ for the uniform and $\gamma = 1.167$ for the Gaussian distribution points to a similar distribution type (cf. $\gamma = 1.287$ for the symmetrical two-point distribution). The closest distribution of type (3.80) would be with about $b = 2.181$ (the uniform case) or $b = 2.594$ (the Gaussian
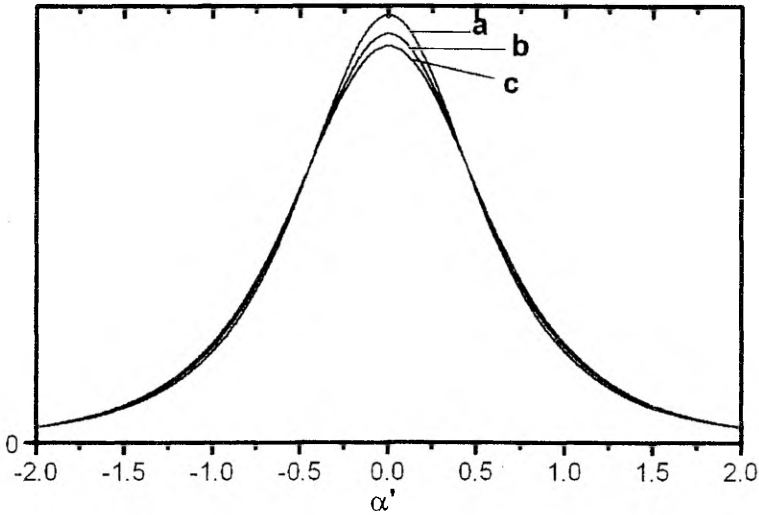
Figure 6. The comparison of central pressure kernels for Gaussian (a), uniform (b) and two-point symmetrical (c) effective amplificability distributions with standard deviations all equal to unity.

case). And indeed, the central pressure kernel for the uniform distribution differs from (3.80) with adjusted standard deviation and b values nowhere by more than 1%.

Also the least-square fitting of the central kernel with (3.80) gives good results with similar parameter outcomes (within a few %). It is noteworthy that the parameter that is reproduced especially well is the FWHM of the kernel.

At high ω' values the assimilation effect is clearly observable. This is illustrated in Fig. 7 for the uniform distribution where the pressure kernel shape shows a clear tendency towards the rectangular shape (the kernels have been compressed in the α'-dimension to remove broadening). The asymptotic approaching of the frequency-dependent γ values of the kernel to the corresponding values of the effective amplificability distribution is also confirmed by the calculations (see Fig. 8).
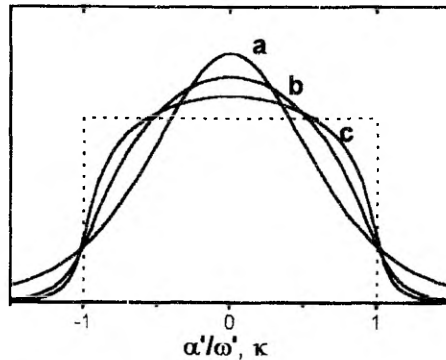

Figure 7. The assimilation effect: the pressure coefficient distributions at various ω' values for the uniform effective amplificability distribution with $\kappa_1 = -1$, $\kappa_2 = 1$ (dotted line). The values are: $\omega' = 1$ (a), $\omega' = 5$ (b), $\omega' = 10$ (c). The distributions are normalized to the same area and the α' axis is scaled with ω', as discussed in text. Note the box-like shape that the distribution acquires at large detunings from the centre of the IDF.

43

Let us now summarize what we have found out about the general properties of the joint distribution $\rho_\alpha(\omega', \alpha')$ for the diaelastic model:

- The hole shifting coefficient relative to the IDF maximum exhibits the color effect: it is a linear function of the position within the IDF (also relative to the maximum), the coefficient being $\bar{\kappa}_{eff}$.
- The broadening of the IDF as a whole is, similarly to the previous models, governed by the same color effect phenomenon.
- In the center of the IDF, the pressure coefficient distribution is symmetrical and single-peaked; its standard deviation equals to that of the effective amplificability distribution. The shape should match well with an inverted fourth-order even polynomial (3.80).
- Far on the wings of the IDF the pressure coefficient distribution acquires the shape of the effective amplificability distribution.
- The width of the pressure coefficient distribution, i.e. the pressure broadening coefficient for narrow spectral holes also depends on the distance from the IDF center (the broadening color effect). The dependence is generally determined by (3.77) for standard deviations. However, when dealing with FWHM-s one also has to take into account the γ-factor which, due to varying pressure kernel shape, also acquires frequency dependence.
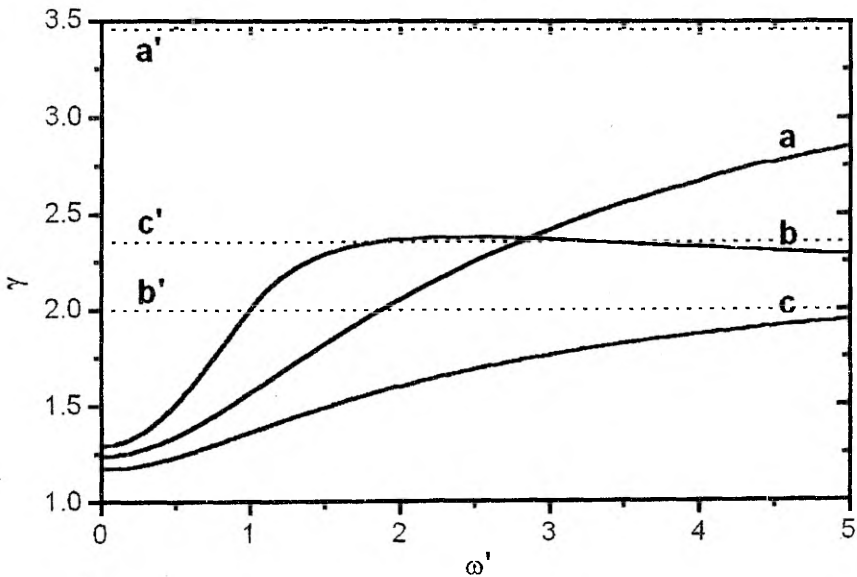

Figure 8. The FWHM to standard deviation ratio (γ) values of the pressure kernels as functions of the position ω' within the IDF in case of uniform (a), symmetrical two-point (b) and Gaussian (c) effective amplificability distributions. The dotted lines, labeled by the corresponding primed characters, represent the γ values of the amplificability distributions themselves, i.e. the asymptotic kernel γ values at large frequencies.

3.2.6. Experimental findings on the diaelastic model

To test various aspects of the diaelastic model, we conducted a series of pressure tuning experiments with crystalline durene (1,2,4,5-tetramethylbenzene). As a dopant, we used dimethyl-s-tetrazine (DMST), in which the main hole burning mechanism is via methyl group tunneling [31, 32]. In durene, the zero-phonon line of DMST S_0–S_1 transition is peaked at 17020 cm^{-1}. The system DMST:durene has been studied by hole burning before [13, 22, 33].

Our goal was to study the pressure effects in crystals with different degree of disorder (inhomogeneity). A general way to control the inhomogenous effects is to modify the density of defects in the lattice. We attempted to do so by mixing a small amount (about 2 mol. %) of hexachlorobenzene into some samples.

The samples were prepared by dissolving DMST and, for mixed samples, also hexachlorobenzene in melted durene (m.p. 82 °C). The concentration of DMST was about 10^{-4} mol/mol. A polycrystalline sample was obtained by slow cooling through the melting point. The sample was kept inside a small two-window pressure cell, which used helium as a pressure transmitter. The cell was kept inside a He-flow cryostat for cooling. The temperature was stabilized at 2.0 ± 0.2 K. The range of available pressures was limited by the pressure regulator to about 1..13 bar. However, this was sufficient to measure the shift and broadening of spectral holes.

Holes were burnt and measured with COHERENT 699-29 single-frequency dye laser with the linewidth of about 1 MHz. For burning the power density at the sample was about 200 $\mu W/cm^2$, for recording it was reduced about 20 times. Burning times were in the order of 100 s. Also the inhomogeneous line was narrow enough to be measured with the same laser. Transmission spectra were recorded that were later converted to optical density. The holes were fitted to Lorentzian curves with a possibly sloped baseline. Note that, theoretically, only the (non-saturated) initial holes are Lorentzian in shape while during the
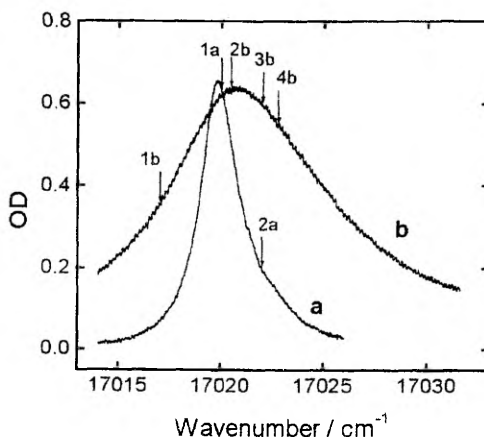

Figure 9. Absorption spectra of the DMST S_0–S_1 transition in neat durene (a) and in durene mixed with hexachlorobenzene (2 mol. %) (b). The linewidths are 2.4 cm^{-1} and 9.6 cm^{-1}, correspondingly. The numbered arrows on each line denote the positions where the pressure tuning series were taken.
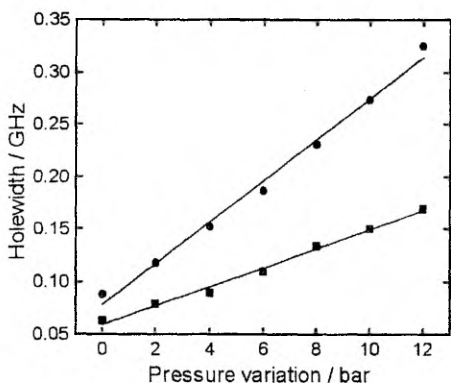
Figure 10. Pressure dependence of the holewidth for spectral holes burnt in the center of the inhomogeneous line in neat (rectangles, series 1a) and mixed (circles, series 2b) crystal. The solid lines indicate the least-squares linear fits. The slopes are 9.0 MHz/bar for neat and 18.8 MHz/bar for mixed crystals.
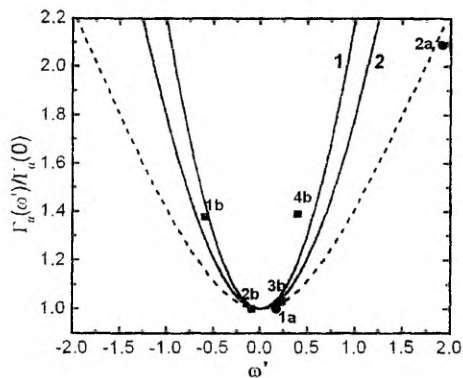
Figure 11. Relative pressure broadenings of all considered holes with respect to the central holes in neat (rectangles) and mixed (circle) crystal as a function of the burning position (scaled with FWHM/2 of the inhomogeneous line). The dashed line represents the corresponding theoretical relative value for the standard deviation, the solid lines for the FWHM-s in case of two-point symmetrical (1) and uniform (2) amplificability distributions.

pressure broadening holes get convoluted with a pressure kernel of a different shape, as discussed in the previous section. However, for the hole widths (FWHM) and baseline characteristics the results should be quantitatively correct.

We first measured the effect of introducing foreign molecules on the inhomogeneous broadening of the absorption line. As seen from Fig. 9, the modification is quite large: in neat samples the linewidth is about 2.4 cm^{-1}, but reaches a value of 9.6 cm^{-1} in mixed samples. This gives us an increase of about 4 times.

We then made several pressure series with spectral holes burnt at different frequencies within the inhomogeneous line, to measure pressure effects on the holes, especially broadening. We chose 6 series (2 for neat and 4 for mixed samples) for closer examination. Arrows 1a, 2a and 1b..4b in Fig. 9 denote the locations where the series were taken. For both neat and mixed samples one of the series was located near the center of the inhomogeneous line which was determined to be 17019.8 cm^{-1} for neat samples (series 1a, position 17020 cm^{-1}) and 17020.9 cm^{-1} for mixed samples (series 2b, position 17020.5 cm^{-1}). In what follows, we will refer to these series and the corresponding pressure quantities as "central".

Fig. 10 shows the pressure dependence of the holewidth within the central series. The broadening values are 9.0 MHz/bar for the neat sample and

18.8 MHz/bar for the mixed sample. It follows from (3.77) that the hole broadening in the center of the inhomogeneous line is proportional to the product $\sigma_\kappa \Gamma_0$, where σ_κ is the standard deviation of the effective amplificability distribution and Γ_0 the zero-pressure inhomogeneous linewidth. According to this, the hole broadening should scale with the inhomogeneous linewidth on a modification of the inhomogeneity if σ_κ is unchanged.

We see, however, that the pressure broadening in mixed system is about 2 times too low to scale with the controlled broadening of the inhomogeneous line: the increase in broadening for central holes as a result of mixing is only 2.1 times while the inhomogeneous linewidth increased 4 times. We therefore have to conclude that the dispersion of the effective amplificability distribution has decreased correspondingly. This could stem from the circumstance that the introduced molecules were all similar and occupied preferably similar sites in the crystal thus in effect narrowing the otherwise perhaps more diverse picture of defects. At the same time the inhomogeneous width, which, above all, is linear with the defect density, is still increased.

We also measured the color effects for both hole shift and broadening. The color effect for the shift was not very pronounced, but still observable. In crystals, as discussed earlier, we have to split the solvent shift in two parts: the constant part, equal for all probes, arising mainly from the surrounding crystal cage and representing the situation in a perfect crystal, and the varying part, responsible for the inhomogeneous broadening. The pressure dependences of the two parts are generally not equal and this could be the main reason that prevents the pressure shift coefficient from extrapolating to zero at the vacuum frequency. In our case, the zero-extrapolated frequency is around 17100 cm^{-1}, indicating that the constant part accounts for at least 4/5 of the total solvent shift (the vacuum frequency for the DMST transition under discussion is about 17500 cm^{-1} [13]). It is, however, clear that the pressure dependence of the varying part of the solvent shift is much stronger than that of the constant part.

To analyze the color effect for the hole broadening, let us rewrite (3.77) as follows:

$$\frac{\sigma_\alpha(\omega')}{\sigma_\alpha(0)} = \sqrt{1 + \omega'^2} \; . \tag{3.90}$$

For the FWHM of the pressure kernel, which represents more precisely the experimentally determined pressure broadening, a similar relation can be written:

$$\frac{\Gamma_\alpha(\omega')}{\Gamma_\alpha(0)} = \frac{\gamma(\omega')}{\gamma(0)} \sqrt{1 + \omega'^2} \; , \tag{3.91}$$

47

where $\gamma(\omega')$ is the previously introduced FWHM to standard distribution ratio which, in this context, is frequency-dependent.

In Fig. 11 the relative pressure broadenings for all non-central holes with respect to the central holes are shown as a function of the burning position. As a guideline, the corresponding theoretical relative value for the standard deviation, as given by (3.90), is plotted, along with relative FWHM values for two choices of amplificability distribution, two-point symmetrical and uniform.

Obviously, in the course of mixing, a notable change in the amplificability distribution must take place. In the clean crystal this distribution seems to be a slowly falling one on the wings (the dropping of the broadening in series 2a even slightly below the standard deviation line, if not an error, is surprising, but, in principle, not impossible). On the other hand, the distribution in the mixed crystal is of a relatively high γ value, as the relative FWHM values are best approximated with those of a uniform or symmetrical two-point distribution, and even exceeding the latter for the series 4b. Note that, in fact, the kind of inhomogeneity modification used here may well result in a multi-maximum amplificability distribution.

3.3. The diffusive mechanism

3.3.1. Counterevidences to the dispersive approach

In most of the doped solids studied so far and exhibiting ZPL-s, the dispersive model in general seems to be appropriate. However, we found one class of solids where it obviously fails, forcing us to think of alternative models (or expand the existing ones). These are the so-called Shpol'skii systems, mainly frozen n-alkanes, which are basically of crystalline nature but show many properties that are more similar to glasses or other disordered systems.

The n-alkanes were introduced into solid state spectroscopy by Shpol'skii [34–36] in the 1960s. They served as paradigms for demonstrating the fundamental features of low temperature optical spectra such as the existence of ZPL-s, phonon sidebands, lifetime limited linewidths etc. [37–39]. Because of their many peculiar features they have been studied in a large number of papers in various aspects, including pressure phenomena [13, 14, 40]. It has been observed [13, 14] that spectral holes in Shpol'skii systems exhibit an unexpectedly large pressure induced broadening which is comparable or even exceeds the respective values for glasses [7–11]. On the other hand, pressure broadening of the inhomogeneous width is moderate and of the same order of magnitude as for ordinary crystals.

Stimulated by these observations, we undertook an experimental study [22] of the *n*-hexane matrix both in the low pressure domain (up to 100 bar) for the pressure tuning measurements on spectral holes and in the high pressure domain (up to 2 kbar), where we studied the pressure dependence of the inhomogeneous line parameters. Again, we used dimethyl-s-tetrazine (DMST) as a probe. The results were compared with the corresponding data from the DMST doped ethanol : methanol glass (3 : 1, volume by volume) and durene crystal.

The experimental setup for the low pressure measurements as well as data processing procedures were similar to those described in subsection 3.2.6 (see [22] for details). Hole shift, broadening and area decrease with pressure were measured. Since a large dependence of the hole pressure behavior on the freezing pressure was observed, two different freezing pressures were used, namely 3 and 50 bar.

High-pressure fluorescence spectra measurements were carried out at 4.2 K in a high-pressure cell with three sapphire windows, placed in a He flow cryostat. Helium gas or solidified helium was used as a pressure transmitting medium. Pressure was created with a two-stage 10 kbar gas compressor. Fluorescence spectra were recorded with a DFS-24 0.8 m double spectrometer under a broadband excitation (Xe lamp + UV filters). The manometer reading from the second compressor stage (at room temperature) combined with the tabulated thermodynamic properties of ^{4}He at high pressures and low temperatures [41, 42] were used to obtain the final pressure at 4.2 K. In high-pressure experiments the freezing pressure was always 50 bar.

The general result is that the Shpol'skii system behaves quite differently when compared to other systems studied. Firstly, let us analyze the shift of holes with pressure. With the dispersive model it is plausible that the pressure shift in different solvents scales with the solvent shift. While in glassy and crystalline matrices this expectation is qualitatively fulfilled, the *n*-hexane with the freezing pressure of 3 bar shows no significant shift with pressure at all. At the same time, the sample frozen under 50 bar shows a shift 4 times larger than for durene (−1 GHz/bar and − 244 MHz/bar, correspondingly), yet the solvent shift for *n*-hexane is
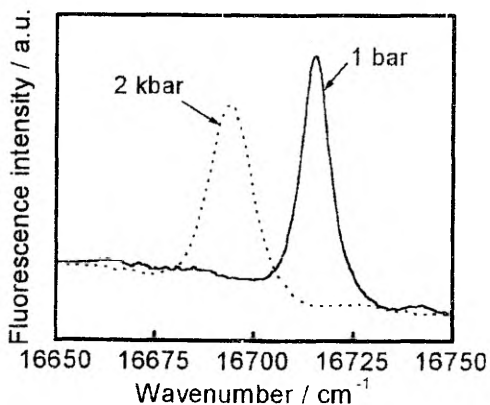

Figure 12. The 531 cm^{-1} vibronic replica in the emission spectra of DMST-doped *n*-hexane frozen under 50 bar. Spectra have been recorded under normal pressure (solid line) and 2 kbar (dotted line), the pressure shift is −310 MHz/bar. The broadening is only about 30 MHz/bar.
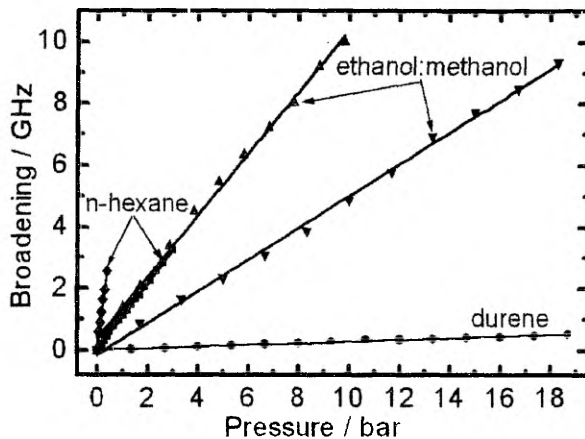
Figure 13. Pressure-induced hole broadening of DMST-doped *n*-hexane frozen at 3 bar (diamonds, slope of the least-squares linear fit 6.5 GHz/bar) and 50 bar (squares, 1.1 GHz/bar), ethanol : methanol glass frozen at 3 bar (up triangles, 1 GHz/bar) and 50 bar (down triangles, 520 MHz/bar), and durene crystal (circles, 27 MHz/bar). Figure kindly provided by the of co-authors of [22] who performed the actual measurements.

smaller. Another observation that does not agree well with the dispersive model is that the pressure shift of the inhomogeneous line and the hole burnt at its maximum do not coincide, the former being more than 3 times smaller, about -300 MHz/bar. This value is roughly reproduced also in the high-pressure experiments, up to a pressure value of 2 kbar (Fig. 12).

Another remarkable observation made is the strong hole area reduction with pressure in *n*-hexane, as compared to the reference systems. The area decreases more strongly in samples with low freezing pressure. In this case the area reduction was found to be not fully reversible. In contrast, in samples with high freezing pressure no residual area decrease was observed after pressure release.

The main difference between the Shpol'skii and other systems is seen from the broadening of the holes under pressure (Fig. 13). For *n*-hexane, frozen under low pressure, broadening is by a factor of 240 larger as compared to durene and by a factor of 6–7 larger as compared to the glass. If freezing is performed under 50 bar, broadening in *n*-hexane is still by a factor of two larger than the respective one in the glass and by a factor of 40 larger than in durene. At the same time we found the broadening of the inhomogeneous line under high pressure (2 kbar) to be relatively small, approximately 30 MHz/bar (Fig. 12). Clearly, the elastic properties of the *n*-hexane depend strongly on the level of freezing pressure. As seen from hole broadening data, this is, to some extent, also true for the glass.

The obtained results, especially the pressure-induced hole area reduction, cannot be explained within the framework of the dispersive mechanism. As

shown in [22], also the hole broadening is about three orders of magnitude too large for the dispersive case, given the inhomogeneous linewidth.

3.3.2. Definition of the diffusive model

Figuring out an alternative model, we are guided by the observations made in the previous section about the behavior of the holes with pressure, which, for short, were the following:

- comparatively large and partly irreversible hole area decrease;
- large hole broadening given the initial width and broadening of the inhomogeneous line;
- general strong freezing pressure dependence;
- no scaling of the hole shift with the solvent shift and the shift of the inhomogeneous line.

To account for these evidences, the defects that cause them must have some special degrees of freedom. It is probably most straightforward to assume that they are bistable and change their state reversibly at a critical external pressure, which is an internal parameter of the defect.

In addition, for the case treated in the previous section, there must be multistable defects to explain the irreversible hole area decrease. However, to get such a large hole area decrease anyway, one has to assume a correlation between defects and probe molecules, i.e. an increased density of defects in the neighborhood of probes. This would account for the large spectral shifts that reduce the area. Multistability of defects may then be a consequence of defect-defect interaction in this region. Although such a phenomenon is probably characteristic for many doped Shpol'skii matrices, we will not consider probe-defect correlation problems in the basic layout of the diffusive model and will take the spatial distribution of defects to be uniform.

Possible candidates for such defects in a Shpol'skii matrix are the lattice vacancies. They can easily hop from one lattice site to another since in an ideal lattice these sites are energetically equivalent. It is also plausible that during crystallization process the system lowers its energy by either attracting to or pushing away from dopant molecules the mobile vacancies. Either way, a zone with increased density of vacancies is created, either around the probe or at some distance. This explains qualitatively the effects connected with the probe-defect correlation.

Compared with the dispersive model, we abandon the assumption (ii) made in subsection 3.2.1 about the defect parameters depending continuously on the external pressure. Hence the expansion (3.1) is inapplicable and we cannot

speak of the pressure coefficients for individual homogeneous lines. Instead, they undergo a random spectral motion with changing pressure as the pressure-induced flips occur. In other words, we are dealing with spectral diffusion (hence also the name of the model), which is driven by pressure and, as such, has a reversible character. An analogous problem for the thermally induced spectral diffusion is treated in [43]. It still uses basically the same statistical method that we have used throughout this chapter – calculating the joint distribution functions. We will use it in the pressure case, too.

Since there are no pressure coefficients we are now limited to the pressure-dependent two-frequency joint distribution (3.4) only. It is generally not appropriate to use the joint distribution function of type (3.5) – even though it may be formally obtainable by the transformation (3.7). The pressure kernel (3.4) for the diffusive model can be generally written as follows:

$$\rho(\omega_1,\omega_2,\Delta p)=\frac{1}{(2\pi)^2}\iint \exp[i\omega_1 x_1 + i\omega_2 x_2 - J(x_1,x_2,\Delta p)]dx_1 dx_2 , \quad (3.92)$$

with J defined as:

$$J(x_1,x_2,\Delta p)= \int p_N(z)[1 - \exp(-i\varepsilon(z,0)x_1 - i\varepsilon(z,\Delta p)x_2)]dz . \quad (3.93)$$

Here the single-defect coordinate set z now also includes the external flipping pressure p_{flip} for the defect while $\varepsilon(z, \Delta p)$ has a discontinuous dependence on p_{flip}.

Next let us review some model calculations regarding the diffusive model.

3.3.3. Calculations on the diffusive model

We start with a simple model case that could be called the two-level diffusive model. It is not directly attributed to any specific process within the real systems; rather the idea of this model is to illustrate the general conclusions of the diffusive approach, with an advantage that it can be treated analytically. Still, as discussed above, it may model some physical processes as well.

The model goes as follows. Suppose we have within the host a sparse population of point defects similar to those described with the diaelastic model. The defects form two subsets with different strengths, C_1 and C_2, correspondingly. Let these subsets be of equal densities. Each of the defects can be attributed an external pressure value p_{flip}, at which it switches its strength from the initial value to the other (i.e. C_1 to C_2 and vice versa). This new value

is maintained at all pressures greater than p_{flip}. Since, as we assume, there is no correlation between a defect's initial strength and its flipping pressure, the two subsets of defects will remain in average equal at any pressure.

For calculations, we will adopt the same inverse cubic form of defect-probe interaction (3.55) as used for the diaelastic model. Then the interaction and coordinate distribution functions can be expressed as follows:

$$\varepsilon(z, \Delta p) = \left[C_1' Y\left(p_{flip} - \Delta p\right) + C_2' Y\left(\Delta p - p_{flip}\right) \right] \frac{\Phi(\theta, \varphi)}{r^3}, \qquad (3.94)$$

$$p_N(z) = \rho \frac{\rho_{flip}\left(p_{flip}\right)}{2} \left[\delta\left(C_1' - C_1\right)\delta\left(C_2' - C_2\right) + \delta\left(C_1' - C_2\right)\delta\left(C_2' - C_1\right) \right], (3.95)$$

where C_1' and C_2' denote the pre- and post-flipping strengths of a defect, correspondingly, Y is the unit step function and ρ_{flip} is the (unity-normalized) distribution function of the flipping pressures among the defects.

It is clear that, from this process only, no pressure broadening of the IDF as a whole can be obtained. Indeed, since the whole density of defects as well as partial densities of both defect subsets remain the same irrespective to pressure, there is nothing to influence the shape of the IDF. This also follows from (2.10), (2.12) giving – like in case of the diaelastic model – for the IDF a Lorentzian with the central position and width expressed as:

$$v_0 = a_I \rho \frac{C_1 + C_2}{2}, \qquad (3.96)$$

$$\Gamma_{ih} = a_R \rho \frac{|C_1| + |C_2|}{2}, \qquad (3.97)$$

where a_I and a_R are given by (3.67), (3.68). These expressions are pressure-independent. On the other hand, the flipping defects still cause a spectral motion of individual homogeneous lines, so one would expect some pressure dependence of the spectral holes.

To obtain the joint distribution function (3.92), (3.93), we once again change to the frequency coordinates originated at v_0 and normalized with Γ_{ih}:

$$\omega_i' = \left(\omega_i - v_0\right)/\Gamma_{ih}, \quad i = 1, 2 \qquad (3.98)$$

Then (3.92) can be rewritten as:

$$\rho(\omega_1', \omega_2', \Delta p) = \frac{1}{(2\pi \Gamma_{ih})^2} \iint \exp\left[i\omega_1' x_1 + i\omega_2' x_2 - S_2(\Delta p)|x_1 + x_2| - \right.$$
$$\left. - \frac{S_1(\Delta p)}{|C_1| + |C_2|}\left(|C_1 x_1 + C_2 x_2| + |C_2 x_1 + C_1 x_2|\right)\right] dx_1 dx_2 \qquad (3.99)$$

where

$$S_1(\Delta p) = \int_0^{\Delta p} \rho_{flip}(p)dp, \qquad (3.100)$$

$$S_2(\Delta p) = \int_{\Delta p}^{\infty} \rho_{flip}(p)dp = 1 - S_1(\Delta p) \qquad (3.101)$$

(see Fig. 15). We will express all our following results in terms of S_1 only.

The evaluation of integral (3.99) depends on the signs and mutual relations of C_1, C_2. In what follows, let us view the case $0 \le C_1 \le C_2$. Then we get for the joint distribution function:

$$\rho(\omega_1', \omega_2', \Delta p) = \frac{8c^3}{(\pi \Gamma_{ih})^2} \frac{S_1(\Delta p)}{\left[(\omega_2' - \omega_1')^2 + 4c^2 S_1(\Delta p)^2\right]} \times$$
$$\times \frac{\left[(\omega_2' - \omega_1')^2 + 4c^2\right]\left(1 + S_1(\Delta p)\right) + c^2(\omega_2' + \omega_1')^2\left(1 - S_1(\Delta p)\right)}{\left[(\omega_1'(c-1) + \omega_2'(c+1))^2 + 4c^2\right]\left[(\omega_1'(c+1) + \omega_2'(c-1))^2 + 4c^2\right]} \qquad (3.102)$$

where

$$c = \frac{C_2 - C_1}{C_2 + C_1}. \qquad (3.103)$$

Fig. 14 depicts the shape of the pressure diffusion kernel and its dependence on the initial burning frequency within the IDF and the pressure (represented by S_1). We see that in the center of the IDF the kernel is symmetrical and its shape is given by the ratio of two polynomials, yielding a $\omega_2'^{-4}$-type asymptotic behavior, similarly to the diaelastic model. The kernel width shows a saturative pressure dependence, as is to be expected (Fig. 16). If we assume that our typical pressures are small in the scale of the full range of the flipping pressures
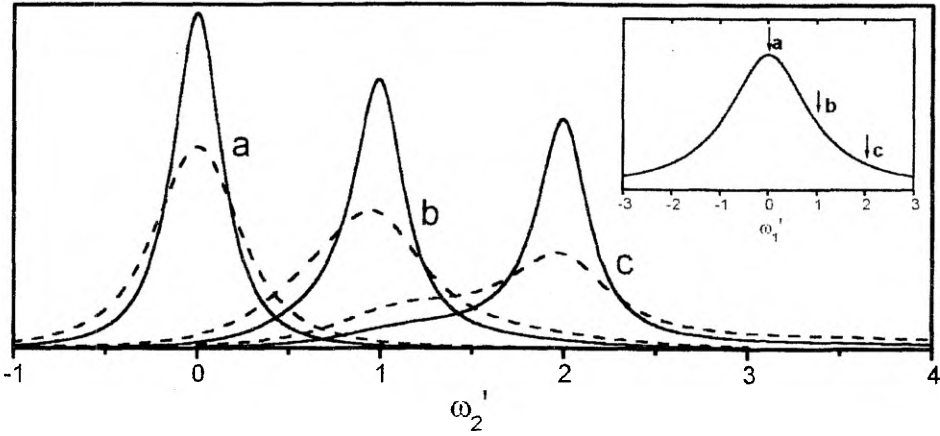
Figure 14. Pressure diffusion kernels for the two-level diffusive model with $c = 1/3$. The kernels are taken on three different positions on the IDF (see insert): $\omega_1' = 0$ (a), $\omega_1' = 1$ (b) and $\omega_1' = 2$ (c) and at two different pressure levels: $S_1(\Delta p) = 0.25$ (solid lines) and $S_1(\Delta p) = 0.5$ (dashed lines). All kernels are normalized to the same area.

of the defects, we probably hit with Δp an approximately uniform part of ρ_{flip} (see Fig. 15). Then the shape of $S_1(\Delta p)$ is close to linear. Combined with the S_1-dependence for the central kernel width, which is also near to linear for small pressures, it may well explain the observable linear pressure broadening.

The off-center shape of the diffusion kernel is generally asymmetric. This is reasonable if we bear in mind that the probes with a given initial frequency must be redistributed by pressure in such a manner as not to influence the overall inhomogeneous distribution, i.e. more towards the center than towards the wing. From a certain point the kernel also exhibits multiple maxima, more pronouncedly farther on the wings and at higher pressures.

These phenomena evidently express the counterpart of what we called the assimilation effect in the case of diaelastic model. We can clarify this again by making an approximation, justified far on the wings, that each probe is influenced by only a single defect, the one that
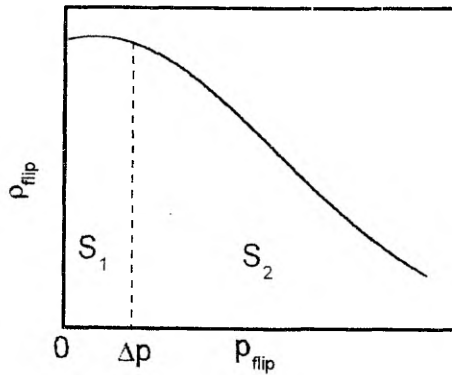

Figure 15. Schematic explanation of the definition of the quantities $S_1(\Delta p)$, $S_2(\Delta p)$ (see (3.100), (3.101)) on a hypothetic probability density curve $\rho_{flip}(p_{flip})$ for the defect flipping pressures. For small pressures ρ_{flip} is nearly uniform with pressure, yielding for S_1 a quasi-linear character.

55

is nearest (the single defect limit). Then, given the assumptions of this model, the probe population that is resonant with a fixed frequency ω', consists of two subsets – one where a defect with strength C_1 is situated at a distance r_1 and another with strength C_2 and distance r_2. Since $r_1 < r_2$, the latter subset is more numerous, as the surface of the sphere around the probe with the corresponding radius is larger and it is more probable for a defect to be located on it. When pressure is applied, the defects start to flip their strengths but the distances remain the same.

This way the resonant frequencies of the probes are transferred to two new values, according to the two subsets mentioned. A simple calculation shows that these two new frequency values are $C_1\omega'/C_2$ ($<\omega'$, larger subset) and $C_2\omega'/C_1$ ($>\omega'$, smaller subset). So at medium pressures and sufficient detunings from the center of the IDF the pressure kernel shape can have three maxima: the initial one near ω', decreasing with pressure, and two maxima near the abovementioned frequency values, increasing with pressure.

The situation is depicted in Fig. 17. In fact, the three Lorentzian-type factors in the denominator of (3.102) represent the discussed components.

At small detunings from the center, on the other hand, the expression of this effect is not prominent enough for new maxima to appear and one sees only kernel asymmetry and a small shift of its maximum. The microscopic mechanism of these phenomena is qualitatively the same; only the result is more blurred because of poor applicability of the single defect limit. This is also the only way of getting a pressure shift from this model; the shift is always towards the center and its maximum theoretical extent over the whole pressure range is from ω' to about $C_1\omega'/C_2$.
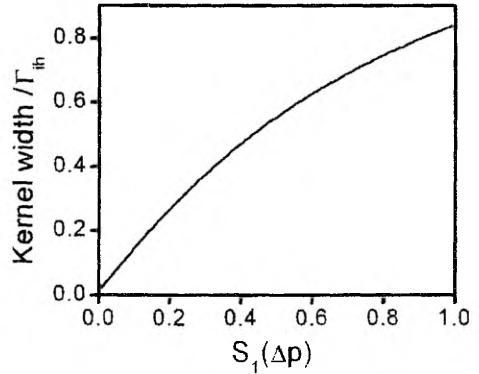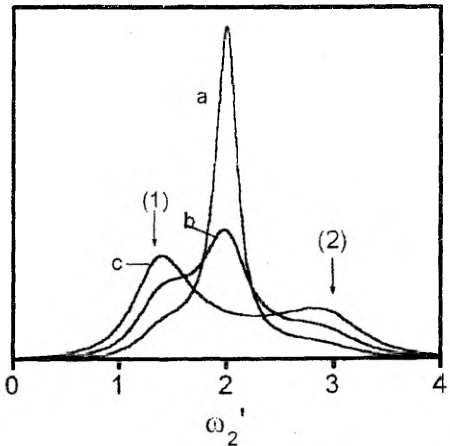

Figure 17. The pressure diffusion kernel for the two-level diffusive model taken at $\omega_1' = 2$ with $c = 0.2$ for three different pressure levels: $S_1 = 0.3$ (a), $S_1 = 0.6$ (b), and $S_1 = 1$ (c). Marked with arrows are the positions where the new maxima are to be expected in the single defect limit: $C_1\omega_1'/C_2 = 1.33$ (1) and $C_2\omega_1'/C_1 = 3$ (2).

56

To give the two-level model
a somewhat more realistic
interpretation, let us point to a
qualitative similarity of its results
with another possible model
situation that can be directly
related to the moving vacancy
case mentioned in the previous
subsection.

probe   **defect**

Figure 18. An illustration of the moving defect model for a single probe-defect pair. At a critical pressure p_{flip} the defect flips into a new position at a distance Δr towards an arbitrary direction represented by the angle β. Correspondingly, its distance from a nearby probe changes from r to r'.

The model is based on the
following assumptions: The
defects, their distribution and
interaction with probes are the
same as for the two-level model.
At a critical external pressure p_{flip} the defect flips to a new position located a
fixed distance Δr (same for all defects) away from its initial site, towards an
arbitrary direction (see Fig. 18). It is also assumed that Δr is small compared to
the mean distance between the defects. For moving vacancies, for example, Δr
could be the lattice constant. The flipping pressure is distributed among the
defects by ρ_{flip}, as before.

By an argument similar to that used with the two-level case we see that here,
too, the overall shape of the IDF is not altered as there is no change in the
density or average placement of defects with respect to probes as a result of
flipping.

This model differs from the two-level case by two aspects: Firstly, the
relative effect of the defect flipping on the probe transition frequency also
depends on the defect-probe distance and secondly, the defect-probe interaction
change upon flipping can have a value from a continuous range rather than just
two discrete values. However, for the central kernel the difference between the
two models should not be very remarkable. This follows from the fact that the
probes that contribute to the center of the IDF are influenced by a number of
defects located at nearly equal distances. Because of the averaging effect the
difference between the flipping natures should not play too much a role for the
central kernel. This is to be compared with the situation viewed with the
diaelastic model in subsection 3.2.4, where the central pressure coefficient
distributions for different effective amplificability distributions were
qualitatively similar.

A further similarity is that while the joint distribution function of pre- and
post-flipping frequencies for a fixed pre-flipping frequency in the two-level case
consisted of two δ-functions (located at $C_1\omega'/C_2$ and $C_2\omega'/C_1$), the same
distribution for the moving defect model has also two prominent peaks, namely
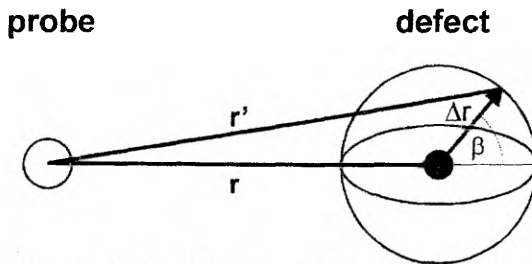two edge singularities, for a fixed defect-probe distance. These singularities

correspond to flipping directions $\beta = 0$ and $\beta = \pi$ (see Fig. 18). However, the picture is blurred by the fact that different defect-probe distances can yield the same transition frequency. But if the distribution of distances for a fixed frequency has a clear maximum, the resulting single-defect joint distribution function of pre- and post-flipping frequencies for a fixed pre-flipping frequency may still have two outstanding maxima. Hence the situation is rather similar to the two-level model.

3.4. A technique to study the pressure mechanisms

Previously, we have outlined the general properties of both dispersive and diffusive mechanisms of pressure behavior of spectral holes. The differences between them should, in principle, provide an opportunity to decide from experiments which mechanism is operative in each case. However, occasionally the expressions of these properties may be obscured for one or another reason or else, some of our assumptions made in interpreting them may be inappropriate.

The question about the operative pressure mechanism is still largely a question about the prevailing one since they can be, and most probably are, both active at the same time. For example, the moving defects as sources of the diffusive broadening can, apart from flipping, act diaelastically, thus accounting for the hole shift. Let us also recall that the spectral holes in ethanol-methanol glass showed some properties that could be attributed to the diffusive mechanism, like area decrease with pressure. It has been pointed out [44] that in glassy and amorphous solids internal buckling is an inherent ingredient of their structural stability.

To clarify the situation, one needs an experimental technique to address the basic foundations of each of the mechanisms. In this section we will propose such a procedure. It takes advantage of the fact that with dispersive mechanism each of the homogeneous lines has a distinct pressure coefficient while with diffusive mechanisms each line moves stochastically with pressure.

We will argue as follows: The two-frequency distribution $\rho(\omega_1, \omega_2, \Delta p)$, fixed on a reference pressure, undergoes a mechanism-specific transformation when the pressure is changed. The details of this transformation are not revealed on a simple pressure tuning experiment that only allows a comparison of initial and final states of the process. An idea to obtain more information could be to label an intermediate state e.g. by additional burning. With this in mind, we propose an experimental procedure consisting of following four steps (depicted graphically in Fig. 19):

1) a spectral hole is burnt with an irradiation dose Q at a frequency v_0 within the IDF;
2) an extra pressure Δp is applied to the system;
3) the sample is irradiated again with the same dose Q at the spectral position $v_0 + \Delta v_0$, where Δv_0 is the shift of the hole minimum due to the pressure;
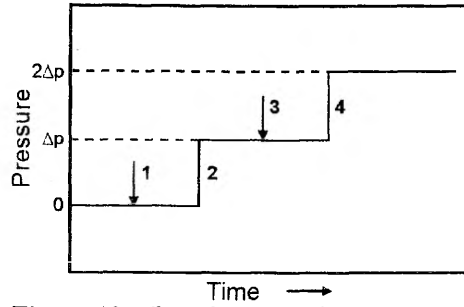4) the applied pressure is increased up to $2\Delta p$.

With this technique, as we will see in the following, the dispersive mechanism should produce a characteristic

Figure 19. The schematic of the proposed four-step process. Steps are denoted by numbers: 1 and 3 correspond to burning, 2 and 4 to applying the pressure. The pressure scale is relative to the pressure of the initial burning; the time scale is arbitrary.

double-minimum holeshape while with the diffusive mechanism the hole should retain a single minimum.

Let us view the situation analytically. Given the initial two-frequency distribution $\rho_0(\omega_1, \omega_2, \Delta p)$, its evolution through the steps 1–3 can be expressed for both mechanisms as follows:

$$\rho_1(\omega_1, \omega_2, \Delta p) = f_{hb}(\omega_1, v_0, Q)\rho_0(\omega_1, \omega_2, 0), \qquad (3.104)$$

$$\rho_2(\omega_1, \omega_2, \Delta p) = f_{hb}(\omega_1, v_0, Q)\rho_0(\omega_1, \omega_2, \Delta p), \qquad (3.105)$$

$$\rho_3(\omega_1, \omega_2, \Delta p) = f_{hb}(\omega_1, v_0, Q)f_{hb}(\omega_2, v_0 + \Delta v_0, Q)\rho_0(\omega_1, \omega_2, \Delta p), (3.106)$$

where f_{hb} is the hole-burning exposure function (2.33). To obtain actual hole shapes, these distributions need to be integrated over ω_1 and convoluted with the homogeneous spectrum.

The algorithm for finding the two-frequency distribution at step 4 should be "ρ_3 transformed by Δp taken at Δp", giving us the necessary pressure change $2\Delta p$ in total. Here we need to view both mechanisms separately. For the dispersive mechanism the required transformation is readily expressed by (3.8), yielding

$$\rho_4^{dsp}(\omega_1, \omega_2, \Delta p) =$$
$$= f_{hb}(\omega_1 - \Delta\omega, v_0, Q)f_{hb}(\omega_2 - \Delta\omega, v_0 + \Delta v_0, Q)\rho_0(\omega_1 - \Delta\omega, \omega_2 - \Delta\omega, \Delta p) , (3.107)$$

where $\Delta\omega = \omega_2 - \omega_1$.

To obtain a similar transformation expression for the diffusive mechanism, we make an assumption that the ensemble of homogeneous lines is homogeneous in terms of their individual pressure flipping probability distributions, both at any given frequency and at all frequencies within the range under consideration. Though, as shown in subsection 3.3.3, this is not necessarily strictly true, it is probably a reasonable assumption given the narrowness of the active frequency range compared to the width of the whole inhomogeneous distribution. Then the two-frequency distribution can be factorized:

$$\rho(\omega_1, \omega_2, \Delta p) = \rho_{ih}(\omega_1)\rho'(\Delta\omega, \Delta p). \qquad (3.108)$$

Under the assumption made, the ρ'-part will then remain unchanged at any base pressure, while the inhomogeneous part transforms on a pressure change Δp_0 into its convolution with the function $\rho'(\Delta\omega, \Delta p)$:

$$\rho_{ih}(\omega) \rightarrow \rho'_{ih}(\omega) = \int \rho_{ih}(\omega')\rho'(\omega - \omega', \Delta p_0)d\omega'. \qquad (3.109)$$

We thus get for the step 4 in the diffusive case:

$$\rho_4^{dif}(\omega_1, \omega_2, \Delta p) = f_{hb}(\omega_1, \nu_0 + \Delta\nu_0, Q)\rho'(\Delta\omega, \Delta p)\times$$
$$\times \int f_{hb}(\omega', \nu_0, Q)\rho_{ih}(\omega')\rho'(\omega_1 - \omega', \Delta p)d\omega' \qquad (3.110)$$

In order to carry out some numerical calculations, we have to specify the model to some extent. Firstly, let us adopt some further assumptions:

- By a similar argument as used to justify the factorization (3.108), we take the IDF to be constant within the frequency range of interest ($\rho_{ih}(\omega) = const$);
- Still by the same argument we expand the scope of factorization (3.108) to include the dispersive case as well;
- We assume a Lorentzian homogeneous line of width (FWHM) Γ_h;
- We take the burning position to be at the origin, $\nu_0 = 0$.

Now we only have to specify the function $\rho'(\Delta\omega, \Delta p)$. We choose it to be a single-maximum symmetric function of $\Delta\omega$, which is preferably peaked at zero. This enables us to discard the hole shift and set $\Delta\nu_0 = 0$. We stress that the results are not qualitatively sensitive to the particular shape of distribution. It would also be illustrative here to use the same function for both mechanisms. According to section 3.2, for the dispersive mechanism justified choices would be a Gaussian for glassy and polymeric systems or an inverse fourth-order

60

polynomial (e.g. the square of a Lorentzian) for crystalline matrices. For the diffusive case, however, we have to take into account that not all choices of $\rho'(\Delta\omega, \Delta p)$ are *a priori* possible. Since, as seen from (3.110), the application of pressure means convoluting the inhomogeneous structure with this function, it must be of such a form as to ensure the additivity of this process. The most straightforward way to achieve this is to choose a function that retains its shape when convoluted with itself. The simplest known functions to possess such a property are the Gaussian and Lorentzian curves. For a Gaussian, unlike the Lorentzian, the additive parameters on a convolution are not the widths but their squares, which means that we would have to define the Gaussian width to be proportional to the square root of the pressure to maintain additivity. But this, again, prohibits the simultaneous use of the same function for the dispersive case.

Following these considerations, we use a Lorentzian with a width $\Gamma_p\Delta p$:

$$\rho'(\Delta\omega, \Delta p) = \frac{2}{\pi} \frac{\Gamma_p \Delta p}{(\Gamma_p \Delta p)^2 + 4\Delta\omega^2} . \qquad (3.111)$$

In what follows, let us use dimensionless quantities for Q, v, ω, and Δp, by the following scaling

$$\left.\begin{array}{l} Q \to Q/\sigma\eta \\ v, \omega \to \Gamma_h v, \ \Gamma_h \omega \\ \Delta p \to (\Gamma_h/\Gamma_p)\Delta p \end{array}\right\} \qquad (3.112)$$

We also take into account that the widths of the Lorentzians add up on convolution, and normalize the spectra to unity at $Q = 0$. We can then write down the hole spectra for all four steps as follows (see $(3.104) - (3.107)$, (3.110)):

$$I_1(v) = \frac{1}{\pi} \int \frac{1}{1 + (2v - \omega)^2} \exp\left(-Q\frac{1}{1+\omega^2}\right) d\omega , \qquad (3.113)$$

$$I_2(v, \Delta p) = \frac{1}{\pi} \int \frac{1 + \Delta p}{(1 + \Delta p)^2 + (2v - \omega)^2} \exp\left(-Q\frac{1}{1+\omega^2}\right) d\omega , \qquad (3.114)$$

$$I_3(v, \Delta p) = \frac{1}{\pi^2} \iint \frac{1}{1 + (2v - \omega_2)^2} \frac{\Delta p}{\Delta p^2 + (\omega_2 - \omega_1)^2} \times$$
$$\times \exp\left(-Q\left[\frac{1}{1 + \omega_1^2} + \frac{1}{1 + \omega_2^2}\right]\right) d\omega_1 d\omega_2 \qquad , \qquad (3.115)$$

$$I_4^{dif}(v, \Delta p) = \frac{1}{\pi^2} \iint \frac{1 + \Delta p}{(1 + \Delta p)^2 + (2v - \omega_2)^2} \frac{\Delta p}{\Delta p^2 + (\omega_2 - \omega_1)^2} \times$$
$$\times \exp\left(-Q\left[\frac{1}{1 + \omega_1^2} + \frac{1}{1 + \omega_2^2}\right]\right) d\omega_1 d\omega_2 \qquad , \qquad (3.116)$$

$$I_4^{dsp}(v, \Delta p) = \frac{1}{\pi^2} \iint \frac{1}{1 + (2v - \omega_2)^2} \frac{\Delta p}{\Delta p^2 + (\omega_2 - \omega_1)^2} \times$$
$$\times \exp\left(-Q\left[\frac{1}{1 + (2\omega_1 - \omega_2)^2} + \frac{1}{1 + \omega_1^2}\right]\right) d\omega_1 d\omega_2 \qquad . \qquad (3.117)$$

Note again that all the spectra at steps 1 to 3 are identical for both mechanisms. This illustrates that from simple pressure tuning hole spectra it can be hard to decide which mechanism is operative. For step 4, however, the hole shapes for the both cases do not coincide. Moreover, for a certain parameter region (3.117) exhibits a double-minimum shape for the dispersive mechanism. At the same time it is clear that the repetitive convolution of the same symmetrical holeshape for the diffusive case could never yield such a structure. In Fig. 20 the situation is depicted for $Q = 5$ and $\Delta p = 20$.

Qualitatively, this double-minimum shape (Fig. 20(d)) can be explained as follows. The molecules that fill up the primary hole during the first application of pressure are those of medium "speed" whose initial position is far enough from the burning position so as not to get burned out during the first exposure, however, close enough to reach the hole at the pressure change of Δp. Those are the molecules that suffer most from the second burning. After the second increase of pressure they fill in some area near the burning position. For some parameter values it may now occur that the hole in this area gets deeper than at the burning position due to the shortage of molecules expected to fill this region. Contrasted to the diffusive mechanism (Fig. 20(e)) this reflects the existence of a certain memory: a particular probe "keeps in mind" its pressure coefficient for all the times. Note that this result also demonstrates capabilities of spectral hole burning as a specific type of nonlinear spectroscopy. No double-minimum shape
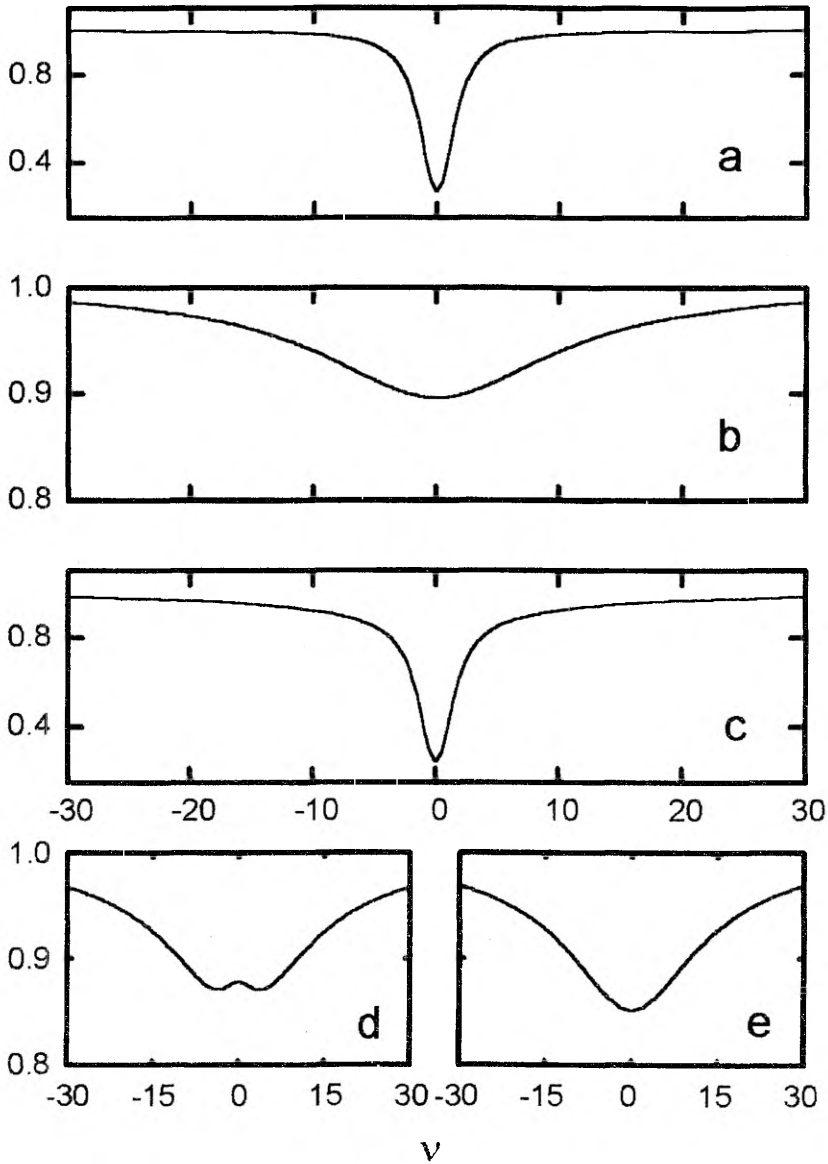
Figure 20. The calculated hole shapes for the four-step procedure for $\Delta p = 20$ and $Q = 5$. The spectrum after the first burning (a), after the subsequent application of pressure (b), after the second burning (c), and after the second application of pressure for dispersive and diffusive mechanisms (d and e, correspondingly) are depicted. For steps 1–3 the hole shapes for both types of pressure broadening mechanisms coincide. The frequency is in units of Γ_h, the intensity of the spectrum is normalized to its initial value. Note the different span of the intensity scale in (a, c) and (b, d, e).

is observable in the linear expansion of (3.117) by Q, it only arises if the higher-order terms are taken into account.

A note should be made on determining the actual parameter values from experiments. From the expansion (2.35) we get for the low dose values:

$$I_1(0) \approx 1 - Q/2, \qquad (3.118)$$

i.e. the dimensionless dose is directly related to the relative hole depth. To scale v back to the dimensional physical value one needs to know the homogeneous linewidth Γ_h. This can be determined from the low-dose holewidths, extrapolating them to the zero-dose limit $2\Gamma_h$. In order to scale Δp back to the real pressure one needs to know Γ_h and Γ_P. The latter is obtainable from the pressure broadening of spectral holes burnt in the linear regime (shallow holes). In other words, saying that $\Delta p = 20$ means using the pressure change which under linear conditions would broaden the hole by 10 widths, i.e. 11 times (keeping in mind that the low-dose holewidth is twice the homogeneous linewidth).

To analyze the magnitude of the hole-splitting effect, let us view the depth of the minimums with respect to the central maximum, i.e. the quantity $I_4^{dsp}(0) - I_4^{dsp}(v_{min})$, where $\pm v_{min}$ are the frequencies corresponding to the minima of the split hole. We will also use here the pressure kernel shapes obtained in section 3.2, namely the Gaussian kernel

$$\rho_G'(\Delta\omega, \Delta p) = \frac{2\sqrt{\ln 2}}{\Gamma_p \Delta p \sqrt{\pi}} \exp\left(-\frac{4\ln 2 \Delta\omega^2}{\Gamma_p^2 \Delta p^2} \right), \qquad (3.119)$$

applicable for glassy and polymeric matrices and the squared Lorentzian

$$\rho_{dia}'(\Delta\omega, \Delta p) = \frac{4\sqrt{\sqrt{2}-1}}{\pi} \frac{\left(\Gamma_p \Delta p\right)^3}{\left(\left(\Gamma_p \Delta p\right)^2 + 4\left(\sqrt{2}-1\right)\Delta\omega^2\right)^2} \qquad (3.120)$$

to account for the situation in the IDF center in crystalline systems according to the diaelastic model. Both of the above distribution functions are normalized to unity and given in a representation that explicitly contains the FWHM $\Gamma_p \Delta p$.

It appears that for every given Δp there exists a dose Q for which the depth of the side holes is maximal. However, for Δp less than about 7 the effect seems to vanish. On the other hand, the maximal obtainable depth increases with Δp, though sublinearly. Simultaneously, the dose needed for the optimal depth increases rapidly with Δp. The position of the optimal minimums (spectral

distance from the burning frequency) also shows a tendency of increasing with Δp. The situation is depicted in Fig. 21. A reasonable choice in crystals would be $\Delta p = 20 - 25$ in which case the maximum depth of the side holes $I_4(0)$-$I_4(\nu_{min})$ would be of about 1/100 from the maximum hole depth.

Keeping this in mind, let us consider the prospects for observation of the discussed effects in real systems. A very convenient way to create tunable pressures is to use helium gas as a pressure-transmitting medium [10, 14]. On the other hand, this confines the maximal obtainable pressure to about 140 bar at 4.2 K, because of the helium solidification. This means, with (3.114), that a ratio ≈ 0.3 bar^{-1} is needed to reach a 1%-effect in a crystalline system (we need to raise the pressure up to $2\Delta p$). For chlorin-doped bensophenone in the crystalline phase [11], this ratio is $0.045 - 0.24$ bar^{-1} depending on the site. This limits the maximum observable effect to 0.8%. This is quite a small value, yet within the reach of careful experiments. From our experiments with DMST-doped durene, described in subsection 3.2.6, a similar value of Γ_P/Γ_h, $0.15 - 0.24$ bar^{-1}, can be estimated for neat samples, depending on the position within the IDF. For mixed samples, i.e. those with enhanced inhomogeneity, the value was somewhat higher, $0.25 - 0.36$ bar^{-1}. This shows that samples with higher defect concentration, expected to exhibit higher absolute values of pressure broadening, are favored for observing the hole-splitting effect. As to the observation of the diffusive mechanism, the above-discussed Shpol'skii systems seem to provide a good opportunity, since values of Γ_P/Γ_h as high as 1.1 bar^{-1} for chlorin-doped n-octane [14] and more than 10 bar^{-1} in dimethyl-s-tetrazine doped n-hexane should favor an observation of the hole splitting or, *vice versa*, to prove its absence and thus verify the proposed diffusive mechanism.

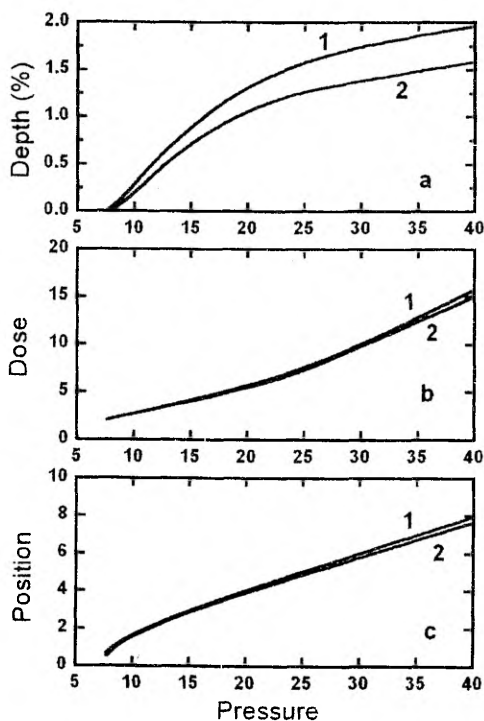As discussed earlier, glasses are quite an intriguing class of materials for the proposed experiments. In

Figure 21. The maximum relative depth of the side minima (a), the optimized dimensionless dose Q to reach this value (b), and the minimum position (c) depending on the dimensionless pressure Δp. Numbers indicate the used pressure kernel type: (1) – the Gaussian kernel (3.119), (2) – the diaelastic kernel (3.120).

glasses the values of Γ_h at 4.2 K are much higher than the corresponding values in crystals with the excited state lifetimes of dopants about or more than 1 ns. High absolute values of pressure broadening, however, yield ratios Γ_P/Γ_h not much different from the molecular crystals, e.g., 0.2 bar^{-1} for chlorin-doped benzophenone in the glassy phase [11]. On the other hand, as can be read from Fig. 21, the dimensionless pressure needed to obtain the same depth of the side minima is lower for the Gaussian kernel (only about $\Delta p = 15 - 20$ for 1%).

In conclusion, the described technique demonstrates the capabilities of spectral hole burning as a specific type of non-linear spectroscopy to explore the pressure-induced processes in various types of solids. Following the proposed lines of thinking, it may well be possible to devise experimental techniques yielding more prominent effects.

4. PRESSURE EFFECTS IN INCOMMENSURATE SYSTEMS

4.1. General considerations

In this section we will discuss some general issues regarding the pressure effects on the impurity spectra in systems where the inhomogeneous effects are caused prevalently by the incommensurate modulation.

There are two main parameters of the modulation wave that mediate the probe-host interaction: amplitude and phase. Both of them can be influenced by the external pressure. Unless a phase transition is involved, the effect on amplitude is expected to be continuous. Hence the pressure phenomena should be governed by the dispersive mechanism, with the distribution of relative amplitude pressure derivatives as the driving force.

The situation with the phase is somewhat different. If all the modulation waves are moving (unpinned), application of low pressure far from the phase boundary will not induce any changes concerning the modulation phase. In that case, the phase at a probe location is continuously changing and the whole inhomogeneous picture can be viewed only dynamically. However, in real systems at low temperatures we can expect a substantial amount of modulation waves to be pinned. Then it is possible that external pressure can add as much energy to the system as to unpin the wave which will then either be free or pinned again in another position. Such a process can even be reversible to some extent. As we can see, it constitutes a pressure mechanism of diffusive type.

The phase-related processes governed by the dispersive mechanism can also be possible, for example via modification of the modulation wavelength by pressure. Note that such a modification will not alter the overall IDF, but individual probes still undergo certain changes in their transition frequencies.

From the IDF viewpoint, the pressure thus primarily compresses (or expands) the whole spectral structure bounded by the edge singularities due to the amplitude modification, while the limited phase modifications do not contribute to the overall picture.

As follows from the above discussion, for persistent hole burning to become possible, the incommensurate modulation waves must be mostly pinned to avoid extensive spectral diffusion. In pressure tuning experiments, both dispersive and diffusive mechanisms may be active. The pressure cycling experiments may show irreversible hole area decrease.

4.2. Pressure effects in incommensurate biphenyl

To get a better understanding of the dynamics and structure of incommensurate solids, we have performed some experimental pressure studies on chlorin-doped biphenyl [45]. In most systems exhibiting incommensurate behavior, the incommensurate phase exists in a narrow temperature interval between higher-temperature commensurate phase and a low-temperature lock-in phase, commensurate with a generally larger unit cell. Incommensurate biphenyl is one of a few systems where such a lock-in transition has not been observed down to very low temperatures (60 mK [46]). Therefore one can use hole-burning methods, including pressure tuning, to investigate this substance.

Biphenyl (diphenyl, phenylbenzene) $C_6H_5C_6H_5$ is a crystalline nonpolar aromatic molecular compound. The molecule of biphenyl consists of two phenyl groups connected by a single C–C bond. Due to the strong pairwise interaction between the central four *ortho* hydrogen atoms (electrostatic repulsion between two closest H atoms on both sides of the C–C bond), isolated molecules of biphenyl in the gas phase are nonplanar, the twist angle between the planes of two phenyl rings being as great as about 42° (see, e.g., [47]). In the solid state of biphenyl this angle is much smaller or even zero, depending on the crystalline phase existing at a given temperature and pressure. The transitions between phases and dynamics in different phases have been studied by various methods, including Raman scattering [48], NMR [49] and EPR [28] techniques.

At ambient pressure and temperatures between 40 K and the melting point of biphenyl (~70°C), it is found in a normal, commensurate phase (high-temperature phase C I). In this phase biphenyl crystals have a monoclinic structure with space group $P2_1/a$ and two molecules in the unit cell. Owing to a strong enough interaction between adjacent biphenyl molecules in the solid state, the equilibrium configuration of all molecules is on the average planar, as was shown by X-ray diffraction [50], but the two phenyl rings in every molecule perform large torsional (twisting) motions relative to each other out of this equilibrium plane.

When the temperature is lowered, a phonon mode related to the twist motion becomes soft and freezes in around 40 K, causing a second-order phase transition to the doubly incommensurate structure (phase IC II), characterized by two different incommensurate wave vectors of the frozen-in modulation (see, e.g., [49]). Here the twist angle in each molecule varies sinusoidally throughout the whole crystal volume. The maximal twist angle 2θ between two phenyl rings in a molecule is strongly temperature-dependent, being about zero at 40 K and increasing up to the value $2\theta \approx 10°$ around 17 K [49]. In fact, the maximal twist angle 2θ can be treated as the order parameter for this transition. At 17 K a partial lock-in transition to another incommensurate structure (phase IC III)

takes place, characterized by a single frozen-in modulation wave vector. This phase transition IC II → IC III was found to be of the first order [51].

The phase transition temperatures T_{I-II} and T_{II-III} rapidly decrease with increasing hydrostatic pressure [48]. In Fig. 22 the known data points of ordinary biphenyl are reproduced, as well as the much more numerous points for its deuterated counterpart $C_6D_5C_6D_5$, which is easier to study, especially in neutron scattering experiments. The figure is redrawn from [48] with the melting / solidification line of helium slightly corrected, based on the paper [42].
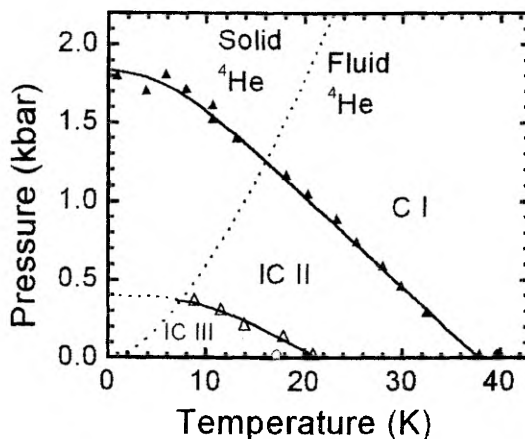
Figure 22. The phase diagram of biphenyl (redrawn from [48]). Filled triangles indicate the experimental points from the C I – IC II and empty triangles from the IC II – IC III phase boundaries for the deuterated biphenyl. Circles (filled and empty) show the phase transition temperatures for the hydrogenated biphenyl at ambient pressure. The helium solidification line (dotted line) is given according to [42].

As seen from Fig. 22, the C I – IC II phase transition line for deuterated biphenyl terminates at $p \approx 1.85$ kbar in the low-temperature limit. As to the hydrogenated compound, the value might be close or a little higher if we consider that also the phase transition temperature at ambient pressure is higher in the hydrogenated case. However, different experimenters have reported slightly different values (see [45] for a review). For example, in [52] it is found that the transition pressure at $T \rightarrow 0$ K is lower for the hydrogenated than for the deuterated biphenyl, the values being 1.5 kbar and 1.35 kbar, correspondingly. The same pressure values for the IC II – IC III transition are found to be 400 and 200 bar [53]. In the absence of new, more reliable data, let us adopt in this study for our purposes the following pressure values at $T \rightarrow 0$ K: $p \approx 1.8$ kbar for the C I – IC II phase transition and $p \approx 200$ bar for the IC II – IC III phase transition in hydrogenated biphenyl.

An organic dye chlorin (7,8-dihydroporphin) was used as a dopant in this study. The quantities measured were pressure tuning data in the low pressure range (up to 22 bar) and fluorescence and excitation spectra in the high pressure range (up to 2.7 kbar). The experimental details for the sample preparation and pressure tuning measurements were very similar to those described in the subsection 3.2.6. The power density at the sample was about 100 μW/cm^2 for hole burning, for recording it was reduced by a factor of 50. The high-pressure

fluorescence measurements were described in subsection 3.3.1, for measuring excitation spectra the sample was excited through a MDR-6 monochromator.

Let us first examine the structures in the inhomogeneously broadened spectra. The fluorescence and excitation spectra of chlorin impurity in biphenyl at $T = 4.2$ K are presented in Fig. 23 for ambient pressure (spectra (a) and (b)) and high pressures of 2.6 and 2.7 kbar (spectra (c) and (d), respectively). The ambient-pressure spectrum, belonging to the incommensurate phase IC III of biphenyl, contains a triplet of resonant lines (peak 1 at 15829, peak 2 at 15849 and peak 3 at 15861 cm^{-1}) observed at the same positions in both emission and excitation spectra.

Firstly, the question arises whether the observable triplet structure arises from the probe interaction with the incommensurate
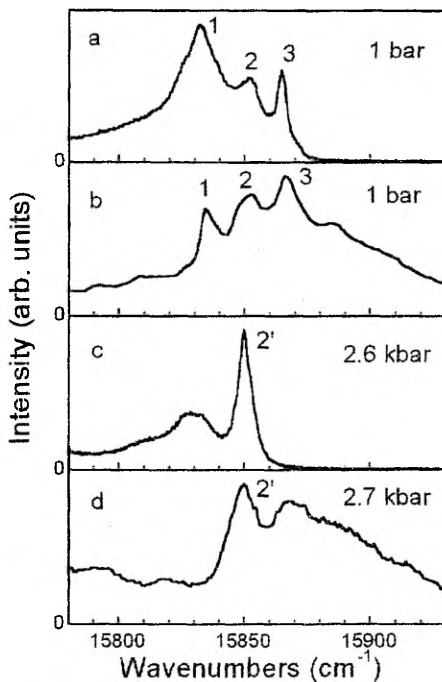

Figure 23. Fluorescence emission (a, c) and excitation (b, d) spectra of chlorin impurity molecules in biphenyl at $T = 4.2$ K under ambient pressure (a, b), at 2.6 kbar (c) and 2.7 kbar (d).

modulation wave or does it correspond to different substitutional sites? Here the fact that the high-pressure spectra of the C I commensurate phase show a single resonant line gives a strong support to the idea that there exists only one major substitutional site for chlorin in the commensurate lattice and that the ambient-pressure splitting arises from incommensuracy. Further evidence is that the solvent shift for the chlorin triplet is rather small (the vacuum frequency for chlorin is 15912 cm^{-1} [54]). Consequently, even though chlorin molecules are significantly larger than biphenyl molecules, they are relatively undisturbed in the biphenyl matrix. This, in turn, justifies the suggestion that the incommensurate structure of bulk biphenyl is probably not too strongly disturbed by chlorin probe molecules and therefore this structure may manifest itself in the probe spectra.

If so, further questions arise as to the nature of the triplet shape. As discussed in section 2.3, a simple sinusoidal modulation should give rise to *two* edge singularities, i.e. to a doublet. And indeed, such a doublet has been observed in ^{2}H NMR experiments for deuterated biphenyl in both IC II and IC III phases [49].

70

This circumstance seems to rule out the possibility that the triplet shape is caused by the modulation in the multi-soliton limit. Instead, one should consider probe-dependent features. We note that a non-monotonous or strongly non-linear dependence of the electronic transition frequency of the probe molecule on the twist angle θ is rather unlikely because of the small amplitude of θ variation (2θ does not exceed $10°$ [49]). To our opinion, the most probable explanation is the pinning of the modulation wave by the probe molecules (see section 2.3). That would mean such a positioning of modulation waves that the probe molecules are more favorably located near the planar biphenyl molecules.

Figure 24. Fluorescence spectra of chlorin molecules in biphenyl recorded at $T = 4.2$ K and various pressures indicated.

The measured high-pressure fluorescence spectra (Fig. 24) show clearly the transformation from the triplet (incommensurate) to singlet (commensurate) shape which takes place at around 1.8 kbar. The resulting resonant line (Fig. 24(c) and (d), peak 2') is peaked at about 15850 cm^{-1} and originates, as we think, from peaks 1 and 3 in the lower-pressure incommensurate phases. A broader feature at about 20 cm^{-1} to lower frequencies is the phonon sideband (see also Fig. 23(c) and (d) where the same phonon sideband is observed in the emission and excitation spectra, respectively).

It is interesting that the pressure dependence of the spectral splitting Δv between peaks 1 and 3 (Fig. 25) turns out to be close to the well-known nonlinear critical character

$$\Delta v(p) = \Delta v_0 \left(1 - p/p_{tr}\right)^n, \qquad (4.1)$$

where Δv_0 is the splitting at ambient pressure, n is the critical exponent and p_{tr} is the IC II – C I phase transition frequency, which equals to about 1.8 kbar. When fitting the experimental data from the high-pressure spectra to the theoretical curve (4.1), one obtains the value $n = 0.39$. Quite intriguing here is the fact that very close values for the critical exponent, characterizing the same phase transition, were obtained in the NMR [49] and EPR [28] studies in the
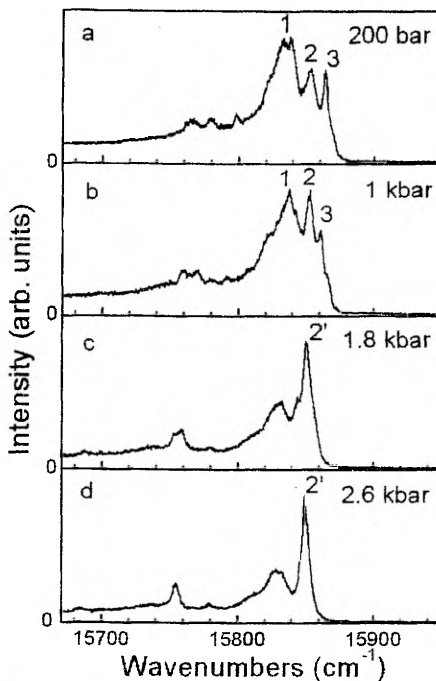
71

temperature domain ($n = 0.35 \pm 0.03$ and $n = 0.4$, respectively). The critical behavior of the maximal twist angle 2θ (treated as the order parameter) in incommensurate biphenyl, clearly established by means of NMR spectroscopy [49], may be regarded as the most decisive evidence that the chlorin spectrum in phases IC II and IC III is governed by the incommensurate modulation and that the observed splitting $\Delta \nu$ is proportional to the magnitude of the maximal 2θ value varying with pressure.

Figure 25. Pressure dependence of the distance (spectral splitting) $\Delta \nu$ between lines 1 and 3 in the emission spectrum of chlorin-doped biphenyl at $T = 4.2$ K. Circles show the experimental points; solid curve indicates the nonlinear least-squares fit to the data points according to (4.1). Dashed line illustrates the linear extrapolation using the low-pressure spectral hole shift data for lines 1 and 3.

In the spectra of Fig. 24 a weaker feature at somewhat lower energies from the main lines 1-3 (in the region of about 15760–15780 cm^{-1}) can be seen, showing in the incommensurate phases a doublet structure with a decreasing splitting under growing pressure and converting to a singlet in the commensurate phase. We attribute these lines tentatively to another substitutional site of chlorin. It also exhibits an incommensurate splitting and behaves qualitatively in a similar manner as the main site (peaks 1-3). A markedly smaller splitting points to a weaker interaction with the modulation wave. This, on the other hand, may be the reason why this wave is more weakly pinned by the probe molecules in this site and the corresponding spectrum exhibits a "classical" doublet structure, thus giving some additional support to the idea of the pinning as a possible mechanism of the main triplet formation.

Next we will analyze the results of the pressure tuning experiments (see also [55]). Here the most surprising observation is a positive (to higher frequencies, blue) shift detected for holes burned in peak 1 (15829 cm^{-1}), i.e. for the line most to the red, in contrast to negative or red shifts of holes burned in more blue peaks 2 and 3. The pressure coefficients for these three lines turned out to be rather diverse: +271 MHz/bar (+9.0 cm^{-1}/kbar) for peak 1, –94 MHz/bar (–3.1 cm^{-1}/kbar) for peak 2 and –174 MHz/bar (–5.8 cm^{-1}/kbar) for peak 3.

As discussed in section 3.2, it is generally plausible from the viewpoint of dispersive pressure models that the pressure shift of spectral holes is at least qualitatively an extension of the solvent shift. This has also been the case in experimental studies (e.g. [7–11]). In a few cases also the positive hole shift with pressure has been observed [56], but then in systems where the probe
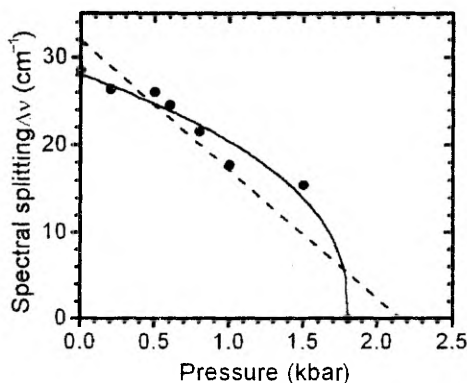
72

molecules exhibit an unusual positive solvent shift. Note that in biphenyl the peak 1 with the positive holeshift is the one with the most negative solvent shift.

Similarly to the above high-pressure results, the situation can be explained by the modification of the amplitude of the incommensurate modulation wave by the pressure. This process takes precedence over the pressure dependence of other probe-host interaction mechanisms that are responsible for most of the solvent shift. As an additional support to this idea we note that if one makes a linear extrapolation of the shifts of spectral holes burned in peaks 1 and 3 from the used low-pressure range to much higher pressures, the corresponding lines should merge at 15848 cm^{-1} under a pressure of 2.16 kbar. The latter value is close to the pressure of phase transition between high-pressure commensurate C I and the intermediate incommensurate IC II phases.

In [55] also the hole broadening and pressure cycling data are considered. A significant observation is a certain (up to 50%) reversible hole area decrease with pressure. This could signal the presence of the diffusive-type pressure mechanisms associated with unpinning-repinning of the modulation wave, as discussed in the previous section. This argumentation is supported by the results of temperature cycling experiments [57], which prove that in biphenyl there exists a presumably similar light- and temperature-driven mechanism of interconversion between the lines 1–3.

The broadening for the holes burnt in peaks 1 and 3 lies generally in the range typical for crystals (32 MHz/bar for peak 1), but is somewhat higher in peak 2 (74 MHz/bar). This could also be viewed as a support for the discussed pressure mechanism: If we relate the hole broadening to small pressure induced shifts of the modulation wave then its magnitude scales with $|dv/dx| \approx |d\theta/dx|$, which is highest in the central region.

APPENDIX I. The relations between the moments of the effective amplificability distribution and the pressure kernel for the diaelastic model

We use an easily obtainable general relation between the moments of a function $f(\alpha)$ and the derivatives of its Fourier transform $F(x)$:

$$\int \alpha^n f(\alpha) d\omega = \frac{F^{(n)}(0)}{(-i)^n},$$
(AI.1)

where the transform conventions are the same as used throughout the thesis. The mean α value $\overline{\alpha}$ and its variance σ_α are given by:

$$\overline{\alpha} = \frac{iF'(0)}{F(0)},$$
(AI.2)

$$\sigma_\alpha^2 = -\frac{F''(0)}{F(0)} + \left(\frac{F'(0)}{F(0)}\right)^2.$$
(AI.3)

Let us calculate the mean α value and its variance from the diaelastic pressure kernel $\rho_\alpha(\omega, \alpha)$ in case of a general amplificability distribution $p_1^{eff}(\kappa)$ (see (3.74), (3.75)):

$$\rho_\alpha(\omega,\alpha) = \frac{1}{(2\pi\Gamma_0)^2} \iint \exp\left(i\omega x_1 + i\alpha x_2 - \int p_1^{eff}(\kappa)|x_1 + \kappa x_2| d\kappa\right) dx_1 dx_2 .$$
(AI.4)

Hence the necessary Fourier transform of the function under question is:

$$F(x_2) = \frac{1}{2\pi\Gamma_0^2} \int \exp\left(i\omega x_1 - \int p_1^{eff}(\kappa)|x_1 + \kappa x_2| d\kappa\right) dx_1 .$$
(AI.5)

First we calculate the derivatives of the x_2-dependent part of this:

$$\frac{\partial}{\partial x_2} \exp(-\int p_1^{eff}(\kappa)|x_1 + \kappa x_2|d\kappa) =$$
$$= \exp(-\int p_1^{eff}(\kappa)|x_1 + \kappa x_2|d\kappa)\left(-\int \kappa \, p_1^{eff}(\kappa)\mathrm{sgn}(x_1 + \kappa x_2)d\kappa\right) \quad , \quad (AI.6)$$

$$\frac{\partial^2}{\partial x_2^2} \exp(-\int p_1^{eff}(\kappa)|x_1 + \kappa x_2|d\kappa) =$$
$$= \exp(-\int p_1^{eff}(\kappa)|x_1 + \kappa x_2|d\kappa)\left[-2\int \kappa^2 \, p_1^{eff}(\kappa)\delta(x_1 + \kappa x_2)d\kappa + \quad (AI.7) \right.$$
$$\left. + \left(\int \kappa \, p_1^{eff}(\kappa)\mathrm{sgn}(x_1 + \kappa x_2)d\kappa\right)^2\right]$$

Here we have taken into account that

$$\frac{d|x|}{dx} = \mathrm{sgn}(x), \quad\quad (AI.8)$$

$$\frac{d\,\mathrm{sgn}(x)}{dx} = 2\delta(x). \quad\quad (AI.9)$$

Now we can also evaluate the quantities required for (AI.2), (AI.3):

$$F(0) = \frac{1}{2\pi\Gamma_0^2}\int \exp(i\omega x_1 - |x_1|)dx_1 = \frac{1}{\pi\Gamma_0^2}\frac{1}{1+\omega^2} = \rho_{ih}(\omega), \quad (AI.10)$$

$$F'(0) = -\frac{1}{2\pi\Gamma_0^2}\int \kappa \, p_1^{eff}(\kappa)d\kappa \int \mathrm{sgn}(x_1)\exp(i\omega x_1 - |x_1|)dx_1 =$$
$$= -i\bar{\kappa}\omega\rho_{ih}(\omega) \quad\quad , \quad (AI.11)$$

$$F''(0) = \frac{1}{2\pi\Gamma_0^2}\int \exp(i\omega x_1 - |x_1|)\left[-2\delta(x_1)\int \kappa^2 p_1^{eff}(\kappa)d\kappa + \bar{\kappa}^2\right]dx_1 =$$
$$= -\frac{\overline{\kappa^2}}{\pi\Gamma_0^2} + \bar{\kappa}^2\rho_{ih}(\omega) \quad\quad . \quad (AI.12)$$

Here we have used the fact that the amplificability distribution is unity-normalized. It is also assumed that the required moments can be calculated for

75

this distribution, i.e., the corresponding integrals converge. The function $\rho_{ih}(\omega)$ in the above expressions represents the IDF, normalized to Γ_0^{-1}.

Substituting these results into (AI.2), (AI.3), we get:

$$\overline{\alpha} = \omega\overline{\kappa}\,, \tag{AI.13}$$

$$\sigma_\alpha^2 = \left(\overline{\kappa^2}\left(1+\omega^2\right)-\overline{\kappa}^2\right)-\overline{\kappa}^2\omega^2 = \left(\overline{\kappa^2}-\overline{\kappa}^2\right)\left(1+\omega^2\right)= \sigma_\kappa^2\left(1+\omega^2\right), \tag{AI.14}$$

which are the required relations.

MAIN ARGUMENTS PROPOSED

1. General statistical theory for the dispersive mechanism of spectral pressure behavior caused by defects in solids is developed. Within the dispersive mechanism, the defect coordinates determining its perturbation level to the active transition of the probe are considered to be continuous with pressure, hence under low pressures the homogeneous lines originating from each of the probes move linearly with pressure and have a distinct pressure coefficient.

2. The general theory is specified for the case of point defects (elastic inclusions) as the perturbers creating within the crystal a stress field that is modified by the external pressure (the diaelastic model). To enable for the hole broadening in pressure tuning experiments, certain heterogeneity in the elastic parameters of the defects is assumed. The influence of the corresponding distribution among the defects is analyzed based on a few simple examples. Some experimental findings about the diaelastic model are presented.

3. A different, diffusive pressure mechanism is introduced to explain the inadequately large pressure broadening of spectral holes observed in Shpol'skii matrices which, as is shown, cannot be related to the dispersive mechanisms. The diffusive mechanism involves discontinuities in the pressure dependence of some of the defects' coordinates (pressure-induced flips). An example of such a defect would be a bi- (or multi-) stable moving vacancy within the matrix structure that changes its state at a critical external pressure. Some novel model situations are constructed and analyzed to study the basic properties of the diffusive mechanism.

4. An experimental technique is proposed for distinguishing between the cases where dispersive or diffusive mechanism prevails in determining the hole broadening. The technique consists of four steps, two burnings and two pressure changes. As a result, with favorable experimental parameters, hole splitting should be observable in the dispersive case, caused by the fundamental properties of this mechanism. However, the reachable effect is predicted to be rather small for studied matrix-probe systems. Some results of parameter optimization are also presented.

5. Pressure effects in the spectra of incommensurate solids are analyzed. In these solids, due to a frozen-in vibration mode, some lattice parameter is spatially modulated with a period incommensurate with the underlying crystal

lattice periodicity. The specific case of chlorin-doped biphenyl is viewed on an experimental basis. It is argued that in this system, originating from the incommensuracy, both dispersive- and diffusive-type pressure mechanisms are operative, the former acting on the amplitude of the modulation and the latter on its phase via unpinning-repinning of the modulation wave.

KOKKUVÕTE

Rõhuefektid tahkiste mittehomogeensetes lisandispektrites

Käesoleva töö põhiliseks eesmärgiks on seatud refereerida olemasolevaid teadmisi tahkiste lisandispektrites mitteisobaarilistes eksperimentides ilmnevate rõhuefektide osas madala hüdrostaatilise rõhu piirjuhul; samuti lisada mõningad omapoolsed mudelid ja analüüsida neid. Arutluste lähtepunktiks on üldine statistiline teooria, mis vaatleb mittehomogeensuse põhjustajana aines hulka ruumiliselt hajutatud häiritusallikaid (defekte). Tulemused on orienteeritud eelkõige sellistele eksperimenditehnikatele nagu mittehomogeense jaotusfunktsiooni rõhusõltuvuse uurimine ja spektraalsälkude rõhktüürimine.

Töös on eristatud on kahte põhimõttelist spektrite rõhulise käitumise mehhanismi: dispersiivne ja difusiivne. Dispersiivse mehhanismi korral sõltuvad defektide koordinaadid, mis määravad tema poolt lisanditsentri aktiivsele elektroonsele üleminekule põhjustatud häirituse, rõhust pidevalt. Seetõttu on madalal rõhul üksikutest tsentritest pärinevate homogeensete joonte spektraalne liikumine rõhu suhtes lineaarne ja igal neist on fikseeritud rõhukoefitsient. On näidatud, et enamus seni antud teemal koostatud nii teoreetilistest kui eksperimentaalsetest töödest käsitlevad just dispersiivse mehhanismi juhtumeid. Olukorra kirjeldamiseks kristallides on välja pakutud nn. diaelastne mudel. See vaatleb häiritusallikatena punktdefekte, mis tekitavad kristallis elastse pingevälja, mida omakorda mõjutab väline rõhk (diaelastne efekt). Et selgitada ka sälkude rõhulist laienemist, on eeldatud teatud heterogeensust defektide ansambli elastsetes parameetrites. Analüüsitud on vastava jaotusfunktsiooni mõju tulemustele. Ka mõningad eksperimentaalsed tulemused diaelastse mudeli kohta on esitatud.

Difusiivne rõhumehhanism on sisse toodud seletamaks dispersiivse juhu jaoks ebaloomulikult suurt sälkude rõhulist laienemist Špolskii maatriksites. See mehhanism eeldab mõnede defektide koordinaatide hüppelisi muutusi rõhu rakendamisel. Sellise defekti näiteks võiks olla bi- (või multi-) stabiilne liikuv vakants aines, mis muudab oma seisundit teatud kriitilise välisrõhu korral. Difusiivse mehhanismi omaduste selgitamiseks on töös koostatud ja analüüsitud mõningaid uudseid mudelsituatsioone.

Välja on pakutud ka põhimõtteline eksperimentaalne protseduur, mille abil on võimalik välja selgitada, kas sälgu rõhulist laienemist määrab dispersiivne või difusiivne mehhanism. See koosneb neljast sammust, vaheldumisi põletamistest ja rõhu rakendamistest. Tulemusena peaks soodsate süsteemi- ja eksperimendiparameetrite korral dispersiivsel juhul olema jälgitav sälgu lõhenemine, mis on seotud mehhanismi fundamentaalsete omadustega. Siiski on

seniuuritud süsteemide puhul ennustatav efekt küllaltki tagasihoidlik. Esitatud on ka mõningad parameetrite optimiseerimise tulemused.

Töö viimases osas on käsitletud rõhuefekte ühismõõduta süsteemides. Nendes süsteemides on sissekülmunud võnkemoodi tõttu mingi kristallvõre parameeter moduleeritud perioodiga, mis ei oma ühismõõtu võrekonstandiga (nende suhe on irratsionaalne). Eksperimentaalselt on uuritud kloriini lisandiga bifenüüli ja leitud, et selles süsteemis on ühismõõdutusest tulenevalt aktiivsed nii dispersiivset kui difusiivset tüüpi mehhanismid. Esimene neist toimib modulatsioonilaine amplituudi ja teine faasi kaudu, põhjustatuna laine kinnituspunkti hüpetest lisanditel.

REFERENCES

1. G. Castro, D. Haarer, R. M. Macfarlane and H. P. Trommsdorff, US Patent No. 4101976.
2. W. E. Moerner and M. D. Levenson, J. Opt. Soc. Am. B **2**, 915 (1985).
3. J. Kikas and K. Leiger, Opt. Comm. **94**, 557 (1992).
4. A. A. Gorokhovskii, R. K. Kaarli and L. A. Rebane, Pis'ma Zh. Eksp. Teor. Fiz. **20**, 474 (1974) [JETP Lett. **20**, 216 (1974)].
5. B. M. Kharlamov, R. I. Personov and L. A. Bykovskaya, Opt. Comm. **12**, 191 (1974).
6. W. E. Moerner (Editor), *Persistent Spectral Hole-Burning: Science and Applications*, (Springer-Verlag, Berlin) 1988.
7. Th. Sesselmann, W. Richter and D. Haarer, Europhys. Lett. **2**, 947 (1986).
8. Th. Sesselmann, W. Richter, D. Haarer and H. Morawitz, Phys. Rev. B **36**, 7601 (1987).
9. Th. Sesselmann, W. Richter and D. Haarer, J.Lumin. **36**, 263 (1987).
10. G. Gradl, J. Zollfrank, W. Breinl and J.Friedrich, J. Chem. Phys. **94**, 7619 (1991).
11. P. Schellenberg, J. Friedrich and J. Kikas, J. Chem. Phys. **100**, 5501 (1994).
12. J. Zollfrank, J. Friedrich, J. Fidy and M. Vanderkooi, J. Chem. Phys. **94**, 8600 (1991).
13. G. Gradl, A. Feis and J. Friedrich, J. Chem. Phys. **97**, 5403 (1992).
14. A. Ellervee, J. Kikas, A. Laisaar, V. Shcherbakov and A. Suisalu, J. Opt. Soc. Am. B **9**, 972 (1992).
15. B. B. Laird and J. L. Skinner, J. Chem. Phys. **90**, 3274 (1989).
16. J. Kikas and K. Leiger, J. Chem. Phys. **104**, 5384 (1996).
17. K. Leiger, *MSc thesis*, Tartu (1995).
18. L. Kador, J. Chem. Phys. **99**, 7 (1993).
19. L. Kador, J. Chem. Phys. **95**, 846 (1991).
20. L. Kador, P. Geissinger and D. Haarer, J. Lumin. **64** 101 (1995).
21. L. Kador and P. Geissinger, Mol. Cryst. Liq. Cryst. **252**, 213 (1994).
22. J. Friebel, J. Friedrich, A. Suisalu, J. Kikas, An. Kuznetsov, A. Laisaar and K. Leiger, J. Chem. Phys. **108**, 1830 (1998).
23. A. M. Stoneham, Rev. Mod. Phys. **41**, 82 (1969).
24. J. Kikas and M. Rätsep, Phys. Stat. Sol. (b) **112**, 409 (1982).
25. J. D. Eshelby, in *Solid State Physics*, edited by F. Seitz and D. Turnbull (Academic Press, New York, 1956), Vol.3, p.79.

26. C. Teodosiu, *Elastic Models of Crystal Defects*, (Editura Academiei, Bucuresti; Springer-Verlag, Berlin - Heidelberg - New-York) 1982.

27. R. Blinc, Phys. Reports, **79**, 33 (1981).

28. A. Veron, J. Emery and M. Spiesser, J. Phys. Chem. Solids **57**, 1201 (1996).

29. L. A. Rebane, A. A. Gorokhovskii and J. V. Kikas, Appl. Phys. B **29**, 235 (1982).

30. L. Kador, J. Chem. Phys. **95**, 5574 (1991).

31. K. Orth, F. Rohlfing and J. Friedrich, Z. Phys. B **95**, 493 (1994).

32. M. R. Johnson and H. P. Trommsdorff, Physica B **226**, 194 (1996).

33. H. de Vries and D. A. Wiersma, Phys. Rev. Lett. **36**, 91 (1976).

34. E. V. Shpol'skii, Sov. Phys. Usp. **3**, 372 (1960).

35. E. V. Shpol'skii, Sov. Phys. Usp. **5**, 522 (1962).

36. E. V. Shpol'skii, Sov. Phys. Usp. **6**, 411 (1963).

37. K. Rebane, P. Saari and T. Tamm, Izv. AN ESSR, Fiz. Mat. **19**, 251 (1970).

38. R. I. Personov, I. S. Osadko, E. D. Godyaev and E. I. Al'shits, Sov. Phys. Solid State **13**, 2224 (1972).

39. S. Voelker, R. M. Macfarlane, A. Z. Genack and H. P. Trommsdorff, J. Chem. Phys. **67**, 1759 (1977).

40. A. Ellervee, J. Kikas, A. Laisaar and A. Suisalu, J. Lumin. **56**, 151 (1993).

41. I. L. Spain and S. Segall, Cryogenics **11**, 26 (1971).

42. A. Driessen, E. van der Poll and I. F. Silvera, Phys. Rev B **33**, 3269 (1986).

43. J. Kikas and J. L. Skinner, Chem. Phys. Lett. **230**, 429 (1994).

44. S. Alexander, Phys.Rep. **296**, 65 (1998).

45. V. Zazubovich, A. Suisalu, K. Leiger, A. Laisaar, An. Kuznetsov and J. Kikas, Chem. Phys. (submitted).

46. A. Suisalu, V. Zazubovich, J. Kikas, J. Friebel and J. Friedrich, Europhys. Lett. **44**, 613 (1998).

47. C. Benkert, V. Heine and E. H. Simmons, J. Phys. C: Solid State Phys. **20**, 3337 (1987).

48. M. H. Lemée-Cailleau, A. Girard, H. Cailleau and Y. Délugeard, Phys. Rev. B **45**, 12682 (1992).

49. L. von Laue, F. Ermark, A. Gölzhäuser, U. Haeberlen and U. Häcker, J. Phys. Condens. Matter **8**, 3977 (1996).

50. G.-P. Charbonneau and Y. Délugeard, Acta Crystallogr. B **33**, 1586 (1977).

51. H. Cailleau, in: R. Blinc, A. P. Levanyuk (Eds.), *Incommensurate Phases in Dielectrics, Part II: Materials (Modern Problems in Condensed Matter Sciences, Vol. 14)*, (North-Holland, Amsterdam, 1986) p. 71.

52. T. Wasiutyński and H. Cailleau, J. Phys.: Condens. Matter **4**, 6241 (1992).
53. M. H. Lemée, P. Launois, F. Moussa, A. Girard, Y. Délugeard and H. Cailleau, Physica B **156&157**, 17 (1989).
54. U. Even and J. Jortner, J. Chem. Phys. **77**, 4391 (1982).
55. V. Zazubovich, Ph. D. Thesis, University of Tartu, 1999.
56. J. Gafert, J. Friedrich and F. Parak, J. Chem. Phys. **99**, 2478 (1993).
57. V. Zazubovich, A. Suisalu, J. Kikas, Phys. Rev. B, **64**, 104203 (2001).

ACKNOWLEDGEMENTS

There are many people and organizations that contributed a great deal to this work.

Firstly, I would like to express my gratitude to my supervisor, Prof. Jaak Kikas for initiating the study and giving it a lot of support and attention.

It was a pleasure to work with the members of the Laboratory of the Laser Spectroscopy of the Institute of Physics of Tartu University. Specifically, I would like to thank Artur Suisalu and Anatoli Kuznetsov for helping me with the experiments, Arlentin Laisaar for discussions and the Head of the Laboratory, Ilmo Sildos for his interest.

My stay in the Institute of Atomic and Molecular Sciences of the Academica Sinica in Taipei, Taiwan was a very interesting and useful experience. I am very grateful to Dr. Ta-Chau Chang and the Director of the Institute, Prof. Sheng Hsien Lin for enabling me this visit.

I would also like to thank my family for support and especially Külli for her understanding and for encouraging me to complete this work.

PUBLICATIONS

Diaelastic pressure-induced effects on spectral holes in crystals

J. Kikas and K. Leiger

*Department of Physics, University of Tartu, Tähe 4, EE 2400 Tartu, Estonia and Institute of Physics,
Estonian Academy of Sciences, Riia 142, EE2400 Tartu, Estonia*

A statistical theory is developed in order to describe the pressure-induced shift and broadening of
spectral holes in pressure-tuning experiments in crystals. The theory accounts for the defect-related
diaelastic effect (induction of internal inhomogeneous strain fields by the applied hydrostatic
pressure due to the host-defect compressibility and/or size mismatch). General results are specified
and analyzed in the case of similar defects and for two different types of point defects. The former
case yields no hole broadening, while the latter one does. A similar consideration applies to electric-
and magnetic-field-induced effects on spectral holes in crystals as well. © *1996 American Institute
of Physics.* [S0021-9606(96)50808-5]

I. INTRODUCTION

Persistent spectral hole burning provides a highly sensi-
tive tool for studying pressure-induced shifts of impurity en-
ergy levels in solids.[1-8] Hole broadening, observable in
pressure-tuning experiments, reflects the inherent inhomoge-
neity (dispersion of pressure coefficients) of the subensemble
of molecules with a fixed transition energy. Such broadening
is especially large in disordered solids such as glasses, where
its magnitude is comparable to that of the pressure-induced
spectral shift.[1-6,8] Relatively large broadening of holes with
pressure has been observed in "soft" crystals of n-alkanes
(Shpol'skii systems).[6,7] However, even in "hard" molecular
crystals such as durene[6] and benzophenone[8] a minor broad-
ening of holes with pressure is readily observable.

Proceeding from the preposition of (microscopically) ho-
mogeneous compression Laird and Skinner developed a sta-
tistical theory of pressure-tuning experiments on spectral
holes in glasses.[9] Within the scope of this theory the pressure
broadening of spectral holes can be understood as a result of
"heteropolar" short-range (attractive r^{-6} and repulsive r^{-12})
intermolecular interactions. No hole broadening is expected
for homopolar interactions. In crystals the inhomogeneous
line shapes are governed by long-range homopolar interac-
tions of the optical transition with comparatively diluted de-
fects (e.g., r^{-3} elastic interactions with point defects).[10] Thus
the observed hole broadening in crystals is puzzling from the
viewpoint of existing theories.

In this paper the diaelastic effect[11] is considered as a
possible origin of the pressure broadening of spectral holes
in crystals. The diaelastic effect is an analog of the diamag-
netic effect, where an additional magnetic moment is in-
duced in a molecule by an external magnetic field. If an
elastic solid contains a region with compressibility different
from the bulk one (an elastic inclusion), the application of
hydrostatic pressure induces a spatially inhomogeneous
strain field around the inclusion. In Sec. II general formulas
for pressure-dependent stress fields around a spherical inclu-
sion in an isotropic homogeneous elastic medium are derived
and specified for some particular cases. In Sec. III the joint
distribution function for the impurity transition energies

governing the pressure evolution of spectral holes is ob-
tained. Based on general results particular cases of identical
defects and of two different types of defects are analyzed. In
Sec. IV the results are discussed in connection with experi-
ments and other theories.

II. POINT DEFECTS AS ELASTIC INCLUSIONS

Let the homogeneous and isotropic host material be
characterized by the Lamé constants λ_h and μ_h [μ_h being the
shear modulus and $\kappa_h = (\lambda_h + 2\mu_h/3)^{-1}$, the volume com-
pressibility]. We consider the following model for a point
defect.[11] From a spherical cavity of the radius r_h and the
volume $V_h = (4\pi/3)r_h^3$ at zero external pressure the host ma-
terial is removed. It is replaced by a sphere of the initial
radius r_g and the volume $V_g = (4\pi/3)r_g^3$ made of a material
with the Lamé constants λ_g and μ_g in general differing from
those of the host material. Assuming for the sample a spheri-
cal shape cocentric with the cavity and of the radius
$R_0 \gg r_h, r_g$, the spherical symmetry is preserved in the
course of strain relaxation. In spherical coordinates the dis-
placement vector has only a radial nonzero component given
by [see Ref. 11, Eq. (21.5)]

$$u(r) = Cr^{-2} + \bar{C}r. \qquad (1)$$

Equation (1) describes the displacement field inside as well
as outside the inclusion. The constants C and $\bar{C}$ (different for
the interior and the exterior of the inclusion) can be ex-
pressed via the elastic constants $\kappa_g, \mu_g, \kappa_h, \mu_h$ and the geo-
metrical characteristics r_g, r_h. First we note that
$C_g \equiv C(\text{inside}) = 0$ due to the absence of singularity at the
origin, i.e.,

$$u_r(r) = \begin{cases} \bar{C}_g r, & r < r_0 \\ Cr^{-2} + \bar{C}_h r, & r > r_0 \end{cases}, \qquad (2)$$

where r_0 is the final radius of the inclusion after strain relax-
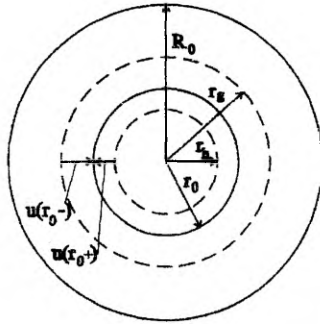ation (see Fig. 1).

23

FIG. 1. A model of a point defect. A spherical elastic inclusion of the initial radius r_g (larger dashed-line circle) is forced into a spherical cavity of the initial radius r_h (smaller dashed-line circle) formed in a homogeneous isotropic elastic sample of the radius $R_0 \gg r_g, r_h$ (large solid-line circle). The radius of the inclusion after the strain relaxation (small solid-line circle) is r_0. Such relaxation is accompanied by changes of the initial dimensions of the cavity and the inclusion, by $u(r_0+)$ and $u(r_0-)$, respectively.

In spherical coordinates the σ_{rr} component of the stress tensor is given by

$$\sigma_{rr}(r) = \begin{cases} 3\bar{C}_g \kappa_g^{-1} & r < r_0 \\ -4\mu_h C r^{-3} + 3\bar{C}_h \kappa_h^{-1}, & r > r_0 \end{cases} \tag{3}$$

For the determination of the (pressure-dependent) coefficients $C, \bar{C}_h, \bar{C}_g$, we have the following equations:
(i) for the change of the radius of the inclusion,

$$r_0 - r_g = u_r(r \to r_0-); \tag{4a}$$

(ii) for the change of the cavity radius,

$$r_0 - r_h = u_r(r \to r_0+); \tag{4b}$$

(iii) from continuity of the stress at the guest–host interface,

$$\sigma_{rr}(r \to r_0-) = \sigma_{rr}(r \to r_0+); \tag{4c}$$

(iv) and from the equilibrium of the sample surface (strain counterbalanced by the external pressure p),

$$\sigma_{rr}(r \to \infty) + p = 0. \tag{4d}$$

Equations (2)–(4) yield

$$C = \frac{\left(r_g + \frac{4}{3}\mu_h \kappa_g r_h \right)^2 \left[(r_g - r_h) + (\kappa_h r_g - \kappa_g r_h)\frac{p}{3} \right]}{\left[\left(1 + \frac{4}{3}\mu_h \kappa_g \right) + \left(1 + \frac{4}{3}\mu_h \kappa_h \right)\frac{\kappa_g p}{3} \right]^3}, \tag{5}$$

$$\bar{C}_h = -\frac{\kappa_h}{3} p, \tag{6}$$

$$\bar{C}_g = \frac{\frac{4}{3}\mu_h \kappa_g(r_g - r_h) + \left(1 + \frac{4}{3}\mu_h \kappa_h \right)r_g \frac{\kappa_g p}{3}}{r_g + \frac{4}{3}\mu_h \kappa_g r_h}, \tag{7}$$

and

$$r_0 = \frac{r_g + \frac{4}{3}\mu_h \kappa_g r_h}{\left(1 + \frac{4}{3}\mu_h \kappa_g \right) + \left(1 + \frac{4}{3}\mu_h \kappa_h \right)\frac{\kappa_g p}{3}}. \tag{8}$$

In Cartesian coordinates the stress tensor outside the cavity is given by

$$\sigma_{kl} = -p\,\delta_{kl} + \frac{2\mu_h C}{r^3}\left(\delta_{kl} - \frac{3x_k x_l}{r^2} \right), \quad k,l = 1,2,3. \tag{9}$$

We specify now the coefficient C for some particular cases.

A. Incompressible defects

In this case $\kappa_g = 0$ and from Eq. (8) $r_0 = r_g$. One obtains

$$C = (r_g - r_h)r_g^2 + \frac{1}{3}\kappa_h r_g^3 p. \tag{10}$$

Equation (10) can be represented as

$$C = C^0(1 + \alpha p), \tag{10'}$$

where

$$\alpha = \frac{r_g \kappa_h}{3(r_g - r_h)} = \frac{V_g}{\Delta V}\kappa_h \tag{11}$$

and

$$C^0 = r_g^2(r_g - r_h) = \frac{\Delta V}{4\pi}. \tag{12}$$

In Eqs. (11) and (12) $V_g = (4\pi/3)r_g^3$ is the guest volume introduced earlier and $\Delta V = 4\pi r_g^2(r_g - r_h)$, for $\Delta V \ll V_g$ the latter value is approximately the change of the cavity volume.

For further discussions the following points are of importance:

(i) the coefficient α depends not only on the bulk parameters (κ_h) but on the local ones ($V_g/\Delta V$) as well, i.e., for the same host material defect-dependent variations of α are possible;

(ii) depending on the sign of ΔV α can acquire both positive and negative values;

(iii) the variations of C^0 and α (arising from the variations of V_g and ΔV) need not be absolutely correlated.

B. Equal host and guest compressibilities

For $\kappa_g = \kappa_h = \kappa$ one obtains from Eq. (5),

$$C = \frac{(r_g - r_h)\left(r_g + \frac{4}{3}\,\mu_h \kappa r_h\right)^2}{\left(1 + \frac{4}{3}\,\mu_h \kappa\right)^3 \left(1 + \frac{\kappa p}{3}\right)^2}. \tag{13}$$

Linearizing Eq. (13) for small pressure values, one obtains a result formally coinciding with Eq. (10') but with the C^0 and α values different from Eqs. (11) and (12),

$$C^0 = \frac{(r_g - r_h)\left(r_g + \frac{4}{3}\,\mu_h \kappa r_h\right)^2}{\left(1 + \frac{4}{3}\,\mu_h \kappa\right)^3} \tag{14}$$

and

$$\alpha = -\frac{2}{3}\,\kappa. \tag{15}$$

Note that now α is independent of the defect characteristics r_g, r_h.

C. Highly compressible defects

In this case $\kappa_g \to \infty$ and

$$C = -\frac{16\mu_h^2 r_h^3 p}{\left[4\mu_h + \left(1 + \frac{4}{3}\,\mu_h \kappa_h\right)p\right]^3}. \tag{16}$$

Note that $C \neq 0$ only if $p \neq 0$. Linearization of Eq. (16) for small pressure values yields

$$C = -(4\mu_h)^{-1} r_h^3 p. \tag{17}$$

III. JOINT DISTRIBUTION FUNCTION OF TRANSITION ENERGIES

What one is looking for in order to interpret the pressure-tuning experiments on spectral holes is the pressure kernel or, more generally, the joint distribution function $I(\omega_1, \omega_2)$ of the transition energies at the initial (ω_1) and final (ω_2) pressure values.[9] The method used to calculate it is essentially a multidimensional generalization[12,13] of Stoneham's statistical theory for inhomogeneous line shapes.[10]

Suppose we have n different types of defects in the lattice, with the densities ρ_j, $j = 1,\dots,n$. The joint distribution function is then given by

$$I(\omega_1, \omega_2) = \frac{1}{(2\pi)^2} \int_{-\infty}^{\infty} \int_{-\infty}^{\infty} \exp[i(\omega_1 - \omega_1^0)x_1$$
$$+ i(\omega_2 - \omega_2^0)x_2 - J(x_1, x_2)]dx_1 dx_2, \tag{18}$$

where ω_1^0 and ω_2^0 are the respective unperturbed frequencies and

$$J(x_1, x_2) = \sum_{j=1}^{n} \rho_j \int \{1 - \exp[-ix_1 \epsilon_{1j}(z)$$
$$-ix_2 \epsilon_{2j}(z)]\}dz. \tag{19}$$

Integration in Eq. (19) is carried out over the coordinates z of the defect. $\epsilon_{1i}(z)$ and $\epsilon_{2i}(z)$ are the frequency shifts caused by a defect of jth type located at z for the initial (p_1) and the final (p_2) pressure value, respectively,

$$\epsilon_{1j}(z) = \epsilon_j(z, p_1); \quad \epsilon_{2j}(z) = \epsilon_j(z, p_2). \tag{20}$$

In what follows we specify the general theory for the case of elastic interaction of the impurity transition with point defects. We suppose that the frequency perturbation caused by elastic interaction is linear in the stress components

$$\epsilon = \sum_{k,l=1}^{3} a_{kl} \sigma_{kl}, \tag{21}$$

where the coefficients a_{kl} give the coupling of the stress components to the transition energy. Here we have omitted the index $i = 1,2$ referring to different pressure states and the index $j = 1,\dots,n$ referring to different defect types, characterized by the values of μ_g, κ_g, r_g, and r_h in our model. In what follows we omit in Eq. (9) the hydrostatic term $-p\delta_{kl}$ yielding a uniform pressure shift independent of defects. From the second (r^{-3}) term one obtains

$$\epsilon = C\,\frac{\Phi(\theta, \varphi)}{r^3}, \tag{22}$$

where $C = C(\mu_h, \kappa_h, \kappa_g, r_h, r_g, p)$ is given by Eq. (5). The function Φ in Eq. (22) depends only on the symmetry of the states involved in the actual transition and their coupling to the stress field and *does not* depend on the defects. The spherical angles θ and φ give the direction of the impurity (or defect, if one takes the impurity location for the origin). Substituting ϵ from Eq. (22) with C from Eq. (10') into Eq. (19) and integrating over r, one obtains

$$J(x_1, x_2) = \sum_{j=1}^{n} \rho_j \{|C_j^0|[(1 + \alpha_j p_1)x_1 + (1 + \alpha_j p_2)x_2]a_R$$
$$+ iC_j^0[(1 + \alpha_j p_1)x_1 + (1 + \alpha_j p_2)x_2]a_I\}, \tag{23}$$

where

$$a_R = \frac{\pi}{6} \int_0^{2\pi} \int_0^{\pi} |\Phi| \sin\theta \, d\theta \, d\varphi \tag{24}$$

and

$$a_I = -\frac{1}{3} \int_0^{2\pi} \int_0^{\pi} \Phi \ln|\Phi| \sin\theta \, d\theta \, d\varphi. \tag{25}$$

Note that the site energy distribution is Lorentzian for all pressures, its width (FWHM/2) is given by

$$\Gamma_i = a_R \sum_{j=1}^{n} \rho_j |C_j^0 (1 + \alpha_j p_i)|, \quad i = 1,2. \tag{26}$$

Note that, depending on the sign of α, a pressure-induced broadening $(\alpha > 0)$ as well as a pressure-induced narrowing

($\alpha < 0$) of inhomogeneous lines are possible. For hard (incompressible) defects the former case corresponds to $r_g > r_h$ and the latter one to $r_g < r_h$. It is also possible that a counterbalance between the defects of both positive and negative α values can result in rather a weak pressure broadening of inhomogeneous lines even in crystals with high concentration of defects.

As to the maximum position, we make the following remarks:

(i) In this paper we do not consider the pressure dependence of the unperturbed frequency. For simplicity we take $\omega_2^0 = \omega_1^0 = 0$.

(ii) Due to surface effects there is a homogeneous (the same for all impurities) contribution to the frequency shift (the Eshelby term[14]) at finite defect densities. We do not consider this term either, as it does not influence the effects we are interested in.

With these assumptions the maximum positions for the inhomogeneous line at the initial and the final pressure are given by

$$\omega_i^M = a_I \sum_{j=1}^{n} \rho_j C_j^0 (1 + \alpha_j p_i), \quad i = 1,2. \tag{27}$$

In what follows, we analyze $I(\omega_1, \omega_2)$ in the simple (it can be said trivial) case of similar defects as well as in the case of two different types of defects (the type here refers to a point defect with the given values of the parameters C_j^0 and α_j). The latter brings us to several nontrivial effects and gives some guidance to what may happen in more complicated situations (larger numbers or, as a limiting case, a continuous distribution of defect parameters).

A. Similar defects

With a single type of defect ($n = 1$), Eq. (23) yields

$$J(x_1, x_2) = \rho a_R |C^0| |(1 + \alpha p_1) x_1 + (1 + \alpha p_2) x_2|$$
$$+ i \rho a_I C^0 [(1 + \alpha p_1) x_1 + (1 + \alpha p_2) x_2] \tag{28}$$

and Eq. (18) can be calculated to give

$$I(\omega_1, \omega_2) = \frac{1 + \alpha p_1}{\pi} \delta[(1 + \alpha p_1)\omega_2 - (1 + \alpha p_2)\omega_1]$$
$$\times \frac{\Gamma_1}{\Gamma_1^2 + (\omega_1 - \omega_1^M)^2}, \tag{29}$$

where the Lorentzian factor is the site energy distribution at the initial pressure with Γ_1, ω_1^M introduced in Eqs. (26) and (27) ($n = 1$), respectively. For $|\alpha p_i| \ll 1$, Eq. (29) can be represented as

$$I(\omega_1, \omega_2) = \frac{1}{\pi} \delta\{\omega_2 - [1 + \alpha(p_2 - p_1)]\omega_1\}$$
$$\times \frac{\Gamma_1}{\Gamma_1^2 + (\omega_1 - \omega_1^M)^2}. \tag{29'}$$

As readily seen from Eq. (29'), the case of similar defects yields no pressure broadening—the pressure kernel reduces
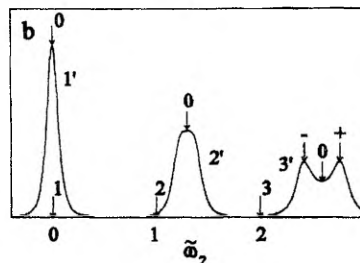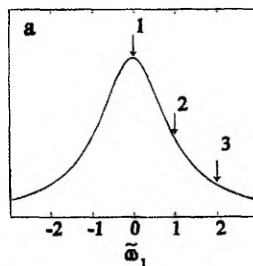

FIG. 2. Pressure kernel for the interaction with two types of point defects (the symmetric case, $K = \rho_2 C_2^0 / \rho_1 C_1^0 = 1$). The inhomogeneous line (frequency distribution) at the initial pressure is depicted at the top (a). The arrows 1–3 indicate the initial frequencies for which the frequency distributions (pressure kernels) after a pressure variation are depicted (b, curves 1'–3'). The distributions are normalized to the same area. Note that the splitting occurs at larger deviations from the line maximum (arrows 0, +, and − indicate the maxima and the minimum of the pressure kernel).

to a δ-function. We point to a subtle but important circumstance in the use of the term "pressure kernel." Equation (29'), though quite similar, is not exactly of the shape

$$I(\omega_1, \omega_2) = K(\omega_2 - \omega_1) I(\omega_1). \tag{30}$$

Hence, the frequency distribution at the final pressure $I(\omega_2, p_2)$ is not related to the frequency distribution at the initial pressure $I(\omega_1, p_1)$ by an integral transformation

$$I(\omega_2, p_2) = \int K(\omega_2 - \omega_1) I(\omega_1, p_1) d\omega_1, \tag{31}$$

with the kernel K depending solely on the frequency difference. This statement is of a general nature and applies to Sec. III B as well. In a simple particular case considered here it is expressed in the frequency dependence of the pressure shift. The pressure coefficient

$$(\omega_2^m - \omega_1^m)/\Delta p = \alpha \omega_1^m \tag{32}$$

(ω_1^m and ω_2^m denote the hole positions at pressures p_1 and p_2, respectively) is a linear function of the initial frequency.
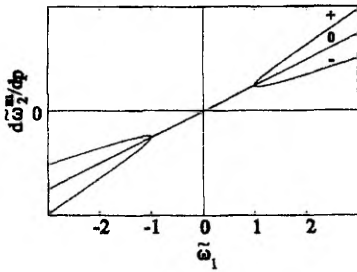
FIG. 3. Dependence of the pressure coefficient (spectral shift per unit pressure variation) for the maxima and the minimum of the pressure kernel from Fig. 2(b) on the initial frequency.

FIG. 4. The same as Fig. 2(b) for an asymmetric case $(K = \rho_2 C_2^0 / \rho_1 C_1^0 = 2.33)$.

B. Two types of defects

For $n=2$ joint distribution Eq. (18) is most easily calculated by changing to new Fourier variables, $y_1 = (1 + \alpha_1 p_1)x_1 + (1 + \alpha_1 p_2)x_2$ and $y_2 = (1 + \alpha_2 p_1)x_1 + (1 + \alpha_2 p_2)x_2$. One gets

$$I(\omega_1, \omega_2) = \frac{|\Delta p||\Delta a|}{\pi^2} \frac{\gamma_1}{\Omega_1^2 + \gamma_1^2} \frac{\gamma_2}{\Omega_2^2 + \gamma_2^2}, \tag{33}$$

where $\Delta p = p_2 - p_1$, $\Delta \alpha = \alpha_2 - \alpha_1$,

$$\Omega_j = (1 + \alpha_{\bar{j}} p_1)\omega_2 - (1 + \alpha_{\bar{j}} p_2)\omega_1 \pm a_1 \rho_j C_j^0 \Delta \alpha \Delta p \tag{34}$$

with + for $j=2$ and − for $j=1$, and $\bar{j}=2$ for $j=1$, $\bar{j}=1$ for $j=2$,

$$\gamma_j = a_R \rho_j |C_j^0| |\Delta \alpha| |\Delta p|, \quad j=1,2. \tag{35}$$

Equation (33) is, in fact, a product of two shifted Lorentzians, generally of different widths. Note that if $\alpha_1 = \alpha_2$, the case of two different types of defects reduces essentially to the one of identical defects considered in Sec. III A. For $|\alpha_j p_i| \ll 1$, Eq. (34) transforms to

$$\Omega_j = \omega_2 - (1 + \alpha_j \Delta p)\omega_1 \pm a_1 \rho_j C_j^0 \Delta \alpha \Delta p \tag{34'}$$

in the first order by Δp.

In order to depict and analyze Eq. (33) we choose for the spectral origin the maximum of the inhomogeneous line in the initial state

$$\omega_1^M = a_1(\rho_1 C_1^0 + \rho_2 C_2^0) \tag{36}$$

and change to the dimensionless frequency $\tilde{\omega}$ scaling with the inhomogeneous width $\Gamma_1 = a_R(\rho_1 |C_1^0| + \rho_2 |C_2^0|)$,

$$\tilde{\omega}_i = (\omega_i - \omega_1^M)/\Gamma_1. \tag{37}$$

Figure 2(b) depicts the pressure kernel (i.e., the joint frequency distribution as a function of the final frequency for a fixed initial frequency) for three positions, 1–3, in the inhomogeneous line [Fig. 2(a)] for $\Delta p \Delta \alpha = 0.2$ in the "symmetric" $(\rho_1 C_1^0 = \rho_2 C_2^0)$ case. The main difference from the results for a single type of defects is the finite width of the
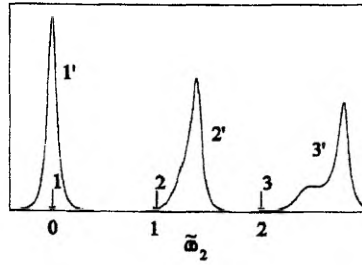
pressure kernel, i.e., there is a pressure broadening of spectral holes proportional to $\Delta \alpha$. Note that according to Eqs. (33), (34'), (35) pressure kernels for different pressure changes are obtainable from each other by a linear frequency rescaling, i.e., their shape does not depend on the pressure variation but on the initial frequency only.

Depending on the spectral position the pressure kernel exhibits either one or two maxima. In Fig. 3 the frequency $(\tilde{\omega}_1)$ dependence of the pressure coefficients for these maxima (and the corresponding minimum) are depicted.

If $K = \rho_2 C_2^0 / \rho_1 C_1^0 \neq 1$, the pressure kernel is of an asymmetric shape, as depicted in Fig. 4 for $K=2.33$. Such asymmetry inhibits to a certain extent the splitting observable at larger deviations from the line maximum. A full $|K| - \tilde{\omega}_1$ diagram for the appearance of a single maximum and of two maxima is given in Fig. 5. Note that at $|\tilde{\omega}_1| > \tilde{\omega}_c = 2\sqrt{2}$ the splitting occurs for all values of K and for $|\tilde{\omega}_1| < 1$ no splitting ever occurs. According to the remark made above, the diagram of Fig. 5 does not depend on pressure. However, to observe such a hole splitting in real experiments one has to overcome the hole broadening related to the finite homogeneous and instrumental widths, i.e., for a given initial frequency there exists a certain pressure threshold to observe
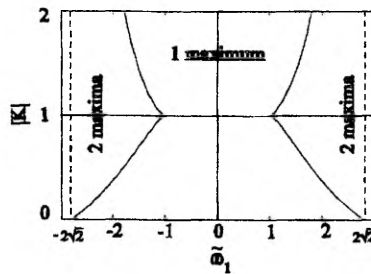

FIG. 5. Single- and two-maxima regions for the pressure kernel in the $\tilde{\omega}_1 - K$ plane.

the splitting. Contributions from other defects, not accounted in the model, may enlarge the single-maximum frequency region.

IV. DISCUSSION

Splitting and broadening of spectral lines (holes) in the applied external fields (electric, magnetic, uniaxial stress) is quite a general phenomenon and is usually related to the symmetry reduction of the impurity center itself. Thus degenerate energy levels may split in a field of lower symmetry and geometrically equivalent impurity centers may become inequivalent. This is, particularly, the hole broadening mechanism in Stark experiments in amorphous solids with orientational disorder.[14-16]

The effects considered in this paper, though similar in appearance, are of basically different nature. No local symmetry reduction is needed in order to get the splitting and/or the broadening of spectral lines. The latter results from and reflects the heterogeneity of the ensemble of defects interacting with the impurity transition. The possibility of observing hole splitting in the case of two different types of defects stems from the circumstance that for r^{-3} interactions large spectral deviations are mainly caused by interaction with a single nearby defect. A specific feature of such splitting is the color effect; the magnitude of splitting depends on the position in the inhomogeneous line (band). We also demonstrated that the split components may exhibit asymmetry, depending on the relative densities of defects of different types.

Speaking generally, the pressure kernel gives (in the case of large detunings from the maximum of the inhomogeneous line) a rough representation of the distribution $\rho(\alpha)$ [weighted by the factor $C^0(\alpha)$] and may thus be quite a valuable source of physical information. A larger number of defect types or a continuous distribution of defect parameters may apparently obscure the observability of the above-discussed hole splitting. However, the blurred splitting appears then as a color effect in the hole broadening and may also manifest itself in an essentially non-Lorentzian pressure-induced hole broadening. Indeed, even in crystals Gaussian pressure kernels have been observed experimentally.[6-8]

The behavior of spectral holes with pressure in pressure-tuning experiments in glasses has earlier been considered theoretically within the frame of the same statistical theory.[9] Here we point to the following differences of the present consideration from that of Ref. 9. In the latter a microscopically *homogeneous* compression of the host was supposed, i.e., the pressure change Δp results in a decrease of a host particle distance r from the impurity by an amount of

$$\Delta r = -\frac{\kappa}{3} \Delta p r, \tag{38}$$

where κ is the volume compressibility. If the transition energy perturbation by a host particle is given by a "homopolar" interaction

$$\epsilon(r) = A r^{-n}, \tag{39}$$

then

$$\Delta \epsilon(r) = A \frac{\kappa n}{3} \Delta p r^{-n} = \frac{n}{3} \kappa \Delta p \epsilon(r). \tag{40}$$

As far as the coefficient of the proportionality A is assumed to be the same for all host particles and their contributions to the transition energy shift are additive, the same proportionality holds also for transition energies and their changes

$$\Delta \omega = \frac{n}{3} \kappa \Delta p \omega. \tag{41}$$

Equation (41) implies that there is only a pressure-induced shift but no pressure broadening. To account for the latter an "heteropolar" (e.g., Lennard-Jones) interaction is assumed in order to break the scaling. Note that in our model similar effects arise from *inhomogeneous* compression of the host material. Another essential difference is that Eq. (41) includes bulk parameters only, whereas in our model there is also the dependence on local (defect) parameters [Eqs. (11), (32)].

Starting from the fundamental intermolecular (Lennard-Jones) interactions one has also to consider the molecular correlations in solids. The simplest way to proceed is to neglect the higher-order intermolecular correlations (Gaussian approximation) or to consider them as corrections to the Gaussian approximation. This approach, naturally, works better in strongly disordered systems (e.g., glasses) were the intermolecular correlations are weaker.[9] The theory developed in the present paper is a phenomenological one as far as the deduction of the (macroscopic) theory of elasticity from the intermolecular interactions is not considered. As perturbers here act not all the host molecules but *defects* of the regular crystalline lattice only. Contrasted to the short-range intermolecular interactions such elastic perturbations are long-range ones (r^{-3} for point defects). The assumption of statistical independence of perturbers now means the statistical independence of defects. Thus the primary area of applicability of the results obtained in this paper are crystals of low defect concentration. However, the results could also be of interest as the first approximation to what happens at higher concentrations of defects (even in glasses, considering the latter ones as crystals of very high defect concentration).

There have been quite a few experimental studies on hole shift and broadening in pressure-tuning experiments in crystals. A small variation of the pressure coefficient for spectral holes within a single-site line in benzophenone-chlorin solid solution has been mentioned, the same system exhibiting a rather weak site-dependent pressure broadening of holes (0.03–0.16 cm^{-1}/kbar).[8] An interesting observation for the n-octane-chlorin solid solution (a Shpol'skii system) has been a relatively large hole broadening (about 2 cm^{-1}/kbar measured in the pressure range of 20–30 kbar) contrasted to the absence of a noticeable pressure broadening of inhomogeneous lines measured at pressures up to 5 kbar. This observation can be explained proceeding from our model as a certain counterbalance of the positive and negative α values in Eqs. (26), (27), while the hole broadening according to Eqs. (33)–(35) is governed by the dispersion of

α values. Sm^{2+}-activated $MeI_yMeII_{1-y}FXI_xXII_{1-x}$ (Me $=Ca,Sr,Ba$; $X=Cl,Br,I$) compounds[18] seem particularly promising for an experimental check as a controllable realization of both the single type of defects and two types of defects (with $r_g > r_h$ as well as with $r_g < r_h$) is possible.

As to the applicability of our model to glasses, we note that in all experimental observations[4-6,8] $\alpha > 0$ (i.e., the inhomogeneous spectral bands in glasses *broaden* with pressure). This rules out certain regions of model parameters.

We have discussed a mechanism of spectral hole broadening due to defect-induced diaelastic effects. Quite a similar approach applies also in the case of electrical dipoles in an external electric field. An external field induces changes of dipole moments of defects. The interaction of the dipole moments with an impurity (coupling to the difference of permanent dipole moments in the excited and the ground state of an impurity) results in the shifts of the impurity transition energy. In the case of dissimilar defect dipoles this is observable as a hole broadening (and splitting under certain conditions). As mentioned above, such an effect must be distinguished from the hole broadening in Stark experiments on amorphous materials.[15-17] One can also speculate about the systems and conditions where an analogous magnetic effect could be observable (cf. with Zeeman experiments in crystals[19] and glasses[20]).

V. CONCLUDING REMARKS

In this paper, a mechanism of spectral hole broadening in crystals due to defect-induced diaelastic effects (and analogous electric and magnetic field effects) was discussed. However, a number of other phenomena can be considered in the same general framework; effects of internal strains arising on cooling from the host-defect thermal contraction mismatch, screening of the external pressure by a hard host matrix for impurities in soft local surroundings, etc. It is also of interest to speculate to what extent the results of this paper, where the assumption of (microscopically) homogeneous compression has been abandoned, could be applied to glasses

as a certain alternative to the homogeneous compression model.[9] An extension of the theory developed in the present paper to linear defects (dislocations, disclinations) would be of interest in this aspect, as far as disclinations have been argued to be an inherent structural constituent of glasses.[21]

[1] Th. Sesselmann, W. Richter, and D. Haarer, Europhys. Lett. **2**, 947 (1986).
[2] Th. Sesselmann, W. Richter, D. Haarer, and H. Morawitz, Phys. Rev. B **36**, 7601 (1987).
[3] Th. Sesselmann, W. Richter, and D. Haarer, J. Lumin. **36**, 263 (1987).
[4] J. Zollfrank, J. Friedrich, J. Fidy, and M. Vanderkooi, J. Chem. Phys. **94**, 8600 (1991).
[5] G. Gradl, J. Zollfrank, W. Breinl, and J. Friedrich, J. Chem. Phys. **94**, 7619 (1991).
[6] G. Gradl, A. Feis, and J. Friedrich, J. Chem. Phys. **97**, 5403 (1992).
[7] A. Ellervee, J. Kikas, A. Laisaar, V. Shcherbakov, and A. Suisalu, J. Opt. Soc. Am. B **9**, 972 (1992).
[8] P. Schellenberg, J. Friedrich, and J. Kikas, J. Chem. Phys. **100**, 5501 (1994).
[9] B. B. Laird and J. L. Skinner, J. Chem. Phys. **90**, 3274 (1989).
[10] A. M. Stoneham, Rev. Mod. Phys. **41**, 82 (1969).
[11] C. Teodosiu, *Elastic Models of Crystal Defects*, Editura Academiei, Bucuresti (Springer, Berlin, 1982).
[12] J. Kikas and M. Rätsep, Phys. Stat. Solidi B **112**, 409 (1982).
[13] D. L. Orth and J. L. Skinner, J. Phys. Chem. **98**, 7342 (1994).
[14] J. D. Eshelby, in *Solid State Physics*, edited by F. Seitz and D. Turnbull (Academic, New York, 1956), Vol. 3, p. 79.
[15] A. P. Marchetti, M. Scozzafava, and R. H. Young, Chem. Phys. Lett. **51**, 424 (1977).
[16] F. A. Burkhalter, G. W. Suter, U. P. Wild, V. D. Samoilenko, N. V. Razumova, and R. I. Personov, Chem. Phys. Lett. **94**, 483 (1983).
[17] U. Bogner, P. Schätz, R. Seel, and M. Maier, Chem. Phys. Lett. **102**, 267 (1983).
[18] R. Jaaniso, H. Hagemann, and H. Bill, J. Chem. Phys. **101**, 10 320 (1994).
[19] A. I. M. Dicker, M. Noort, S. Voelker, and J. H. van der Waals, Chem. Phys. Lett. **73**, 1 (1980).
[20] R. van der Berg, H. van der Laan, and S. Voelker, J. Lumin. **40–41**, 84 (1988).
[21] N. Rivier and D. M. Dufty, J. Phys. (Paris) **43**, 293 (1982).

II

Pressure-induced dynamics in solid n-alkanes as probed by optical spectroscopy,
J. Friebel, J. Friedrich, A. Suisalu, J. Kikas, An. Kuznetsov,
A. Laisaar, K. Leiger,
J. Chem. Phys. **108** (1998) 1830.

Pressure-induced dynamics in solid *n*-alkanes as probed by optical spectroscopy

J. Friebel
Technische Universität München, Lehrstuhl für Physik Weihenstephan, D-85350 Freising, Germany, and Physikalisches Institut und Bayreuther Institut für Makromolekülforschung, Universität Bayreuth, D-95440 Bayreuth, Germany

J. Friedrich
Technische Universität München, Lehrstuhl für Physik Weihenstephan, D-85350 Freising, Germany

A. Suisalu
Institute of Physics, Riia 142, EE2400 Tartu, Estonia

J. Kikas
Institute of Materials Science, University of Tartu, Tähe 4, EE2400 Tartu, Estonia

An. Kuznetsov and A. Laisaar
Institute of Physics, Riia 142, EE2400 Tartu, Estonia

K. Leiger
Institute of Physics, Riia 142, EE2400 Tartu, Estonia, and Institute of Materials Science, University of Tartu, Tähe 4, EE2400 Tartu, Estonia

The dependence of frequency, width, and area of spectral holes on pressure were measured at 1.6 K in the pressure range up to 2.5 MPa for dimethyl-s-tetrazine (DMST) doped *n*-hexane (Shpol'skii system), and as reference systems, for DMST-doped durene ("hard" molecular crystal) and ethanol:methanol glass. For the Shpol'skii system, in addition the inhomogenous fluorescence spectra were measured for normal and high (200 MPa) pressures. The main observations were the following: (i) spectral holes in the Shpol'skii system exhibit very large pressure-induced broadening (up to 65 GHz/MPa) depending essentially on the prehistory (freezing pressure) and exceeding the corresponding values for durene (by far) and glass; (ii) spectral holes in the Shpol'skii system exhibit strong, and to a large extent, reversible, area reduction with applied pressure; and (iii) the inhomogeneous fluorescence lines show quite a moderate (as compared to holes) pressure broadening of about several GHz/MPa. The results for the Shpol'skii system are shown to be inconsistent with existing theories. They are qualitatively explained by pressure-induced dynamics of vacancy defects in the frozen *n*-alkanes. © *1998 American Institute of Physics.*
[S0021-9606(98)50504-1]

I. INTRODUCTION

Different classes of solids loosely characterized as "crystals" can exhibit quite different physical behavior, some of them being in particular aspects even more similar to glasses or other disordered phases. In this paper we address specific elastic–plastic properties of frozen *n*-alkanes as revealed in the pressure dependence of the optical spectra of dye probes. The *n*-alkanes were introduced into solid state spectroscopy by Shpol'skii[1-3] in the 1960s. They served as paradigms for demonstrating the fundamental features of low temperature optical spectra such as the existence of zero phonon lines, phonon sidebands, lifetime limited linewidths, etc.[4-6] Despite the intensive studies in the 1960s and 1970s, several problems remained unexplained: for instance, the nature of the diffusive spectral background, or the peculiar dependence of the spectra on concentration.[7,8] Although less attention has been paid to these systems since, they have never ceased to attract experimentalists. We mention the nonphotochemical site conversion hole burning experiments,[9] the comparative hole burning experiments be-tween zero phonon lines and spectral background,[9,10] the Stark-effect experiments on spectral holes,[9,11] the spectroscopic experiments with single molecules,[12] and our papers on pressure phenomena in Shpol'skii matrices.[13-15]

The present study has been stimulated by our observation[13,14] that spectral holes in Shpol'skii systems exhibit an unexpectedly large pressure-induced broadening which is comparable to or even exceeds the respective values for glasses.[16-20] Compared to ordinary organic molecular crystals like durene or benzophenone,[13,20] pressure broadening of spectral holes in Shpol'skii systems is larger by orders of magnitude. On the other hand, pressure broadening of the inhomogeneous width is moderate and of the same order of magnitude as for ordinary crystals. In this paper we address this problem on the basis of new experimental data from both the low pressure regime (up to 10 MPa) and the high pressure regime (up to 200 MPa).

II. EXPERIMENT

Dimethyl-s-tetrazine (DMST) was used as a probe. It undergoes a spectral hole burning transformation either due

to an irreversible photodissociation[21] or to optically induced nuclear spin conversion.[22,23] In order to stress the specific features of the Shpol'skii system, we compared the behavior of DMST in *n*-hexane with the respective one in an ethanol: methanol glass (3:1, volume by volume) and in a durene crystal. The liquid solutions (*n*-hexane and ethanol:metha-nol) were poured into small plastic bags to prevent the samples from getting stuck to the walls of the pressure cham-ber during freezing.[13] Freezing was performed under two different conditions, namely under a pressure of 0.3 and 5 MPa, respectively. Spectral hole burning was performed at 1.6 K under a prepressure between 0.1 and 0.3 MPa, respec-tively. Pressure was transmitted via He gas. The accuracy of the pressure control was about 10^{-3} MPa. The *n*-hexane sample used in the high pressure experiment (200 MPa) was also crystallized under 5 MPa. The details of the high pres-sure experiment are described elsewhere.[14]

Hole burning was performed with a single mode dye laser operating with R6G. Holes were detected in the trans-mission mode. The laser scan range of 30 GHz was sufficient for probing the holes in the accessible pressure range whose upper limit (2.5 MPa) was determined by the liquid–solid phase boundary of [4]He. The holes were probed with a laser power of about 10 μW. The power level for burning was about 3 orders of magnitude higher. Burning times were a few minutes. Under these conditions the relative depths of the holes were about 30%–50%. The quantities measured were the shift, the broadening, and the area of the hole as a function of pressure. In the Shpol'skii—as well as in the durene crystal, the holes could be very well fitted to Lorent-zian line shapes. Hence, in these cases, the pressure-induced broadening was determined as the difference between the holewidth with and without pressure. In the ethanol:metha-nol glass the holes were fitted to a Voigt-profile. In this case, the respective pressure-induced broadening is to a good ap-proximation given by $(\sigma_v^2 - \sigma_v\sigma_0)^{1/2}$, where σ_v is the full width at half maximum (FWHM) of the Voigtian line shape and σ_0 is the width of the initial hole. In order to improve the accuracy of the determination of the area of the hole, we burnt holes with almost rectangular shapes by sweeping the laser frequency over a range that was large compared to the initial width (Fig. 5). In this way, the background could be kept rather low. For the glass sample, however, this proce-dure could not be applied because the initial holewidths were already too broad given the limited scan range of the laser.

The inhomogeneously broadened absorption spectra were recorded at 4.2 K with a resolution of about 3 wave numbers.

III. RESULTS

Figure 1 shows an overview of the 00-bands of the DMST absorption in the various matrices investigated. The band where hole burning was performed has its maximum at 17 238 in *n*-hexane, at 17 020 in durene, and at 17 800 cm^{-1} in ethanol:methanol glass.

Figure 2 shows hole spectra of the *n*-hexane system as they deform under pressure for two freezing conditions,
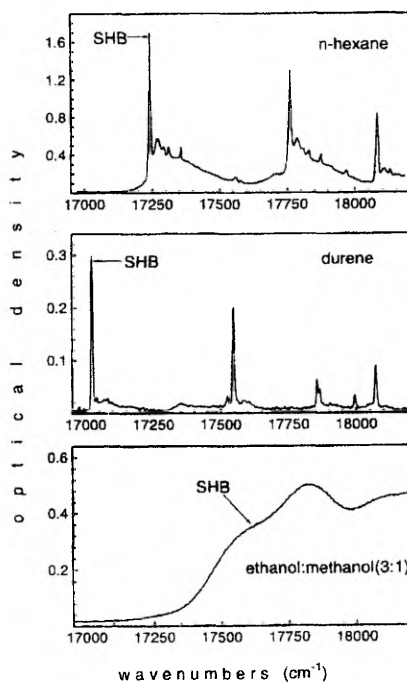

FIG. 1. Absorption spectra of DMST in *n*-hexane, in durene crystal, and in ethanol:methanol glass at 4.2 K. Arrows point to the lines/bands used for spectral hole burning.

namely for a freezing pressure of 0.3 [Fig. 2(a)] and 5 MPa [Fig. 2(b)], respectively. The spectra show antihole features, demonstrating that nuclear spin conversion contributes to the spectral transformation process as well. However, the area of
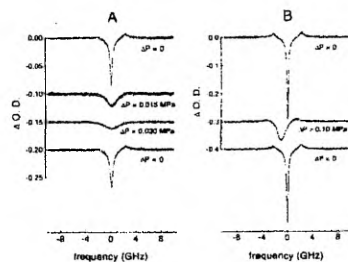

FIG. 2. Spectral holes in the absorption of DMST-doped *n*-hexane frozen under 0.3 MPa (A) and 5 MPa (B). Top spectra—initial holes at $P = 0.3$ MPa; for intermediate spectra the pressure variation ΔP is indicated. Bottom spectra—holes recovered at the initial pressure value after pressure cycle.
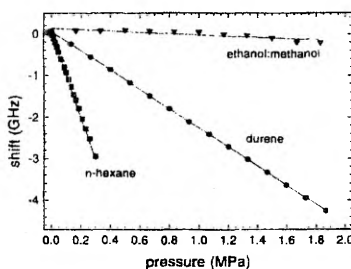
FIG. 3. Pressure-induced hole shift of DMST-doped *n*-hexane (squares, slope of the least-squares linear fit—10 GHz/MPa), durene crystal (circles, −2.44 GHz/MPa), ethanol:methanol glass (triangles, −0.15 GHz/MPa). All samples are cooled from room temperature to 4.2 K under a pressure of 5 MPa.

FIG. 5. Hole area as a function of pressure in DMST-doped *n*-hexane frozen at 0.3 MPa (filled diamonds) and 5 MPa (squares) and durene (circles). The empty diamond refers to data taken after pressure release. Durene and the prepressurized (5 MPa) *n*-hexane are fully reversible. Solid curves are guides for the eye. The insert shows artificially broadened holes which were used to measure the influence of pressure on the hole area.

the hole exceeds that of the antiholes, demonstrating that photochemical or photophysical hole burning processes prevail under our experimental conditions.

There is quite a remarkable feature: Hole A broadens very strongly with pressure; however, there is no significant spectral shift. We hasten to stress that this behavior is very sensitive to the level of freezing pressure. In Fig. 2(b), for instance, pressure broadening is still remarkably strong but less than in Fig. 2(a). The decrease in pressure broadening is accompanied by an increase in pressure shift.

Figures 3–5 show how the center frequency, the width, and the area change as a function of pressure. Figure 3 compares the pressure shifts of the three systems which were, in this case, frozen under a pressure of 5 MPa. Under this condition, the shift per unit pressure change is larger by a factor of 4 for the *n*-hexane matrix as compared to durene. Remember that there was no shift if freezing was performed under low pressure. This is a surprising observation. According to simple models,[16,17] one would expect that the pressure shift scales with the solvent shift. The solvent shift for *n*-hexane, however, is less than for durene because its absorption is

more to the blue (Fig. 1), yet the pressure shift is larger. The pressure shift of the glass system, on the other hand, seems to corroborate the respective scaling with the solvent shift: its absorption is further to the blue, hence, the respective pressure shift is low.

The pressure shift of the hole should be compared with the pressure shift of the inhomogeneous line: For *n*-hexane the latter is much smaller, namely about 3 GHz/MPa (Fig. 6). This value roughly pertains even up to a pressure level of 200 MPa (Fig. 7). For durene, on the other hand, the pressure shift of the hole and of the inhomogeneous line are the same (Fig. 6).

Figure 4 shows the broadening of the holes under pressure. It demonstrates that the Shpol'skii systems are something quite special: For *n*-hexane, frozen under low pressure, broadening is by a factor of 240 larger as compared to durene, and by a factor of 6–7 larger as compared to the glass. If freezing is performed under 5 MPa, broadening in *n*-hexane is still by a factor of two larger than the respective one in the glass and by a factor of 40 larger than in durene.
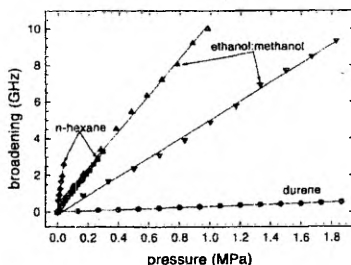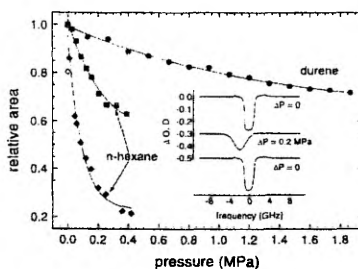

FIG. 4. Pressure-induced hole broadening of DMST-doped *n*-hexane frozen at 0.3 MPa (diamonds, slope of the least-squares linear fit 65 GHz/MPa) and 5 MPa (squares, 11 GHz/MPa), ethanol:methanol glass frozen at 0.3 MPa (up triangles, 10 GHz/MPa) and 5 MPa (down triangles, 5.2 GHz/MPa), and durene crystal (circles, 0.27 GHz/MPa).
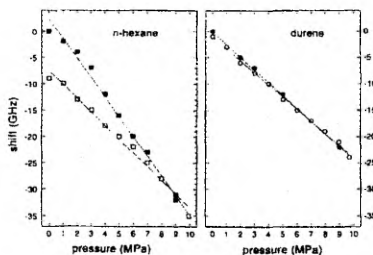

FIG. 6. Shift of the inhomogeneous line of *n*-hexane frozen at 5 MPa (left) and durene frozen at 1.1 MPa (right) under pressure. Filled symbols: pressure increase, empty symbols: pressure decrease. Corresponding slopes from the least-squares linear fits are −3.72 and −2.59 for *n*-hexane and −2.43 and −2.30 GHz/MPa for durene, temperature: 4.2 K.
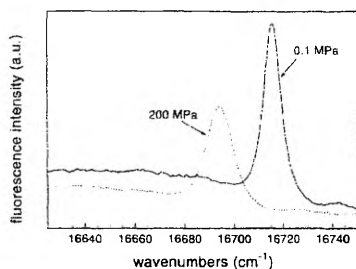
FIG. 7. The 531 cm⁻¹ vibronic replica in the emission spectra of DMST-doped *n*-hexane frozen under 5 MPa. Spectra have been recorded under normal pressure (solid line) and 200 MPa (dotted line), the pressure shift is 3.1 GHz/MPa. No major broadening is observable.

Interestingly, the broadening of the inhomogeneous line under high pressure (200 MPa) is relatively small, on the order of a few GHz/MPa (Fig. 7). It is obvious from the data that, for the Shpol'skii system, everything that is measured depends strongly on the history of the sample. The same is true for the glass but to a lesser extent. The durene data, on the other hand, do not seem to significantly depend on the history.

Figure 5 shows the decrease of the area of the hole with pressure for different freezing pressure levels. The insert shows artificially broadened holes which were used to increase the accuracy of the area determination. Clearly, the area decreases with pressure and the decrease is strongest for the sample frozen under the lowest pressure, very similar to the behavior of the linewidth under pressure.

IV. DISCUSSION

Our results show that the Shpol'skii systems are characterized by very specific features such as irreversible (plastic) deformations under pressure, reduction of the hole area under pressure, and different behavior of holes and inhomogeneous lines under pressure. In the following we focus on the large broadening of the holes as compared to the rather small broadening of the inhomogeneous lines and discuss it in light of recently developed theories.

A. Pressure broadening of spectral holes: The static defect model

Let us briefly recall the models of pressure broadening of spectral holes:[24,25] Pressure broadening is assumed to arise from an inhomogeneous distribution of pressure-dependent coupling coefficients between the probe molecules and the lattice. The transition frequencies of the individual molecules are supposed to be linear and, hence, continuous with pressure. The main difference between the two models[24,25] concerns the way they take into account the strong molecular correlations present in solids. Laird and Skinner[24] start from the pure molecular interaction, hence, correlations between molecules have to be introduced separately. Kikas and Leiger,[25] on the other hand, start from the phenomenological

theory of elasticity which includes molecular correlation automatically. Accordingly, their theory is limited to highly ordered solids, i.e., to crystals with low defect concentrations. In the following, we call their model the "static defect model."

Since the Shpol'skii systems seem to be of crystalline character, we ask whether we can interpret our results within the frame of the static defect model. In the framework of this theory, pressure broadening of spectral holes is attributed to inhomogeneous elastic strain fields which are induced by point defects and which are modified by the applied pressure (diaelastic effect[26]). Note that the observed Lorentzian shape of the inhomogeneous line[27] points to interactions with point defects (elastic dipoles) as the major source of inhomogeneous broadening.[28] The pressure-dependent inhomogeneous strain fields give rise to both inhomogeneous broadening of optical transitions as well as pressure broadening of spectral holes. The magnitude of both effects are determined by the host compressibility and the characteristic features of the defects involved. These latter are the volume V of the defects and the respective change in volume ΔV. For incompressible defects, V can be associated with the volume of the removed host material and ΔV with the change of the cavity volume after substitution of the defect material. We stress that physically reasonable models for defects require $\Delta V/V \lesssim 1$. As shown in detail in Ref. 25, the defect model can, in principle, explain a strong broadening of spectral holes while maintaining the almost unchanged inhomogeneous width. For this one has to assume a balance between defects with positive and negative ΔV. The overall broadening of the inhomogeneous line per pressure is then given by [see Eq. (26) of Ref. 25],

$$d\Gamma/dp \propto \Sigma V_i \ \text{sign}(\Delta V_i), \tag{1}$$

and may be quite small if positive and negative ΔV-values mutually compensate. On the other hand, the broadening of the hole per pressure at the maximum of the inhomogeneous band is roughly given by [see Eq. (35) of Ref. 25],

$$d\Gamma_{\text{hole}}/dp \propto \text{aver}|\Delta V| \text{var}|V/\Delta V|, \tag{2}$$

and may be quite large at high defect densities and/or strong coupling to the optical transition considered. In simpler words, one can say that a large broadening of spectral holes may be balanced by a negative color effect in their shifts, i.e., if the pressure shift is weaker for those probe molecules with the larger solvent shift.

Although the defect model can in principle explain strong pressure broadening of spectral holes while simultaneously maintaining an inhomogeneous width which is rather insensitive to pressure, we have to check whether the characteristic parameter of the defects, namely $\Delta V/V$, is in a physically reasonable range. Following again Ref. 25, it is possible to derive an approximate relation between measurable quantities, such as the inhomogeneous width Γ, the pressure broadening of the hole $d\Gamma_{\text{hole}}/dp$, the bulk compressibility κ, and the defect parameter $\Delta V/V$:

$$\kappa^{-1}\Gamma^{-1}d\Gamma_{\text{hole}}/dp \approx \text{var}(\Delta V/V). \tag{3}$$

Taking the variation var($\Delta V/V$) as a lower limit estimate for $\Delta V/V$ and substituting the experimental values $\Gamma \approx 100$ GHz, $d\Gamma/dp \approx 10$ GHz/MPa and $\kappa \approx 10^{-4}$ MPa^{-1}, one obtains $\Delta V/V \approx 10^3$, a value at least three orders of magnitude too high. We stress that the respective estimates for the ordinary molecular crystals, like durene or benzophenone, are close to unity.[13,20] Hence, the behavior of these materials under pressure shows that the static defect model is physically reasonable and seems to describe the ordinary crystals reasonably well. As to the Shpol'skii systems, however, it fails completely. This failure signals that Shpol'skii systems are indeed very specific materials and cannot be characterized by models suitable for ordinary crystals. We have to look for other, more efficient mechanisms for pressure broadening, explaining other observations as well, for instance, the observed decrease of the area of the hole with increasing pressure.

B. Pressure dependence of hole area: The moving vacancy model

The reversible decrease of the area of the hole is a surprising observation which seems to be characteristic for the Shpol'skii systems[14] and which cannot be accounted for within the frame of the models.[24,25] It should be stressed that a destabilization of the photoproduct with increasing pressure and a subsequent enhanced back reaction from the product state to the educt state can be ruled out in the present experiments, although such a process is possible and was observed for chlorine doped n-octane at a pressure level of 500 MPa.[14] In our case, the reduction of the hole area with increasing pressure is due to a redistribution of part of the hole area over a much wider spectral range within the inhomogeneous line. In order for this to occur, special degrees of freedom with special properties are required:

(1) They must be bistable and must, of course, interact with the probe molecule. In addition to bistable defects which account for the reversible pressure deformation, there must also be multistable defects which account for the irreversible deformation. These multistable defects could be induced by defect–defect interactions if their concentration is sufficiently high.

(2) There must be a strong correlation between probe molecules and the density of these degrees of freedom. More precisely, the spatial density of pressure-induced flips must be higher in the neighborhood of the probe molecules as compared to the average density. Such an increased density would account for large spectral shifts, which reduce the area.

Some of these degrees of freedom must reversibly change their state already at very low pressure levels.

As possible candidates for such defects we propose vacancies in the host lattice. Let us check whether they comply with the above requirements:

(1) Under certain conditions, vacancies can hop from one lattice site to another. In an ideal lattice these sites are energetically equivalent. Since vacancies are defects, they give rise to strain fields which mediate the interaction with the dye probes.

(2) The required correlation of probe and defect can be understood in the following way: The vacancies are formed during the crystallization process. Moreover, they are mobile in the solid state. Their mobility, of course, depends on the temperature of the system. Just below the crystallization temperature their mobility is highest. Suppose the respective interaction with the probe is positive. In this case the system will lower its energy by pushing the vacancies away from the probe. As a consequence, a vacancy-free zone is created around the probe with a radius R_c. R_c is determined by the fact that for $R > R_c$ the probe–vacancy interaction has dropped below a level too small to move a defect further. However, around R_c an increased density of vacancies has piled up, as required. Similar arguments can be used in case the interaction is attractive. In this case it is plausible that the density of defects in the neighborhood is higher as compared to the average density.

(3) External hydrostatic pressure applied to the system creates additional internal strain fields around the probe which change the probe–vacancy interaction,[25,26] and, hence, may induce a vacancy hopping. Note, that due to the statistical nature of the internal strain fields, some of the vacancies are already tuned very closely to the hopping threshold so that only a minor pressure change is needed to force them into a new position.

The model of probe correlated vacancies as specific defects for Shpol'skii systems could account for many of the observed features:

(a) First of all, it gives a simple explanation of the observed differences between shift and broadening of the hole and the inhomogeneous line. The pressure-induced shift of the inhomogeneous line is governed both by spectral hopping (redistribution), caused by pressure-induced jumps in the nearby vacancy zone, and by "diffusional" dynamics from more distant defects. However, only the latter contributes to the hole shift.

(b) The same reasoning applies to the broadening as well. In fact, the proposed mechanism of pressure broadening of holes has much in common with spectral diffusion caused by moving defects as considered in Ref. 29. Pressure as an inducing force for such a dynamics, however, gives to the process a reversible character in contrast to thermal mechanisms.

(c) The observed reversible decrease of hole area is explained naturally by large (as compared to the hole-width) spectral jumps of probe molecules induced by dynamics of nearby defects. Note, that models which assume strongly nonlinear in pressure compressibility of frozen n-alkanes, and thus largely different pressure coefficients of the probe transition energy, for different pressure regions, can, in principle, account for the fea-

tures A and B, but fail completely to describe this observation.

Related to Shpol'skii systems, there are other experimental observations, such as unusual thermal line broadening in pressurized perylene *n*-octane solid solution[30] and single molecule spectral hopping,[12] which all hint at the existence of some nonphononic degrees of freedom in these systems. It seems reasonable to assume that in all these observations (including ours) dynamics (thermal or pressure-induced) of specific defects of frozen *n*-alkanes shows up.

V. CONCLUDING REMARKS

Shpol'skii crystals are peculiar systems which show very specific spectral features when put under pressure. We showed that this behavior can not be understood on the basis of models adequate for ordinary molecular crystals. In our view, Shpol'skii matrices are very weakly bound crystalline systems with an unusual high density of vacancies. It is the vacancies which are responsible for the fact that Shpol'skiis exhibit unusual elastic–plastic properties and share common features with both crystals and glasses.

ACKNOWLEDGMENTS

[1] E. V. Shpol'skii, Sov. Phys. Usp. **3**, 372 (1960).
[2] E. V. Shpol'skii, Sov. Phys. Usp. **5**, 522 (1962).
[3] E. V. Shpol'skii, Sov. Phys. Usp. **6**, 411 (1963).
[4] K. Rebane, P. Saari, and T. Tamm, Izv. AN ESSR, Fiz. Mat. **19**, 251 (1970).
[5] R. I. Personov, I. S. Osadko, E. D. Godyaev, and E. I. Al'shits, Sov. Phys. Solid State **13**, 2224 (1972).
[6] S. Voelker, R. M. Macfarlane, A. Z. Genack, and H. P. Trommsdorff, J. Chem. Phys. **67**, 1759 (1977).
[7] T. B. Tamm, Ya. V. Kikas, and A. E. Sirk, J. Appl. Spectrosc. **24**, 218 (1976).
[8] J. W. Hofstraat, I. L. Freriks, M. E. J. de Vreeze, C. Gooijer, and N. H. Velthorst, J. Phys. Chem. **93**, 184 (1989).
[9] T. Attenberger, U. Bogner, and M. Maier, Chem. Phys. Lett. **180**, 207 (1991).
[10] P. Geissinger, S. Reul, D. Haarer, and K. Rieckhoff, Chem. Phys. Lett. **190**, 67 (1992).
[11] G. Gradl, B. E. Kohler, and C. Westerfield, J. Chem. Phys. **97**, 6064 (1992).
[12] L. Kador, Phys. Status Solidi **189**, 11 (1995); A. Myers and W. E. Moerner, J. Phys. Chem. **98**, 10377 (1994); W. E. Moerner, T. Plakhotnik, T. Irngartinger, M. Croci, V. Palm, and U. P. Wild, *ibid.* **98**, 7328 (1994); T. Plakhotnik, D. Walser, M. Pirotta, A. Renn, and U. P. Wild, Science **271**, 1703 (1996).
[13] G. Gradl, A. Feis, and J. Friedrich, J. Chem. Phys. **97**, 5403 (1992).
[14] A. Ellervee, J. Kikas, A. Laisaar, V. Shcherbakov, and A. Suisalu, J. Opt. Soc. Am. B **9**, 972 (1992).
[15] A. Ellervee, J. Kikas, A. Laisaar, and A. Suisalu, J. Lumin. **56**, 151 (1993).
[16] Th. Sesselmann, W. Richter, and D. Haarer, Europhys. Lett. **2**, 947 (1986).
[17] Th. Sesselmann, W. Richter, D. Haarer, and H. Morawitz, Phys. Rev. B **36**, 7601 (1987).
[18] Th. Sesselman, W. Richter, and D. Haarer, J. Lumin. **36**, 263 (1987).
[19] G. Gradl, J. Zollfrank, W. Breinl, and J. Friedrich, J. Chem. Phys. **94**, 7619 (1991).
[20] P. Schellenberg, J. Friedrich, and J. Kikas, J. Chem. Phys. **100**, 5501 (1994).
[21] D. M. Burland and D. Haarer, IBM J. Res. Dev. **23**, 534 (1979).
[22] C. Borczyskowski, A. Oppenländer, H. P. Trommsdorff, and J.-C. Vial, Phys. Rev. Lett. **65**, 3277 (1990).
[23] K. Orth, F. Rohlfing, and J. Friedrich, Z. Phys. B **95**, 493 (1994).
[24] B. B. Laird and J. L. Skinner, J. Chem. Phys. **90**, 3274 (1989).
[25] J. Kikas and K. Leiger, J. Chem. Phys. **104**, 5384 (1996).
[26] C. Teodosiu, *Elastic Models of Crystal Defects* (Editura Academiei, Bucuresti; Springer, Berlin, 1982).
[27] F. Rohlfing, Thesis, Bayreuth, 1994.
[28] A. M. Stoneham, Rev. Mod. Phys. **41**, 82 (1969).
[29] J. Kikas and J. L. Skinner, Chem. Phys. Lett. **230**, 429 (1994).
[30] O. N. Korotaev, I. P. Kolmakov, M. F. Shchanov, V. P. Karpov, and E. D. Godyaev, JETP Lett. **55**, 424 (1992).

III

Pressure-Induced Broadening of Spectral Holes in Molecular Crystals and Glasses as a Measure of Disorder

J.KIKAS[1] and K.LEIGER[1,2]

[1]*Institute of Materials Science, University of Tartu, Tähe 4, 51010 Tartu, Estonia*
[2]*Institute of Physics, University of Tartu, Riia 142, 51014 Tartu, Estonia*

Experimental evidence on local elastic properties of disordered molecular solids is far from being exhaustive. In this report we discuss the potentialities of persistent spectral hole burning (SHB) [1] to contribute to these studies. SHB provides a sensitive tool for studying small shifts of impurity energy levels in solids. In so called pressure tuning experiments [2] the hole is burnt at a frequency ν_i and recorded at the initial hydrostatic pressure value p_1. After this pressure is set to a new value $p_2 = p_1 + \Delta p$ and the hole is recorded again. The extreme narrowness of spectral holes makes them sensitive to minor changes in physical conditions, e.g. changes in hydrostatic pressure as small as $\Delta p = 0.1$ MPa (1 bar) may have observable effects on holes [3]. Beside the shift of the hole maximum $\Delta \nu = \nu_2 - \nu_1$ more or less expressed broadening of holes is observable in pressure tuning experiments as well. Such broadening reflects the inherent inhomogeneity of the subensemble of molecules with a fixed transition energy and, hence, can be used as a measure of disorder in solids.

Hole broadening in molecular systems: experimental evidence. Different types of solids (crystals, glasses) exhibit large variations in the magnitude of pressure broadening of holes (see Fig. 2a). For a direct study of the influence of structural disorder we have compared the pressure-tuning features of spectral holes in crystalline and glassy phases of polymorphic benzophenone [4]. In the glassy phase the hole broadening $d\Gamma/dp \approx 3$ GHz/MPa and exhibits a weak dependence on frequency within the broad spectral band. The crystalline phase spectrum consists of a number of narrow lines ascribed to different local environments (sites). Within a single line the pressure broadening is about two orders of magnitude smaller, varying from line to line (0.01-0.05 GHz/MPa). However, the dispersion of pressure *shifts* $d\nu/dp$ for all sites around an averaged frequency dependence yields a much higher value of about 0.6 GHz/MPa, comparable to the broadening in glass. Thus the pressure broadening in glass may be understood as arising from disorder in the vicinity of probe molecule. Still the results point to some differences in the statistics of «crystalline» and «glassy» sites.

Diaelastic mechanism of hole broadening in crystals. Proceeding from the preposition of (microscopically) homogeneous compression Laird and Skinner have developed a statistical theory [5] of pressure-tuning experiments on spectral holes in glasses. Within the scope of this theory the pressure broadening of spectral holes can be understood as a result of breaking the scaling between attractive (r^{-6}) and repulsive (r^{-12}) intermolecular interactions. A complication for the theory [5] is the account of strong molecular correlations in solids. In order to describe the pressure broadening of spectral holes in crystals we used a different approach proceeding from the elastic models of crystalline defects and taking into account the so called diaelastic effect [6]. If an elastic solid contains a region with compressibility different from the bulk one (an elastic inclusion), the application of hydrostatic pressure induces a spatially inhomogeneous strain field around the inclusion. Considering point defects as spherical inclusions, we can describe the effect of pressure on spectral holes.

As a result, we get the r^{-3} defect-probe interaction, giving for the inhomogeneous broadening a Lorentzian shape. As to the spectral holes no pressure broadening arises if the coupling coefficients are equal for all the defects (defects of the same type). To analyse the

possible effect of dispersion of the coupling parameters, we considered the case of two defect types. It yields a hole broadening and, possibly, splitting with pressure (Fig. 1). The latter is obviously an effect specific to the systems with two defect types. However, the main idea is that the pressure broadening of spectral holes can be explained by dispersion of certain parameters of the sources of inhomogeneous strains (in our case the point defects).
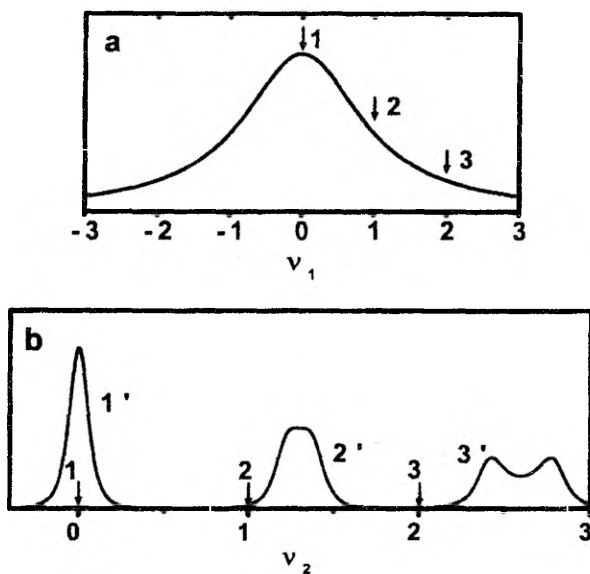

Figure 1. Pressure kernel for the interaction with two types of point defects. The inhomogeneous frequency distribution at the initial pressure is depicted at the top (a). The arrows 1–3 indicate the initial frequencies for which the frequency distributions (pressure kernels) after a certain pressure variation are depicted (b, curves 1'–3'). The distributions are normalised to the same area. Note that the splitting occurs at larger deviations from the line maximum.

We call the pressure broadening mechanism of this type the dispersive mechanism. Also the Laird-Skinner model belongs to this category. More generally, we can describe such a mechanism by assigning a statistical distribution to pressure coefficients $d\nu/dp$ of individual molecules. An important point is that the homogeneous lines corresponding to individual probe molecules shift linearly with pressure (fixed pressure coefficients).

Frozen n-alkanes: failure of the dispersive mechanism. While many crystalline systems fit well into the dispersive model of pressure broadening, there exist other examples. Our pressure tuning experiments [7] on a Shpol'skii system, n-hexane, doped with dimethyl-s-tetrazine (DMST) revealed a large pressure broadening of spectral holes, in contrast with quite a moderate pressure broadening of the inhomogeneous band as a whole (Fig. 2). In fact, it can be shown by a simple argument
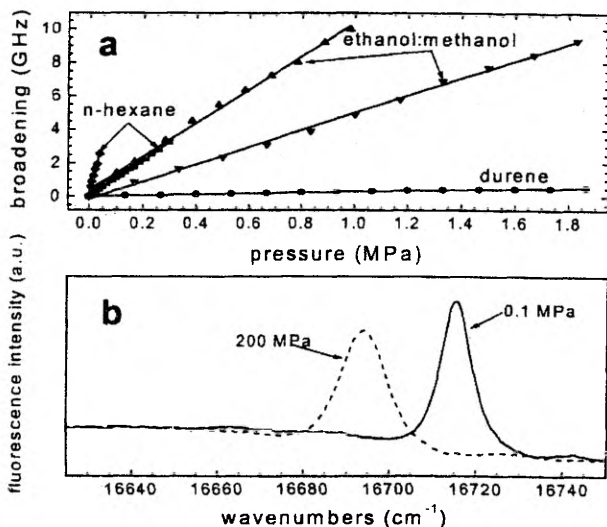
Figure 2. (a) Pressure-induced hole broadening of DMST-doped n-hexane frozen at 0.3 MPa (diamonds, slope of the least-squares linear fit 65 GHz/MPa) and 5 MPa (squares, 11 GHz/MPa), ethanol:methanol glass frozen at 0.3 MPa (up triangles, 10 GHz/MPa) and 5 MPa (down triangles, 5.2 GHz/MPa), and durene crystal (circles, 0.27 GHz/MPa). (b) The 531 cm^{-1} vibronic replica in the emission spectra of DMST-doped n-hexane frozen under 5 MPa. Spectra have been recorded under normal pressure (solid line) and 200 MPa (dashed line), the pressure shift is 3.1 GHz/MPa. No major broadening is observable.

that the dispersive model fails to explain such a situation leading to unphysical values of the defect parameters. It is possible to derive an approximate relation between the measurable quantities, such as the inhomogeneous width Γ_{ih} of the spectral line, the pressure broadening of the hole dΓ/dp, the bulk compressibility κ, and the defect parameter $\Delta V/V$ (relative volume defect):

$$\kappa^{-1} \Gamma_{ih}^{-1} \, \mathrm{d}\Gamma/\mathrm{d}p \approx \mathrm{var}(\Delta V/V).$$

Taking the variation var($\Delta V/V$) as a lower limit estimate for $\Delta V/V$ and substituting the experimental values $\Gamma_{ih} \approx 100$ GHz, dΓ/d$p \approx 10$ GHz/MPa and $\kappa \approx 10^{-4}$ MPa^{-1}, one obtains $\Delta V/V \approx 10^{3}$, a value at least three orders of magnitude too high.

To account for this unexpectedly large hole broadening, we proposed a new mechanism of hole broadening with pressure. It involves spatially (or otherwise) bistable (possibly multistable) vacancies within the host lattice that change their positions and/or are created (destroyed) reversibly with pressure changes. This modifies the transition energies of probe molecules and thus shifts the corresponding homogeneous lines. Within such a model is possible to explain the difference between the pressure broadening of the hole and that of the inhomogeneous line: dopants can perform finite spectral jumps «out of the hole» towards the band maximum. Such a preposition is supported by the observed reversible area reduction of spectral holes with pressure.

Within the frame of this model it is not appropriate to speak of pressure coefficients of individual homogeneous lines. Instead, each of them undergoes quite a random spectral motion as the pressure changes. In other words, we are dealing with pressure-induced

(reversible!) spectral diffusion. We therefore call the hole-broadening model based on this mechanism the diffusive model.

Dispersive or diffusive mechanism: how to distinguish? In general, it may not be easy to establish which of the two mechanisms (diffusive or dispersive) is operative, in a particular case: one observes some hole shift and broadening all the same. We have designed an experimental procedure [8] to distinguish between these two possible mechanisms. The method is based on non-linear saturation properties of the hole burning process. The proposed four-step procedure consists of burning a hole, applying hydrostatic pressure to the system, additional burning at the hole minimum at this second pressure, and then applying more pressure. By model calculations we have demonstrated (Fig. 3) that under certain conditions (sufficient pressure and optimal dose values), the dispersive model yields a double-minimum hole, while the diffusive model does not.
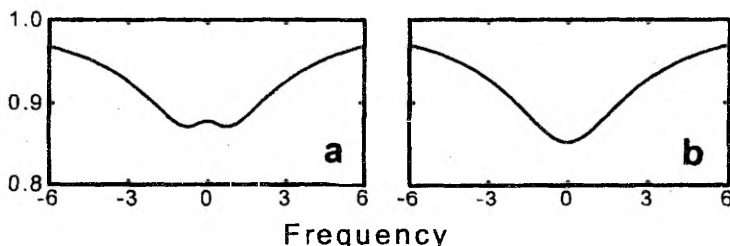

Figure 3. The calculated hole shapes for the four-step procedure for dispersive and diffusive mechanisms (a and b, correspondingly). The frequency is in units of homogeneous linewidths; the intensity of the spectrum is normalised to its initial value.

Conclusions. The existing data point to a peculiar intertwining of continuity and discontinuity, reversibility and irreversibility in pressure-induced microscopic processes in disordered molecular solids. Spectral hole burning seems to be a versatile technique for the studies of these effects.

[1] W. E. MOERNER (Editor), *Persistent Spectral Hole-Burning: Science and Applications*, (Springer-Verlag, Berlin) 1988.
[2] Th. SESSELMANN et al., Phys. Rev. B, **36** (1987) 7601.
[3] A. ELLERVEE et al., J. Opt. Soc. Am. B, **9** (1992) 972.
[4] P. SCHELLENBERG et al., J. Chem Phys., **100** (1994) 5501.
[5] B. B. LAIRD and J. L. SKINNER, J. Chem. Phys., 90 (1989) 3274.
[6] J. KIKAS and K. LEIGER, J. Chem. Phys. **104** (1996) 5384.
[7] J. FRIEBEL at al., J. Chem. Phys. **108**, (1998) 1830.
[8] K. LEIGER and J. KIKAS, J. Chem. Phys., submitted.

IV

Pressure effects on the spectra of dye molecules in incommensurate and commensurate phases of biphenyl,
V. Zazubovitch, A. Suisalu, K. Leiger, A. Laisaar, An. Kuznetsov, J. Kikas,
Chem. Phys. (submitted).

Pressure effects on the spectra of dye molecules in incommensurate and commensurate phases of biphenyl

V. Zazubovich [a,b,†], A. Suisalu [a], K. Leiger [a,b], A. Laisaar [a], An. Kuznetsov [a], J. Kikas [b,*]

[a] *Institute of Physics, University of Tartu, Riia Street 142, 51014 Tartu, Estonia*
[b] *Institute of Materials Science, University of Tartu, Tähe Street 4, 51010 Tartu, Estonia*

[†] Present address: Department of Chemistry and Ames Laboratory–U.S. Department of Energy, Iowa State University, Ames, Iowa 50011, USA

[*] Corresponding author. Tel.: +372-7-375-541; fax: +372-7-375-540. E-mail address: jaakk@physic.ut.ee (Jaak Kikas).

Abstract

Low-pressure tuning of spectral holes, burned in the spectra of chlorin molecules doped into polycrystalline biphenyl, was studied for the incommensurate phase III of biphenyl at $T = 2$ K and $P = 0.1–2.5$ MPa. A blue pressure shift of holes burned in the outermost red line of an inhomogeneous spectral triplet was found, in contrast to the red pressure shifts of the other two lines. Extrapolation of these shifts to higher pressures shows the convergence of that triplet at a pressure above 200 MPa. Such a behavior was confirmed by high-pressure measurements of the luminescence emission and excitation spectra at $T = 4.2$ K and P up to 270 MPa. The pressure variation of the spectral splitting between the most blue and red lines in the triplet was found to obey a power law with a critical exponent $n = 0.39$. This value is close to those obtained for incommensurate biphenyl from NMR and EPR experiments in the temperature domain. The results prove that the optical spectra reflect an interaction of the impurity molecule with the incommensurate modulation wave in biphenyl host matrix disappearing at transition to the normal commensurate phase.

1. Introduction

Incommensurate systems [1,2] represent a specific class of solids showing a long-range order but lacking the translational lattice periodicity of crystals. In these systems some property (e.g., relative arrangement of neighboring atoms or molecules) is modulated with a period incommensurate with that of the crystal lattice, i.e. the period of modulation is not an integer multiple of the crystal unit cell size. As such, incommensurate systems are interesting intermediates between ordinary periodic crystals and aperiodic amorphous solids or noncrystalline biopolymers. They show a number of new phenomena, which are found neither in regular crystals nor in glasses.

1

In most systems exhibiting incommensurate behavior, the incommensurate phase exists in quite a narrow temperature interval between an ordinary higher-temperature commensurate phase and a low-temperature lock-in phase, which is commensurate again, but generally has a larger unit cell. Incommensurate biphenyl is one of a few systems where such lock-in transition to a low-temperature commensurate structure has not been observed down to the lowest temperatures (60 mK [3]). This makes it a suitable subject of investigation by using a powerful method of spectral hole burning (SHB) [4,5]. (Note that some of the recent results concerning temperature broadening and thermal cycling of spectral holes in doped biphenyl can be found in our papers [3,6]).

SHB in combination with hydrostatic pressure has been successfully applied to studies of crystals [7,8,9] (including Shpol'skii systems [7,9]), organic glasses [8,10,11], polymers [12,13] and more complicated biological systems (proteins [14], photosynthetic complexes [15-18]), see also recent reviews [19-20]. The low-pressure tuning of spectral holes [7-16,19,20] is better suited for investigation of the unperturbed interaction mechanisms and properties of solids, whereas from high-pressure SHB studies [7,17-27], performed at fixed pressures of some kilobars (1 kbar = 0.1 GPa = 100 MPa), one can learn, how pressure modifies processes in solids and alters their characteristics (e.g., density of states for soft localized vibrational modes in glasses [25]).

Biphenyl (diphenyl, phenylbenzene) $C_6H_5C_6H_5$ is a crystalline nonpolar aromatic molecular compound, being the first member in the series of so-called *para*-polyphenyl (oligophenyl) crystals (biphenyl, *p*-terphenyl, *p*-quaterphenyl, ...). Each molecule of biphenyl consists of two phenyl groups C_6H_5- connected by a single C–C bond in *para* position. Due to the strong pairwise interaction between the central four *ortho* hydrogen atoms (electrostatic repulsion between two closest H atoms on both sides of the C–C bond), isolated molecules of biphenyl in the gas phase are nonplanar, the twist angle between the planes of two phenyl rings being as great as about 42° (see, e.g., [28]). In the solid state of biphenyl this angle is much smaller or even zero, depending on the crystalline phase existing at a given temperature and pressure. The transitions between these phases and also dynamics in different phases have been extensively studied by using absorption and fluorescence spectroscopy [29,30], Raman [31,32] and neutron [33-35] scattering as well as NMR [36,37] and EPR [38,39] techniques.

At ambient pressure and temperatures between 40 K and the melting point of biphenyl (~70°C), it is found in a normal, commensurate phase (high-temperature phase C I). In this phase biphenyl crystals have a monoclinic structure with space group $P2_1/a$ (C_{2h}^5) and two molecules in the unit cell.

2

Owing to a strong enough interaction between adjacent biphenyl molecules in the solid state, the equilibrium configuration of all molecules is on the average planar, as was shown by X-ray diffraction [40], but the two phenyl rings in every molecule perform large torsional (twisting) motions relative to each other out of this equilibrium plane.

When the temperature is lowered, a phonon mode related to the twist motion becomes soft and freezes in around 40 K, causing a second-order phase transition to the doubly incommensurate structure (phase IC II), characterized by two different incommensurate wave vectors of the frozen-in modulation (see, e.g., [37]). Here the twist angle in each molecule varies sinusoidally throughout the whole crystal volume. The maximal twist angle 2φ between two phenyl rings in a molecule is strongly temperature-dependent, being about zero at 40 K and increasing up to the value $2\varphi \approx 10°$ around 17 K [37].

At 17 K a partial lock-in transition to another incommensurate structure (phase IC III) takes place, characterized by a single frozen-in modulation wave vector [41]. This phase transition IC II → IC III was found to be of the first order [41]. In deuterated biphenyl $C_6D_5C_6D_5$, at atmospheric pressure, both these transitions occur at temperatures of 37 K and 20 K, respectively [33,42] (also slightly different values 38 K and 21 K can be found [32,43]).

As was shown in several experimental [32,33,42,44-50] and theoretical [51-53] studies, the phase transition temperatures T_{I-II} and T_{II-III} rapidly decrease with increasing hydrostatic pressure in the range 0.1–200 MPa. In Fig. 1 we reproduce the known data points on the phase diagram for ordinary (hydrogenated) biphenyl as well as much more numerous points for its deuterated counterpart $C_6D_5C_6D_5$, which is easier to study, especially in neutron scattering experiments. This figure was redrawn from the latest publication [32] by Cailleau's group on the phase transitions in biphenyl (see Fig. 2 in [32]) with some modifications: addition of a few phase transition points from other works and representation of the corrected (at pressures below 60 MPa) melting/solidification line of helium (it is well known that at $T \to 0$ K liquid ^{4}He solidifies under pressure of about 2.5 MPa and not ~16 MPa as can be seen from Fig. 2 of Ref. [32]). For the temperatures down to 2 K, the melting temperature and pressure values of ^{4}He were taken from the paper [54] (the values of T_{ms} and P_{ms} from Table VI of Ref. [54]). At the lowest temperatures between 0.3 and 2 K, the very precise data points from Ref. [55] were plotted.

As can be seen from Fig. 1, the C I – IC II phase transition line with many experimental points for deuterated biphenyl terminates at the point $P \approx$ 185 MPa, $T \to 0$ K. The same critical pressure value (as well as the whole transition line) is also given in papers [33,42,45,47], whereas somewhat lower value of about 170 MPa is reported in [44,51,52]. Standing separately are

results obtained in [53] where it was stated that the phase transition temperature T_{I-II} drops to absolute zero at pressures of about 150 and 135 MPa for deuterated and hydrogenated biphenyl crystals, respectively (see Fig. 1 where corresponding theoretical transition lines [53] and experimental points [49] are reproduced).

On the other hand, from the report [48] one finds that T_{I-II} decreases to 0 K at about 180–190 MPa for both biphenyl modifications, while T_{II-III} approaches zero at about 40 MPa for deuterated and at about 20 MPa for hydrogenated compound. In the absence of new, more reliable data, we adopt in this study for our purposes the pressure value $P \approx 180$ MPa at $T \to 0$ K for the C I – IC II phase transition in hydrogenated biphenyl. Note that both the pressures and temperatures needed for generating the phase transitions C I – IC II and IC II – IC III in biphenyl are well within the reach of SHB experiments, which makes this material also appealing for SHB studies of phase transitions (see [24] for related results on doped *p*-terphenyl).

This work, involving investigation of the ordinary optical spectra and the hole burning spectra of doped biphenyl under pressure, was intended to lend some further support to the view that observable spectral features are manifestations of the incommensurate character of biphenyl at low temperatures.

2. Experimental

An organic dye chlorin (7,8-dihydroporphin) was used as a dopant in this study. A small amount of chlorin was dissolved in hydrogenated biphenyl at a concentration of about 10^{-4} mol/mol. A polycrystalline sample was obtained by slowly cooling the molten biphenyl down to the room temperature. In the SHB experiments, all performed at 2 K, the range of applied pressures did not exceed 2.5 MPa (25 bar), which is well below the solidification pressure of 3.8 MPa at 2.0 K for ^{4}He, used as the pressure transmitting medium (see the melting line of ^{4}He in Fig. 1 and also Tables V and VI in Ref. [54]). The sample was kept in a small two-window pressure cell under a variable (tunable) pressure of liquefied helium, condensed inside the cell from gaseous state. The pressure cell was placed in a helium-bath cryostat where the temperature of liquid helium surrounding the cell was stabilized at 2.0±0.1 K. Every spectral hole under study was first burned and recorded at atmospheric pressure. Thereafter the pressure was raised stepwise up to about 2–2.2 MPa and at each pressure value the same hole was repeatedly recorded. The results were well reproducible and after the pressure release the hole entirely restored its spectral position and shape (width). All the holes were burned and measured using a Coherent Radiation CR-699-29 single-frequency tunable ring dye laser with the linewidth of about 1 MHz. For burning the power density at the sample

4

was about 100 µW/cm^2, whereas for recording it was reduced by a factor of ~50. Obtained transmission spectra were converted to optical density and the holes were fitted to Lorentzian curves. Rigorously speaking, the pressure tuning of spectral holes needs not preserve their Lorentzian profiles [7,56]. However, as far as our main interests in this study were limited to the pressure-induced shifts of holes and only qualitatively also to their broadening, it is of little importance here.

Complementary to SHB measurements, the ordinary photoluminescence emission and excitation spectra were measured at high pressures up to 270 MPa. In this case a special high-pressure low-temperature system was used. It consists of a 1500-MPa helium gas compressor, a high-pressure cell with three sapphire windows and a temperature-controlled liquid-helium cryostat. The pressure cell with a sample inside it was placed into the cryostat and filled with compressed gaseous helium at room temperature through a flexible capillary tube connecting the cell and compressor. Then the cell was cooled down to the measurement temperature, 4.2 K, by liquid helium surrounding the cell in cryostat. Meanwhile the gaseous helium inside the pressure cell solidified at a certain temperature depending on an initial pressure of gas (see the melting/freezing line for ^{4}He in Fig. 1). Emission spectra of the compressed sample were recorded with a DFS-24 double-grating spectrometer under broad-band excitation (a powerful Xe lamp + UV filters). For measuring excitation spectra the sample was excited through a MDR-6 monochromator. Further experimental details of our high-pressure measurements can be found elsewhere [7,21-24].

3. Results and discussion
3.1. The inhomogeneous spectra

The luminescence emission and excitation spectra of chlorin impurity in biphenyl at $T = 4.2$ K are presented in Fig. 2 for ambient pressure [spectra (a) and (b)] and high pressures of 260 and 270 MPa [spectra (c) and (d), respectively]. The ambient-pressure spectrum, belonging to the incommensurate phase IC III of biphenyl, contains a triplet of resonant lines (peak 1 at 15 829, peak 2 at 15 849 and peak 3 at 15 861 cm^{-1}) observed at the same positions in both emission and excitation spectra. The basic question to interpret these spectra is: does the ambient-pressure triplet in the inhomogeneous spectrum correspond to different substitutional sites or is it a manifestation of interaction of an impurity molecule with the incommensurate modulation wave? By analogy with incorporation of perylene impurity in biphenyl host matrix [57] and terrylene in *p*-terphenyl [58], which is isomorphic with biphenyl, we assume that each chlorin molecule replaces a

pair of biphenyl molecules along the *b* axis of a monoclinic unit cell, as sketched in Fig. 3. Still its orientation in the crystal lattice of biphenyl remains unclear. Obviously, for the depicted orientation a 180° rotation yields a spectrally identical position. However, it is not excluded that some other, more stable orientations may be possible. The high-pressure spectra of the C I commensurate phase [Fig. 2(c) and (d)], exhibiting a *single* resonant line, however, give a strong support to the idea that there exists only one major substitutional site for chlorin in the commensurate lattice and that the ambient-pressure splitting arises from incommensurability.

Another evidence in this line stems from the fact that the solvent shift for chlorin in biphenyl is rather small (compare frequencies for peaks 1-3 with the vacuum frequency for a free chlorin molecule of 15 912 cm^{-1} from supersonic jet experiments [59]). Even though chlorin molecules are significantly larger than biphenyl molecules, they are relatively undisturbed in the biphenyl matrix. This, in turn, justifies the suggestion that the incommensurate structure of bulk biphenyl is probably not too strongly disturbed by chlorin dopant molecules and therefore this structure may manifest itself in the probe spectra.

Proceeding from the idea that the observed ambient-pressure spectrum is related to incommensurability, the triplet shape of this spectrum raises further questions. First, we note that a simple sinusoidal modulation (plane wave limit [1]) should give rise to a specific spectral shape with *two* edge singularities, i.e., to a doublet. Indeed, such a doublet spectrum was observed in ^{2}H NMR experiments for deuterated biphenyl in both IC II and IC III phases [37]. A certain increase in the relative intensities of these two edge singularities as compared to the central part of the NMR spectrum, observed by lowering the temperature [37], is much in line with what one would expect as a consequence of "squaring up" of the modulation wave [28]. On the contrary, for phenanthrene probe molecules in IC II and IC III phases of biphenyl, studied by EPR spectroscopy, it was noticed that introduction of a middle ("commensurate") component was needed for proper description of the spectra [39]. Such a triplet spectrum can originate from a variety of different mechanisms:

(i) It may arise from the situation where almost commensurate regions with constant φ (the twist of either phenyl ring from the planar, on average, configuration of the biphenyl molecule) alternate with the incommensurate regions (discommensurations) where φ is changing. Such a situation is also called the broad soliton case [1] and it is intermediate between the narrow soliton (domain wall) and plane wave (sinusoidal modulation) regimes. The middle peak in the spectra is then due to the dopant molecules located in the commensurate regions and the two other (outermost) peaks arise from the edge singularities in the energy distribution due to incommensurate modulation

inside discommensurations. The above-discussed NMR data and other evidence on the harmonic (plane wave) modulation in biphenyl seem, however, to rule out this possibility.

(ii)   An alternative explanation for the triplet formation assumes sites being equivalent in the high-temperature structure with lattice constant a and becoming non-equivalent in the low-temperature higher-order commensurate structure with $a' = 3a$. Such an effect was theoretically treated in [1] and observed for Rb_2ZnCl_4 in nuclear quadrupole resonance experiments [60]. For biphenyl, however, the wave vector of the incommensurate modulation (~0.46b^* [41,45]) is quite different from the value $b^*/3$ needed in the above model [1,60] (here b^* denotes the reciprocal lattice vector).

(iii)   Still another possibility may be the pinning of the modulation wave by dopant molecules. As far as the probe–host interaction energy depends on φ, the phase distribution *at the probe location* is not uniform even in the plane wave limit, but is weighted by the respective Boltzmann factor. Such a possibility was discussed in the above-cited work on EPR [39] where the phenanthrene probe apparently introduced quite a strong perturbation. Such a mechanism may likely explain our results as well. The view that the middle peak may be a dopant-dependent feature is further supported by our results on Zn-chlorin dopant in biphenyl, where only a doublet structure in the spectra is observed [61].

(iv)   Formally, additional spectral peaks may also arise from a non-monotonous dependence of the frequency v of an electronic transition in the probe molecule on the twist angle φ. However, owing to the small amplitude of φ variation (2φ does not exceed ~10° [37]) this seems to be rather unlikely (some further counterevidence can be found in Subsection 3.3).

(v)   When comparing the overall shape of the experimental spectrum to that predicted by theory [1], one must in addition keep in mind that the experimental spectrum is in fact a convolution of the inhomogeneous site distribution function with the single-site profile which includes a rather intensive phonon sideband [62].

3.2. Pressure tuning of spectral holes

Spectral hole burning was carried out in all three lines studied (peaks 1-3). The recorded hole shifts with pressure for these lines are depicted in Fig. 4. A surprising observation is a positive (to higher frequencies, or blue) shift detected for holes burned in peak 1 (15 829 cm^{-1}), i.e. for the most red line, in contrast to negative or red shifts of holes burned in more blue peaks 2 and 3. The pressure coefficients for these three lines turned out to be rather diverse: +2.71 GHz/MPa or about +9 cm^{-1}/kbar (1 cm^{-1} = 30 GHz) for peak 1, –0.94 GHz/MPa for peak 2 and –1.74 GHz/MPa for peak 3.

A simple model for pressure tuning of spectral holes (see, e.g., [13]) treats the pressure shift as a small addition to the solvent shift. The frequency of electronic transition in an impurity molecule doped into a solid matrix differs from that in the vacuum due to interactions of that molecule with neighbouring host molecules. This frequency difference is just a quantity called the solvent (or gas-to-solid) shift. We can consider a molecule in the vacuum as having its surroundings moved off to an infinitely large distance. Then the effect of environment can be simulated by gradually reducing this distance down to the equilibrium spacings in the real host matrix. The applied external pressure further decreases distances between the probe and host molecules, and thus the additional frequency shift induced by this pressure should change the electronic transition frequency in the same direction as does the solvent shift. More quantitatively such an approach relates the pressure shift $d\nu/dP$ to the solvent shift $\nu_b - \nu_0$ (where ν_b and ν_0 are the hole burning frequency and the transition frequency in a free molecule, respectively) via a simple relation [13,63]

$$d\nu/dP = 2\kappa(\nu_b - \nu_0),$$

(1)

where $\kappa = (-1/V)(\partial V/\partial P)_T$ is the local volume compressibility, so that the larger the solvent shift, the larger also the pressure shift in the system under study. This simple linear relation holds surprisingly well for glasses [8,63] and, as a tendency, characterizes the pressure shifts for different discrete sites in crystalline samples as well [8].

Usually the solvent shift is negative ($\nu_b - \nu_0 < 0$) and hence the pressure shift is also negative, i.e. to the red. Only in a few cases blue pressure shifts have been observed, e.g., for protoporphyrin IX substituted myoglobin in water/glycerol glass and for protoporphyrin IX in dimethylformamide/glycerol glass [64]. In these cases, however, they occurred for dopant molecules exhibiting an unusual positive solvent shift $\nu_b - \nu_0 > 0$. For chlorin in biphenyl, as mentioned above, a positive pressure shift was detected for the line with the *lowest* peak frequency and hence with the largest negative solvent shift (remind that ν_0 for chlorin molecule is equal to 15 912 cm^{-1} [59]), although according to Eq. (1), the largest (by absolute value) *negative* pressure shift should be expected for this line.

It is interesting to note that if one makes a linear extrapolation of the shifts of spectral holes burned in peaks 1 and 3 from the used low-pressure range to much higher pressures, the corresponding lines should merge at 15 848 cm^{-1} under a pressure of 216 MPa. The latter value is close to the pressure of phase transition between high-pressure commensurate C I and the intermediate incommensurate IC II phases (see Fig. 1). This result (complemented by direct high-pressure measurements described below) gives us a strong support to the idea that the shape of the chlorin impurity spectrum

in biphenyl is determined by influence of the incommensurate modulation wave. Indeed, the splitting between edge singularities depends on the order parameter variation. In the case of biphenyl this is the twist angle between two phenyl rings in the molecule, which may change with pressure.

3.3. The high-pressure spectra

Finally, we discuss the measured high-pressure spectra [Fig. 2(c,d) and Fig. 5], which give a direct confirmation to the extrapolations based on low-pressure tuning of spectral holes. Figure 5 depicts a sequence of luminescence emission spectra of chlorin-doped biphenyl taken at several pressures (at 20 MPa in the incommensurate phase IC III, at 100 MPa in the other incommensurate phase IC II, at 180 MPa in the region of the incommensurate–commensurate phase transition IC II – C I, and at 260 MPa in the high-pressure low-temperature commensurate phase C I). A transformation from the triplet (incommensurate) to singlet (commensurate) shape of the spectrum is well observable. Indeed, at 180 MPa as well as at a higher pressure of 260 MPa (i.e. undoubtedly in the commensurate phase), we see [Fig. 5(c) and (d)] only one peak at about 15 850 cm^{-1} which, as we think, originates from peaks 1 and 3 in the lower-pressure incommensurate phases. A broader feature at about 20 cm^{-1} to lower frequencies is the phonon sideband (see also Fig. 2(c) and (d) where the same phonon sideband is observed in the emission and excitation spectra, respectively). It should also be noted that the value of 15 850 cm^{-1} practically coincides with that of 15 848 cm^{-1} obtained from extrapolation of pressure shifts for the spectral holes burned in peaks 1 and 3.

Quite an interesting picture opens, when one plots the distance (spectral splitting) Δv between peaks 1 and 3 as a function of pressure (Fig. 6). The pressure dependence turns out to be of a widely known nonlinear critical character. From the fit to a theoretical curve

$$\Delta v(P) = \Delta_0 (1 - P/P_{tr})^n , \qquad (2)$$

where Δ_0 is the distance Δv at ambient pressure and P_{tr} is the incommensurate-to-commensurate (IC II – C I) phase transition pressure of about 180 MPa at 4.2 K, one obtains the value $n = 0.39$ for the critical exponent. Excitingly enough, very close values for the critical exponent, characterizing the same phase transition, were obtained in the aforementioned NMR [37] and EPR [39] studies in the *temperature* domain ($n = 0.35\pm0.03$ and $n = 0.4$, respectively). Accordance with some theoretical models should also be mentioned (first of all, with a non-classical 3D *XY*-model [65]). The fact of the critical behavior of the maximal twist angle 2φ (treated as the order parameter) in incommensurate biphenyl, unambiguously established by means of NMR spectroscopy [37],

may be regarded as the most decisive evidence that the chlorin spectrum in phases IC II and IC III is governed by the incommensurate modulation and that the observed splitting Δv is proportional to the magnitude of the maximal 2φ value varying with pressure.

On closer inspection, one can find that the value of the derivative $d\Delta v/dP$ from Eq. (2) in the zero-pressure limit, $d\Delta v/dP|_{P=0} = -n\,\Delta_0/P_{tr} = -1.82$ GHz/MPa (obtained by using for Δ_0 a value of about 28 cm^{-1} or 840 GHz from Fig. 6), does not coincide with the value resulting from SHB measurements, -4.45 GHz/MPa (following from Fig. 4). This is not surprising, since Eq. (2) is expected to describe the situation in the phase IC II, near the incommensurate–commensurate phase boundary, and not in the low-pressure IC III phase. This circumstance and nonlinearity of Eq. (2) are also the reasons why the extrapolated SHB data yield somewhat higher zero-splitting pressure (216 MPa) than the critical pressure of phase transition ($P_{tr} = 180$ MPa). Still the low-pressure SHB data indicate quite correctly that something unusual is happening at higher pressures.

In the spectra of Fig. 5 a weaker feature at somewhat lower energies from the main lines 1-3 (in the region of about 15 760–15 780 cm^{-1}) can be seen, showing in the incommensurate phases a doublet structure [66] with a decreasing splitting under growing pressure and converting to a singlet in the commensurate phase. We attribute these lines tentatively to another substitutional site of chlorin, most probably having a different orientation in the biphenyl crystal a,b plane shown in Fig. 3. It also exhibits an incommensurate splitting and behaves qualitatively in a similar manner as the main site (peaks 1-3). A markedly smaller splitting points to a weaker interaction with the modulation wave. This, on the other hand, may be the reason, why this wave is more weakly pinned by the dopant molecules in this site and the corresponding spectrum exhibits a "classical" doublet structure, thus giving some additional support to a possible mechanism of the main triplet formation discussed in point (iii) of Subsection 3.1.

4. Conclusions

The observed quite uncommon pressure behaviour of inhomogeneous spectra and spectral holes in chlorin-doped biphenyl is qualitatively explained by the interaction of the dopant electronic transition with the incommensurate modulation wave. Drastic changes of spectra with pressure are related to reduction (disappearance) of this modulation when approaching (crossing) the incommensurate–commensurate phase boundary. From the pressure dependence of spectra a critical exponent describing this transition ($n = 0.39$) was obtained. This value matches well the earlier NMR and EPR data derived for the temperature domain. Comparative hole burning measurements in

different crystal phases may shed further light on dynamics and transformations of incommensurate systems. In general, the obtained results demonstrate capabilities of optical molecular probe spectroscopy to tackle such interesting and challenging problems of condensed matter physics as structure and dynamics of partially ordered systems, phase transitions and related issues.

Acknowledgements

References

[1] R. Blinc, Phys. Reports 79 (1981) 331.
[2] R. Currat, T. Janssen, in: H. Ehrenreich, D. Turnbull (Eds.), Solid State Physisc. Advances in Research and Applications, Vol. 41, Academic Press, San Diego, 1988, p. 201.
[3] A. Suisalu, V. Zazubovich, J. Kikas, J. Friebel, J. Friedrich, Europhys. Lett. 44 (1998) 613.
[4] A.A. Gorokhovskii, R.K. Kaarli, L.A. Rebane, Pis'ma Zh. Eksp. Teor. Fiz. 20 (1974) 474 [JETP Lett. 20 (1974) 216].
[5] B.M. Kharlamov, R.I. Personov, L.A. Bykovskaya, Opt. Commun. 12 (1974) 191.
[6] V. Zazubovich, A. Suisalu, J. Kikas, Phys. Rev. B. 64 (2001) 104203.
[7] A. Ellervee, J. Kikas, A. Laisaar, V. Shcherbakov, A. Suisalu, J. Opt. Soc. Am. B 9 (1992) 972.
[8] P. Schellenberg, J. Friedrich, J. Kikas, J. Chem. Phys. 100 (1994) 5501.
[9] J. Friebel, J. Friedrich, A. Suisalu, J. Kikas, An. Kuznetsov, A. Laisaar, K. Leiger, J. Chem. Phys. 108 (1998) 1830.
[10] J. Zollfrank, J. Friedrich, J. Phys. Chem. 96 (1992) 7889.
[11] H. Pschierer, J. Friedrich, H. Falk, W. Schmitzberger, J. Phys. Chem. 97 (1993) 6902.
[12] Th. Sesselmann, W. Richter, D. Haarer, Europhys. Lett. 2 (1986) 947.
[13] Th. Sesselmann, W. Richter, D. Haarer, H. Morawitz, Phys. Rev. B 36 (1987) 7601.
[14] M. Köhler, J. Friedrich, J. Fidy, Biochim. Biophys. Acta (BBA) – Protein Structure and Molecular Enzymology 1386 (1998) 255.
[15] H.-M. Wu, M. Rätsep, R. Jankowiak, R.J. Cogdell, G.J. Small, J. Phys. Chem. B 101 (1997) 7641; 102 (1998) 4023.
[16] J. Pieper, M. Rätsep, R. Jankowiak, K.-D. Irrgang, J. Voigt, G. Renger, G.J. Small, J. Phys. Chem. A 103 (1999) 2412.

[17] H.-C. Chang, R. Jankowiak, N.R.S. Reddy, G.J. Small, Chem. Phys. 197 (1995) 307.
[18] N.R.S. Reddy, R. Jankowiak, G.J. Small, J. Phys. Chem. 99 (1995) 16178.
[19] J. Kikas, A. Laisaar, A. Suisalu, Photonics Science News 6 (2000) 126.
[20] A. Laisaar, J. Kikas, A. Suisalu, J. Low Temp. Phys. 122 (2001) 221.
[21] A. Ellervee, R. Jaaniso, J. Kikas, A. Laisaar, A. Suisalu, V. Shcherbakov, Chem. Phys. Lett. 176 (1991) 472.
[22] A. Ellervee, V.V. Hizhnyakov, J. Kikas, A. Laisaar, A. Suisalu, J. Lumin. 53 (1992) 223.
[23] A. Ellervee, J. Kikas, A. Laisaar, A. Suisalu, J. Lumin. 56 (1993) 151.
[24] J. Kikas, A. Laisaar, A. Suisalu, An. Kuznetsov, A. Ellervee, Phys. Rev. B 57 (1998) 14.
[25] V. Hizhnyakov, A. Laisaar, J. Kikas, An. Kuznetsov, V. Palm, A. Suisalu, Phys. Rev. B 62 (2000) 11296.
[26] T.M.H. Creemers, J.M.A. Koedijk, I.Y. Chan, R.J. Silbey, S. Völker, J. Chem. Phys. 107 (1997) 4797.
[27] A.J. Lock, T.M.H. Creemers, S. Völker, J. Chem. Phys. 110 (1999) 7467.
[28] C. Benkert, V. Heine, E.H. Simmons, J. Phys. C: Solid State Phys. 20 (1987) 3337.
[29] R.M. Hochstrasser, R.D. Mc Alpine, J.D. Whiteman, J. Chem. Phys. 58 (1973) 5078.
[30] T. Suzuki, G. Kudo, K. Nukui, M. Mizuno, K. Abe, T. Shigenari, J. Lumin. 87-89 (2000) 623.
[31] M.H. Lemée-Cailleau, A. Girard, H. Cailleau, Y. Délugeard, P. Pruzan, Ferroelectrics 105 (1990) 147.
[32] M.H. Lemée-Cailleau, A. Girard, H. Cailleau, Y. Délugeard, Phys. Rev. B 45 (1992) 12682.
[33] P. Launois, F. Moussa, M.H. Lemée-Cailleau, H. Cailleau, Phys. Rev. B 40 (1989) 5042.
[34] J. Etrillard, B. Toudic, H. Cailleau, M.H. Lemée-Cailleau, G. Coddens, W. Petry, Physica B 180&181 (1992) 342.
[35] J. Etrillard, B. Toudic, H. Cailleau, G. Coddens, Phys. Rev. B 51 (1995) 8753.
[36] S.-B. Liu, M.S. Conradi, Phys. Rev. Lett. 54 (1985) 1287.
[37] L. von Laue, F. Ermark, A. Gölzhäuser, U. Haeberlen, U. Häcker, J. Phys.: Condens. Matter 8 (1996) 3977.
[38] A. Veron, J. Emery, F. Lari-Guillet, J. Phys. Chem. Solids 56 (1995) 51.
[39] A. Veron, J. Emery, M. Spiesser, J. Phys. Chem. Solids 57 (1996) 1201.
[40] G.-P. Charbonneau, Y. Délugeard, Acta Crystallogr. B 33 (1977) 1586.
[41] H. Cailleau, in: R. Blinc, A.P. Levanyuk (Eds.), Incommensurate Phases in Dielectrics, Part II: Materials (Modern Problems in Condensed Matter Sciences, Vol. 14), North-Holland, Amsterdam, 1986, p. 71.

[42] F. Moussa, P. Launois, M.H. Lemée, H. Cailleau, Phys. Rev. B 36 (1987) 8951.

[43] H. Cailleau, F. Moussa, J. Mons, Solid State Commun. 31 (1979) 521.

[44] H. Cailleau, A. Girard, J.C. Messager, Y. Délugeard, C. Vettier, Ferroelectrics 54 (1984) 597.

[45] H. Cailleau, J.C. Messager, F. Moussa, F. Bugaut, C.M.E. Zeyen, C. Vettier, Ferroelectrics 67 (1986) 3.

[46] P. Launois, Ph. D. Thesis, Université de Paris-Sud, Orsay, 1987.

[47] P. Launois, M.H. Lemée, H. Cailleau, F. Moussa, J. Mons, Ferroelectrics 78 (1988) 137.

[48] M.H. Lemée, P. Launois, F. Moussa, A. Girard, Y. Délugeard, H. Cailleau, Physica B 156&157 (1989) 17.

[49] M.H. Lemée-Cailleau, Ph. D. Thesis, Université de Rennes I, 1989.

[50] M.H. Lemée-Cailleau, A. Girard, H. Cailleau, Y. Délugeard, P. Pruzan, Ferroelectrics 105 (1990) 147.

[51] C. Benkert, V. Heine, Phys. Rev Lett. 58 (1987) 2232.

[52] C. Benkert, J. Phys. C: Solid State Phys. 20 (1987) 3369.

[53] T. Wasiutyński, H. Cailleau, J. Phys.: Condens. Matter 4 (1992) 6241.

[54] A. Driessen, E. van der Poll, I.F. Silvera, Phys. Rev B 33 (1986) 3269.

[55] E.R. Grilly, J. Low Temp. Phys. 11 (1973) 33.

[56] J. Kikas, K. Leiger, J. Chem. Phys. 104 (1996) 5384.

[57] P.J. Walla, F. Jelezko, Ph. Tamarat, B. Lounis, M. Orrit, Chem. Phys. 233 (1998) 117.

[58] S. Kummer, F. Kulzer, R. Kettner, Th. Basché, C. Tietz, C. Glowatz, C. Kryschi, J. Chem. Phys. 107 (1997) 7673.

[59] U. Even, J. Jortner, J. Chem. Phys. 77 (1982) 4391.

[60] A.K. Moskalev, I.A. Belobrova, I.P. Aleksandrova, Fiz. Tverd. Tela 20 (1978) 3288 [Sov. Phys.-Solid State 20 (1978) 1896].

[61] A. Suisalu, V. Zazubovich, J. Kikas, unpublished.

[62] J. Kikas, Chem. Phys. Lett. 57 (1978) 511.

[63] G. Gradl, J. Zollfrank, W. Breinl, J. Friedrich, J. Chem. Phys. 94 (1991) 7619.

[64] J. Gafert, J. Friedrich, F. Parak, J. Chem. Phys. 99 (1993) 2478.

[65] J.C. Le Guillou, J. Zinn-Justin, Phys. Rev. Lett. 39 (1977) 95.

[66] A peak at 15 800 cm^{-1} in Fig. 5(a) seems to be an artifact since it is absent from the other spectra depicted in Fig. 5.

Figure captions

Fig. 1. Phase diagram of biphenyl.
Deuterated compound $C_{12}D_{10}$ (filled symbols):   ▲ [32,33,42,45,47];   ◆ [44,51,52] ($T \to 0$ K, $P \approx 170$ MPa); ■ [49,53]; ▼ [48] ($T \to 0$ K, $P \approx 40$ MPa).
Hydrogenated compound $C_{12}H_{10}$ (open symbols): ○ [32] ($T \approx 40$ K and 17 K, $P = 1$ atm); □ [49,53]; ▽ [48] ($T \to 0$ K, $P \approx 20$ MPa).
Corrected melting line of ^{4}He (replacing the respective curve in Fig. 2 of Ref. [32]): ····· [54,55].

Fig. 2. Photoluminescence emission (a, c) and excitation (b, d) spectra of chlorin impurity molecules in biphenyl at $T = 4.2$ K under ambient pressure (a, b), at 260 MPa (c) and at 270 MPa (d).

Fig. 3. A schematic view of the incommensurate biphenyl lattice with four unit cells in the a, b plane. The guest molecule of chlorin is shown to substitute two adjacent host molecules of biphenyl.

Fig. 4. Pressure-induced shifts at $T = 2.0$ K for spectral holes burned in the absorption lines of chlorin-doped biphenyl at the peaks 1–3. Straight solid lines are the linear least-squares fits to the data points obtained for these peaks; the respective numerical values of the shift rates (pressure coefficients) $d\nu/dP$ are also denoted. Insert shows extrapolation of the peak positions of lines 1 and 3 to much higher pressures. Note that lines 1 and 3 should merge at a pressure of about 216 MPa.

Fig. 5. Emission spectra of chlorin molecules in biphenyl recorded at $T = 4.2$ K and various pressures indicated.

Fig. 6. Pressure dependence of the distance (spectral splitting) $\Delta\nu$ between lines 1 and 3 in the emission spectrum of chlorin-doped biphenyl at $T = 4.2$ K. Circles show the experimental points; solid curve indicates the nonlinear least-squares fit to the data points according to Eq. (2) (see the text). Dashed line illustrates the linear extrapolation using the low-pressure spectral hole shift data for lines 1 and 3 (see inset of Fig. 4).
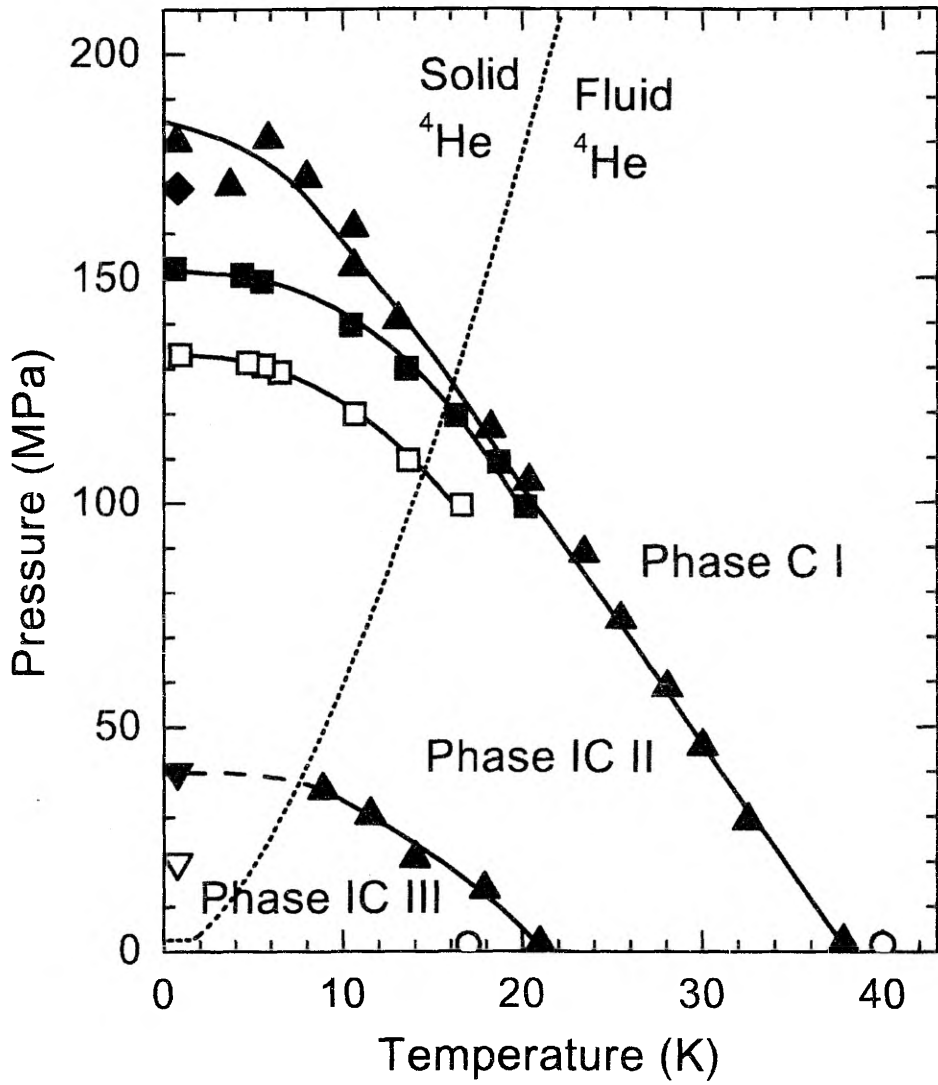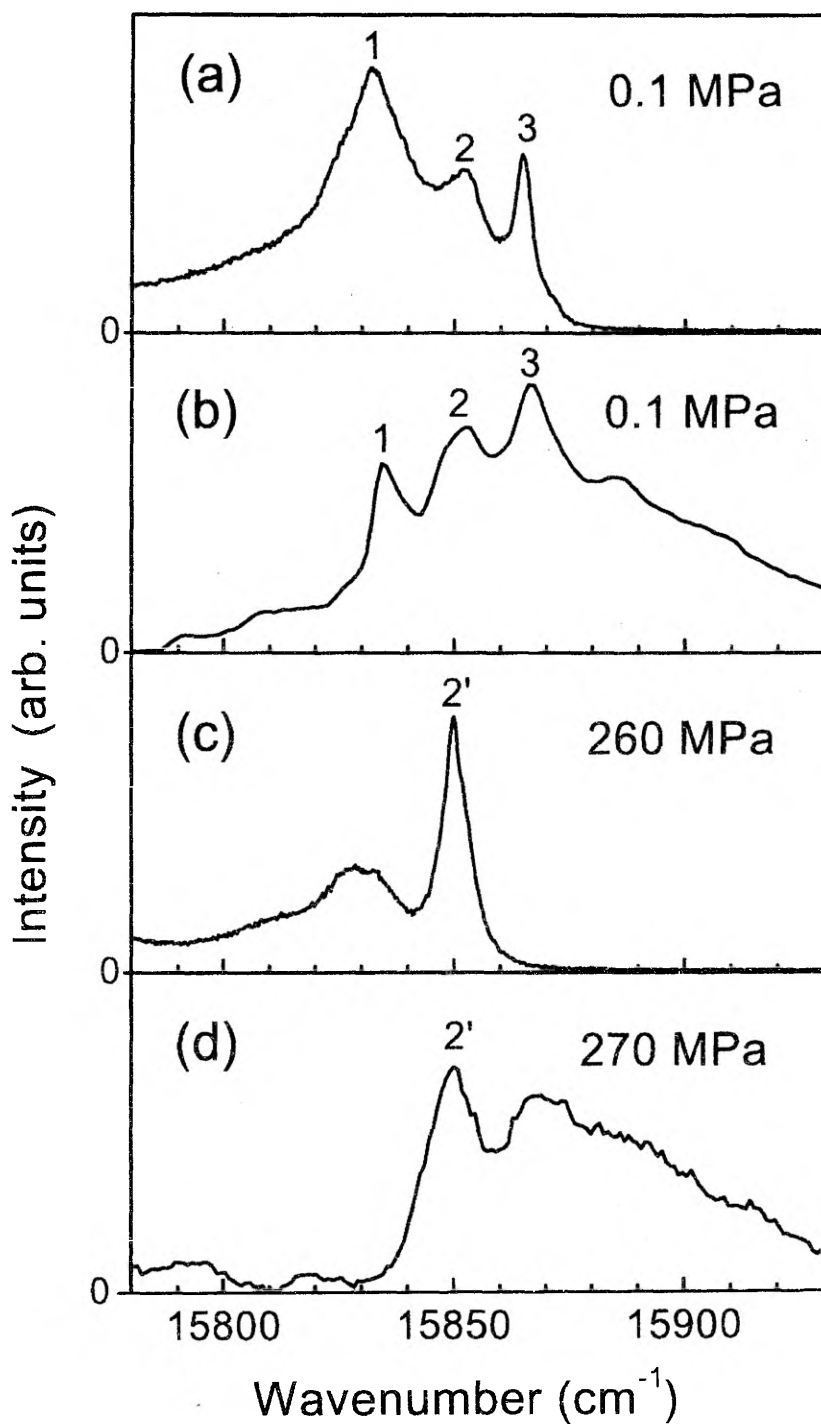
Fig.1. V. Zazubovich *et al*. Chem. Phys.

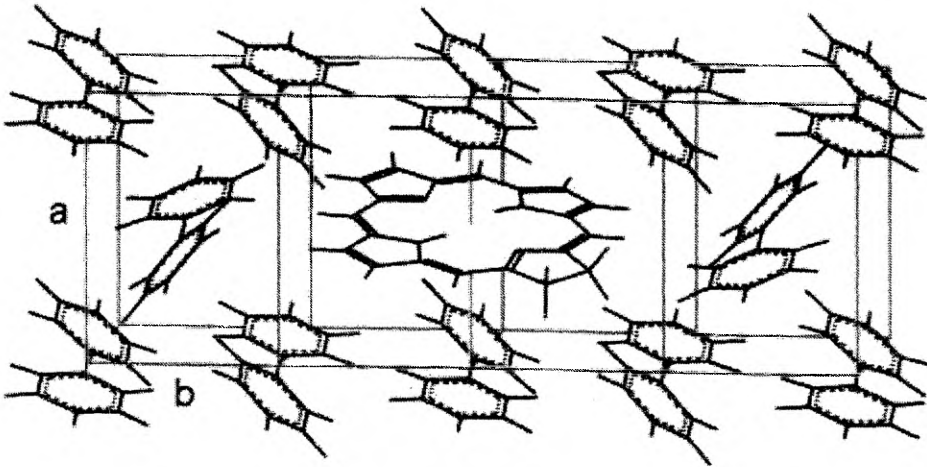Fig. 2. V. Zazubovich, *et al.* Chem. Phys.
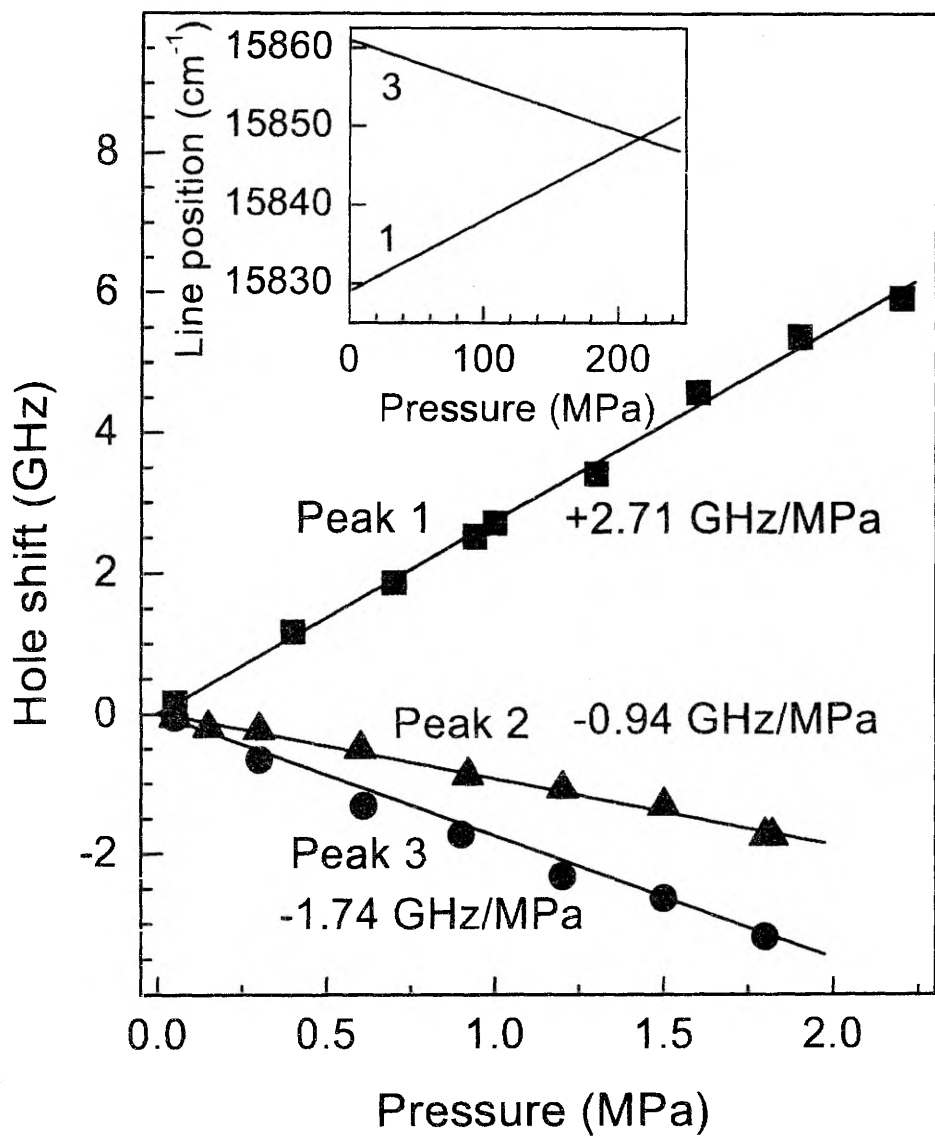
Fig.3 Zazubovich *et al*. Chem. Phys.

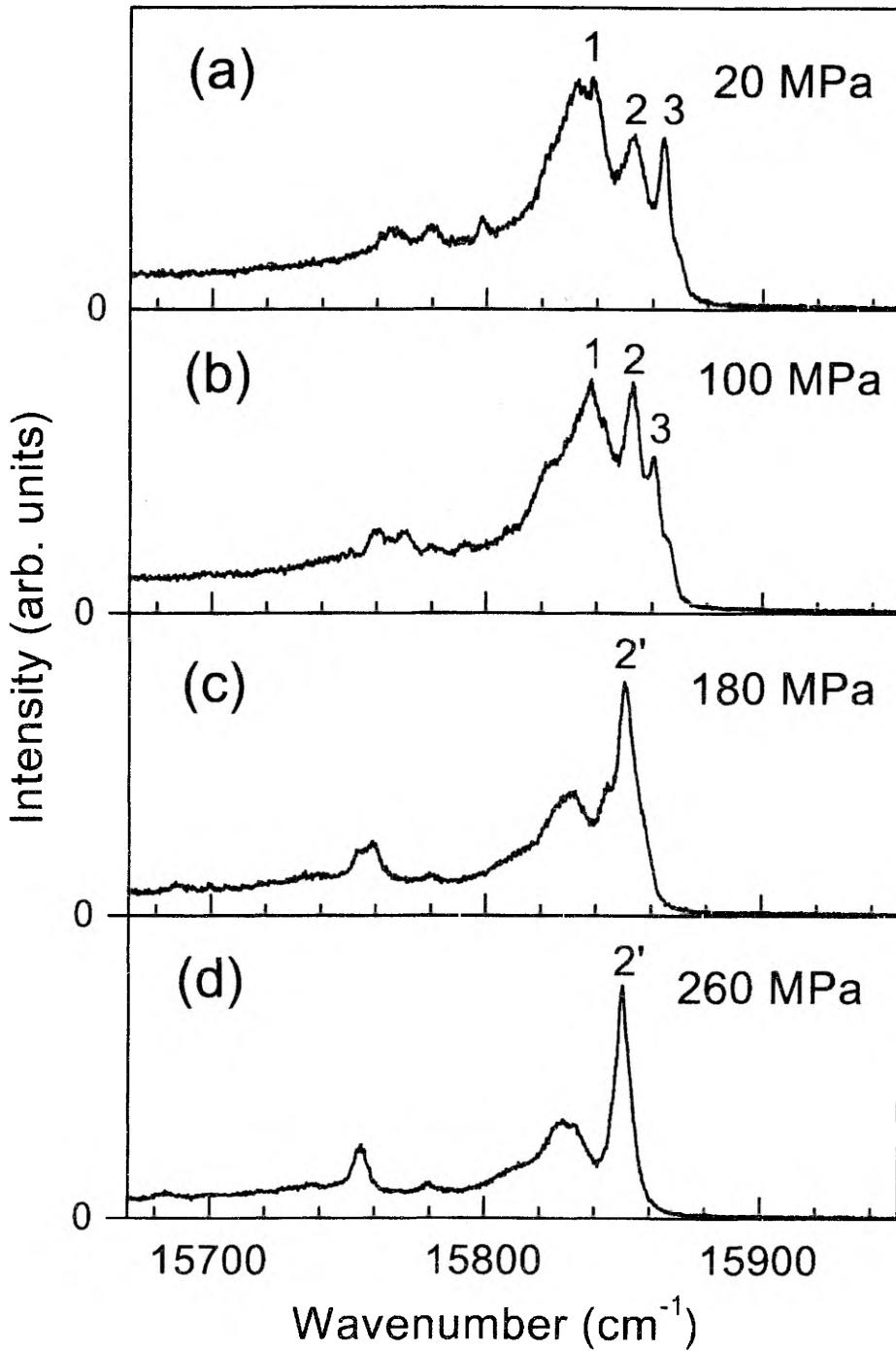Fig. 4. V. Zazubovich, *et al*. Chem. Phys.
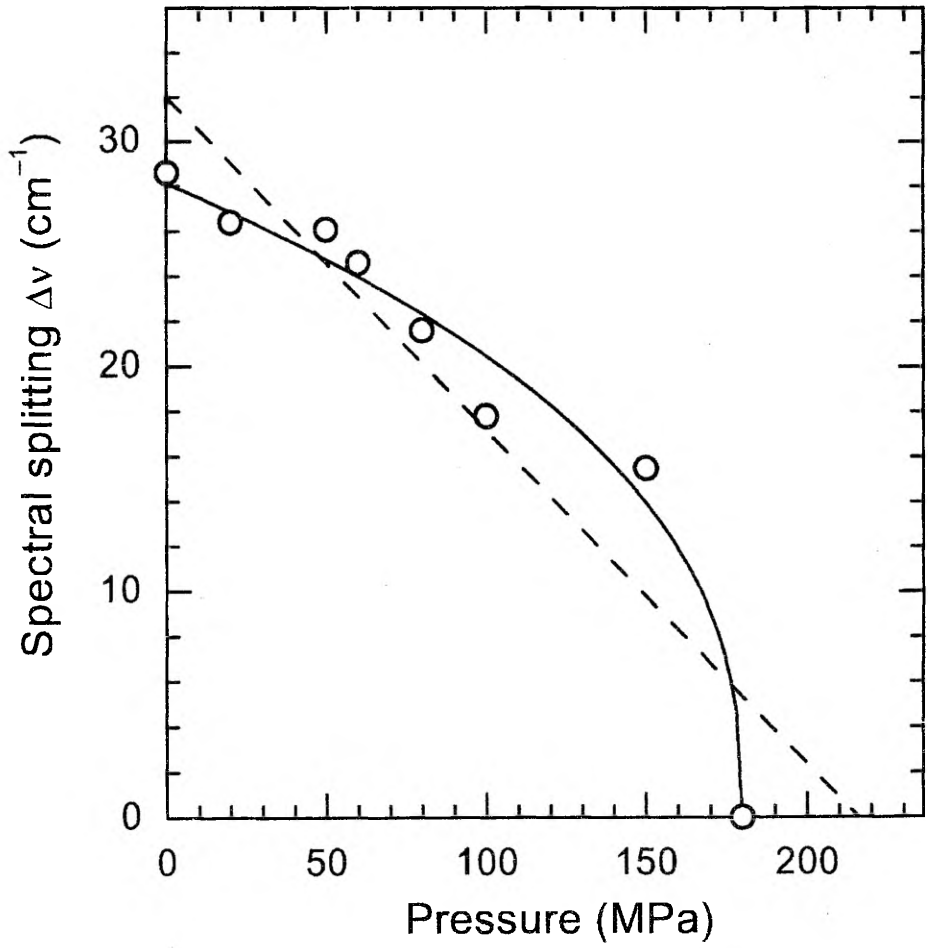
Fig. 5. V. Zazubovich, *et al.* Chem. Phys.

Fig. 6. V. Zazubovich, *et al.* Chem. Phys.

V

Diaelastic pressure-induced broadening of spectral holes in molecular crystals

K. Leiger[1], J. Kikas[2], A. Suisalu[1]

[1]*Institute of Physics, University of Tartu, Riia 142, 51014 Tartu, Estonia*
[2]*Department of Physics, University of Tartu, Tähe 4, 51010 Tartu, Estonia*

Abstract

Broadening and shifts of spectral holes with changing the hydrostatic pressure at 2 K were measured for dimethyl-s-tetrazine (DMST) probe molecules in durene crystals, in both pure and doped with hexachlorobenzene (HCB) at 2 mol%. The HBC molecules act as elastic defects and cause increase in inhomogeneous broadening as well as in the pressure-induced broadening of spectral holes. However, the relative pressure broadening (scaled to the inhomogeneous linewidth) *decreases* with pressure. The HCB concentration affects also the color effect in pressure broadening, i.e. its dependence on the spectral position. The observations are qualitatively interpreted proceeding from the diaelastic model [J. Kikas and K. Leiger, J. Chem. Phys. 104 (1996) 5384].

1. Introduction

Pressure tuning of spectral holes [1–11] is an informative tool for studying local interactions and dynamics in doped solids. Based on a stochastic theory of inhomogeneous broadening by Stoneham [12] and its multidimensional extension by Kikas and Rätsep [13], theoretical models have been worked out to describe the pressure behavior of spectral holes for various types of solids, such as glassy and polymeric systems [1], Shpol'skii systems [2], and molecular crystals [3]. This paper is aimed at testing some aspects of our theoretical model [3] for pressure broadening of spectral holes in crystalline solids. In crystals, the inhomogeneous effects are governed by long-range interactions between probe dye molecules and defects present in the crystal lattice (internal structural defects, guest molecules). In order to describe the

1

dependence of such an interaction on the external hydrostatic pressure, we proceeded from the so-called diaelastic effect. The diaelastic effect is a parallel to the diamagnetic effect, where internal magnetic field in solid is generated as a response to the applied external field. In diaelasticity the spatially varying strain field, generated by the size mismatch between the defect (guest molecule) and host particles is modified by the external pressure. According to this model, no pressure broadening is predicted for spectral holes if all the defects are similar. In this case the subensemble of the dopants selected by hole burning holds no hidden degeneracy that could be lifted away by pressure. Notice that experiments performed on durene [2, 4] and bensophenone [5] still show some pressure broadening of spectral holes even in such well-ordered crystalline matrices.

A deeper insight into the inhomogeneous pressure effects could be obtained by introducing additional (controlled) defects into the lattice. Such defects can be, for instance, guest molecules. When selecting proper dopants, one has to keep in mind the solubility: if too different from the host molecules in size and shape, the guest molecules may be rejected from the host structure.

Proceeding from these considerations we chose durene (1,2,4,5-tetramethylbenzene) for the host matrix and enhanced inhomogeneity by mixing a small amount (about 2 mol. %) of hexachlorobenzene (HCB) into some samples. As the probe dye molecule, we used dimethyl-s-tetrazine (DMST). In durene, the zero-phonon line of DMST S_0–S_1 transition is peaked at 17 020 cm^{-1}. The system durene : DMST has been studied by hole burning before [4, 2, 14], the main hole burning mechanism ascribed to methyl group tunneling [15, 16].

2. Experimental

The samples were prepared by dissolving DMST and, for mixed samples, also hexachlorobenzene in melted durene (m.p. 82 °C). The concentration of DMST was about 0.01 mol% and that of HCB about 2 mol%. A polycrystalline sample was obtained by slow cooling through the melting point. The sample was kept inside a small two-window pressure cell, which used helium as a pressure transmitter. The cell was kept inside a He-flow cryostat for cooling. The temperature was stabilized at 2.0±0.2K. The range of available pressures was limited by the pressure regulator to about 1..13 bar. However, this was sufficient to measure the shift and broadening of spectral holes.

Holes were burnt and measured with COHERENT 699-29 single-frequency dye laser with the linewidth of about 1 MHz. For burning the power density at the sample was about 200 μW/cm^2, for recording it was reduced about 20 times. Burning times were in the order of 100 s. Also the inhomogeneous line was narrow enough to be measured with the same laser. Transmission spectra

were recorded that were later converted to optical density. The holes were fitted to Lorentzian curves with a possibly sloped baseline. Note that the theory does not predict the pressure-broadened holes to be exactly Lorentzian in shape. However, for the hole widths (FWHM) and baseline characteristics the results should be quantitatively correct.

3. Results and discussion

We first measured the effect of introducing guest HCB molecules on the inhomogeneous broadening of the absorption line. As seen from Fig. 1, the modification is quite large: in pure samples the linewidth is about 2.4 cm^{-1}, but reaches a value of 9.6 cm^{-1} in mixed samples. This gives us an increase of about 4 times. "Pure" here and in what follows means "without HCB dopant", all the samples contained, naturally, a small amount of DMST probe molecules.

We then made several pressure series with spectral holes burnt at different frequencies within the inhomogeneous line, to measure pressure effects on the holes, especially broadening. We chose 6 series (2 for pure and 4 for mixed samples) for closer examination. The locations where the series were taken are denoted by arrows in Fig. 1. For both pure and mixed samples one of the series was located near the center of the inhomogeneous line which was determined to be 17019.8 cm^{-1} for pure samples (burning position 17020 cm^{-1}) and 17020.9 cm^{-1} for mixed samples (burning position 17020.5 cm^{-1}). In what follows, we will refer to these series and the corresponding pressure quantities as "central". Fig. 2 shows the pressure dependence of the holewidth within the central series. The broadening values are 9.0 MHz/bar for the pure sample and 18.8 MHz/bar for the mixed sample.

The pressure broadening of spectral holes can be understood as originating from the dispersion of the pressure derivatives of interactions between single defect-probe pairs, keeping in mind that with the applied pressures we are well within the limits of applicability of the linear theory of elasticity. Such interactions typically have a form

$$\varepsilon = C\Phi r^{-n}. \tag{1}$$

Here r is the defect-probe distance. n is a constant specifying the interaction type. Φ is an angular factor whose pressure dependence can be left out of consideration here. Assuming that all the defects are of the same type (a proper assumption for fixed n), Φ also does not depend on defect. Possible variations in the ensemble of defects are described by variations of the coefficient C that can be called the defect strength. In Eq. (1) we have two factors that can

3

contribute to the pressure derivative $d\varepsilon/dp$: the distance and the defect strength. In case of polymers and glassy materials where nearby molecules are regarded as perturbers, the local values of the relative pressure derivative of distance, or the volume compressibility, can have a significant dispersion. In crystals the interaction is of long-range type and local compressibility variations should not play a major role. In this case, given the observable pressure broadening, we have to conclude that the pressure derivatives of the defect strengths have a remarkable dispersion, too. By analogy with the electric and magnetic phenomena, we might call the corresponding relative value (with the opposite sign) the mechanical polarizability of defect.

The situation is analyzed in [3] within the frame of so-called diaelastic model, where point defects are qualitatively described by misfitting spheres of different compressibility within the continuously treated host material. Elastic interaction of such defects with probes is shown to have the form (1) with $n=3$. Defects modelled this way generally possess a finite mechanical polarizability.

The inhomogeneous pressure effects within the diaelastic model are governed by the weighted distribution of the defects' mechanical polarizabilities, with their absolute strengths as weighting factors. It can be shown that the hole broadening in the center of the inhomogeneous line is given by the product $\sigma_\kappa \cdot \Gamma_{ih}$, where σ_κ is the standard deviation of the weighted mechanical polarizability distribution and Γ_{ih} is the zero-pressure width of the inhomogeneous line. According to this, the hole broadening should scale with the inhomogeneous linewidth on modification of the inhomogeneity by changing the defect concentration if σ_κ is unchanged.

We see, however, that in our case the pressure broadening in mixed system is about 2 times too low to scale with the controlled broadening of the inhomogeneous line: the increase in broadening for central holes as a result of mixing is only 2.1 times while inhomogeneous linewidth increased 4 times. We therefore have to conclude that the dispersion of the weighted mechanical polarizability distribution has decreased correspondingly. This does not seem unreasonable. As far as the introduced HCB guest molecules are all similar and occupy preferably similar sites in the crystal, an effective narrowing the otherwise perhaps more diverse distribution of defects may occur. At the same time the inhomogeneous width, which, above all, is linear in the defect density, is still increased.

Next, let us analyze the situation on the wings of the inhomogeneous line. We found rather strong dependence of the pressure behavior parameters of the hole on the burning frequency (the so-called "color effect"). Such dependence for pressure shift is well known and has been observed before (see [6], for example). Its qualitative explanation is simple: each line originating from a single probe has a pressure shift that scales with its previous solvent shift (detuning from the transition frequency of the probe molecule in vacuum), which itself can be viewed as arising from pressure exerted by the crystal field,

varying from probe to probe. In case of crystals we have to split the solvent shift in two parts: the constant part, equal for all probes, arising mainly from the surrounding crystal cage and representing the situation in a perfect crystal, and the varying part, responsible for the inhomogeneous broadening. The pressure dependences of these two parts need not to be equal and this could be the main reason that prevents the pressure shift coefficient from extrapolating to zero at the vacuum frequency. In our case, the zero-extrapolated frequency is around 17 100 cm^{-1}, indicating that the constant part accounts for at least 4/5 of the total solvent shift [8].

The color effect for the hole broadening has deserved less attention. For glasses such a possibility has been pointed out [17,18] as arising formally from the breakdown of the so-called Gaussian approximation valid for high defect densities. This, however, leads to a broadening wavelength-dependence that is of the same type as that of the pressure coefficient for spectral shifts, i.e. decreasing monotonically towards the vacuum frequency and giving a larger broadening value on the red wing than on the blue. The dependence is not linear, though, but of the shape *(A+Bv)*$^{1/2}$ in the first approximation.

The diaelastic model includes the color effect for pressure broadening intrinsically. It can be seen from following considerations. Due to the specific nature of $n = 3$ interaction the situation on the wings of the inhomogeneous line is governed by the interaction with one nearby defect [1]. This is in a very contrast to the situation we have for the Gaussian broadening, where a large number of perturbers contribute comparably. If there is any dispersion of mechanical polarizabilities then, far on the wings, the associated pressure broadening is amplified by smaller distance to defect (and thus stronger interaction). Also the shape of the pressure-broadened hole (the pressure kernel) is more pronouncedly determined by the distribution of mechanical polarizabilities. The pressure kernel is symmetrical with respect to the center of the inhomogeneous line, i.e. the pressure kernel at a given detuning is a mirror image of that at an opposite detuning of the same magnitude. Its width acquires a proportional dependence on the absolute detuning from the center. In the center of the inhomogeneous line, the pressure kernel retains a non-zero width (contributions from a larger number of independent defects become important). Here the pressure kernel is always symmetrical but, depending on the distribution of mechanical polarizabilities, it can become asymmetric on the wings. The following general relation between the standard deviation of mechanical polarizabilities σ_κ and that of the local pressure kernel at a frequency v, $\sigma_\alpha(v)$ holds:

$$\sigma_\alpha(v) = \sigma_\kappa \sqrt{\Gamma_{ih}^2 + (v - v_0)^2} \, , \qquad (2)$$

where v_0 and Γ_{ih} are the peak frequency and FWHM of the inhomogeneous line, correspondingly. Eq. (2) can be shown to hold whenever σ_κ exists, irrespective of the particular shape of the mechanical polarizability distribution, i.e. there exists a simple relation between the spectroscopic (measurable) parameters $\sigma_\alpha(v)$, v_0, Γ_{ih} and an internal characteristic of the system σ_κ. It can be rewritten as follows:

$$\frac{\sigma_\alpha(v)}{\sigma_\alpha(v_0)} = \sqrt{1 + \left(\frac{v - v_0}{\Gamma_{ih}}\right)^2} \ . \tag{3}$$

In Fig.3 the relative pressure broadening for all non-central holes scaled to that of the central holes are shown as a function of the burning position. As a guideline, also the corresponding theoretical value for the standard deviation, as given by (3), is plotted. The seeming discrepancy between the experimental results and the theoretical curve can be readily explained by variance between the FWHM (obtained from experiment) and the standard deviation as different measures of the width of distribution. Let us have a closer look at the issue. Let Γ_α denote the FWHM of the pressure kernel. The ratio $\Gamma_\alpha/\sigma_\alpha$ remains constant as far as the *shape* of the distribution does not change. According to theory, the shape of the central pressure kernel is of the type $(A+B\alpha^2+\alpha^4)^{-1}$, having a FWHM to standard deviation ratio typically about unity. At large detunings from the center of the inhomogeneous line, as discussed earlier, the kernel shape approaches the shape of the weighted mechanical polarizability distribution, which is most likely a Gaussian or other function falling steeply on the wings. For such functions the FWHM to standard deviation ratio is generally higher (2.36 for a Gaussian). This can well explain the difference by a factor of 1.5 between the most detuned from the line maximum data point for the pure crystal (square 2a in Fig. 3) and the corresponding theoretical standard deviation of the pressure kernel. In fact, the discussed seeming discrepancy between the experiment and theory supports the idea, that not only the width but also the shape of the pressure kernel may depend on the spectral position within the inhomogeneous line.

4. Conclusions

We have demonstrated, that disorder in a mixed molecular crystal, introduced by guest molecules and revealed in inhomogeneous broadening of probe dye spectra affects broadening of spectral holes in pressure tuning experiments. Main characteristics of the phenomenon (dependence on concentration of controlled defects, color effect in broadening) qualitatively match the conclusions from diaelastic model [11] with deviations ascribed to

uncontrolled defects. Thus, beside of probing the local elastic properties, the pressure tuning can yield valuable information on the matrix defects, particularly, on the homogeneity / inhomogeneity of the defect ensemble (one prevailing type of defects vs. broad distribution of defect characteristics).

Acknowledgement

References

1. B.B. Laird and J.L. Skinner, J. Chem. Phys. 90 (1989) 3274.
2. J. Friebel, J. Friedrich, A. Suisalu, J. Kikas, An. Kuznetsov, A. Laisaar and K. Leiger, J. Chem. Phys. 108 (1998) 1830.
3. J. Kikas and K. Leiger, J. Chem. Phys. 104 (1996) 5384.
4. G. Gradl, A. Feis and J. Friedrich, J. Chem. Phys. 97 (1992) 5403.
5. P. Schellenberg, J. Friedrich and J. Kikas, J. Chem. Phys. 100 (1994) 5501.
6. G. Gradl, J. Zollfrank, W. Breinl and J. Friedrich, J. Chem. Phys. 94 (1991) 7619.
7. Th. Sesselmann, W. Richter and D. Haarer, Europhys. Lett. 2 (1986) 947.
8. Th. Sesselmann, W. Richter, D. Haarer and H. Morawitz, Phys. Rev. B 36 (1987) 7601.
9. Th. Sesselmann, W. Richter and D. Haarer, J. Lumin. 36 (1987) 263.
10. J. Zollfrank, J. Friedrich, J. Fidy and M. Vanderkooi, J. Chem. Phys. 94 (1991) 8600.
11. A. Ellervee, J. Kikas, A. Laisaar, V. Shcherbakov and A. Suisalu, J. Opt. Soc. Am. B 9 (1992) 972.
12. A.M. Stoneham, Rev. Mod. Phys. 41 (1969) 82.
13. J. Kikas and M. Rätsep, Phys. Stat. Sol. (b) 112 (1982) 409.
14. H. de Vries and D.A. Wiersma, Phys. Rev. Lett. 36 (1976) 91.
15. K. Orth, F. Rohlfing and J. Friedrich, Z. Phys. B 95 (1994) 493.
16. M.R. Johnson and H.P. Trommsdorff, Physica B 226 (1996) 194.
17. L. Kador, J. Chem. Phys. 99 (1993) 7.
18. L. Kador, J. Chem. Phys. 95 (1991) 846.

Figure Captions

Figure 1. Absorption spectra of the DMST S_0–S_1 transition in pure durene (a) and durene mixed with 2 mol. % of hexachlorobenzene (b). Arrows indicate the positions of spectral holes.

Figure 2. Pressure dependence of the width of spectral holes burnt in the center of the inhomogeneous line in pure (rectangles, postion 1a in Fig. 1) and mixed (circles, postion 2b in Fig. 1) crystal. The solid lines indicate the least-squares linear fits. The slopes are 9.0 MHz/bar for pure and 18.8 MHz/bar for mixed crystals.

Figure 3. Relative pressure broadenings of non-central holes with respect to the central holes in pure (rectangles) and mixed (circle) crystal as a function of the burning position. The line represents the corresponding theoretical relative value for the standard deviation (Eq. (3)). The frequency axis is scaled to inhomogeneous linewidth and uses the line maximum as the origin.
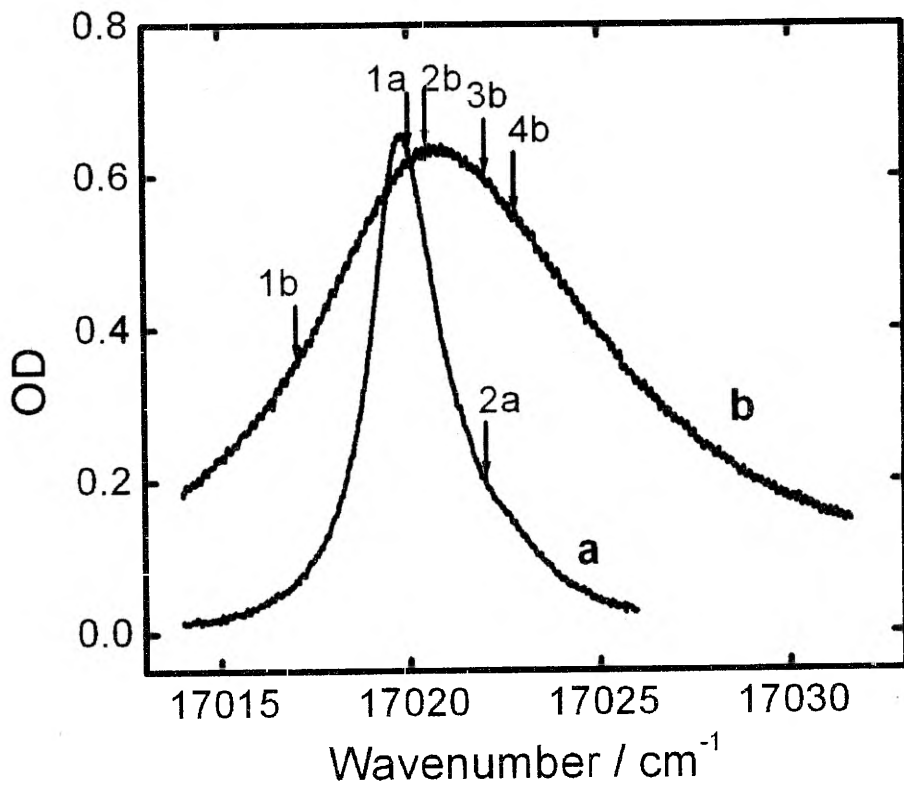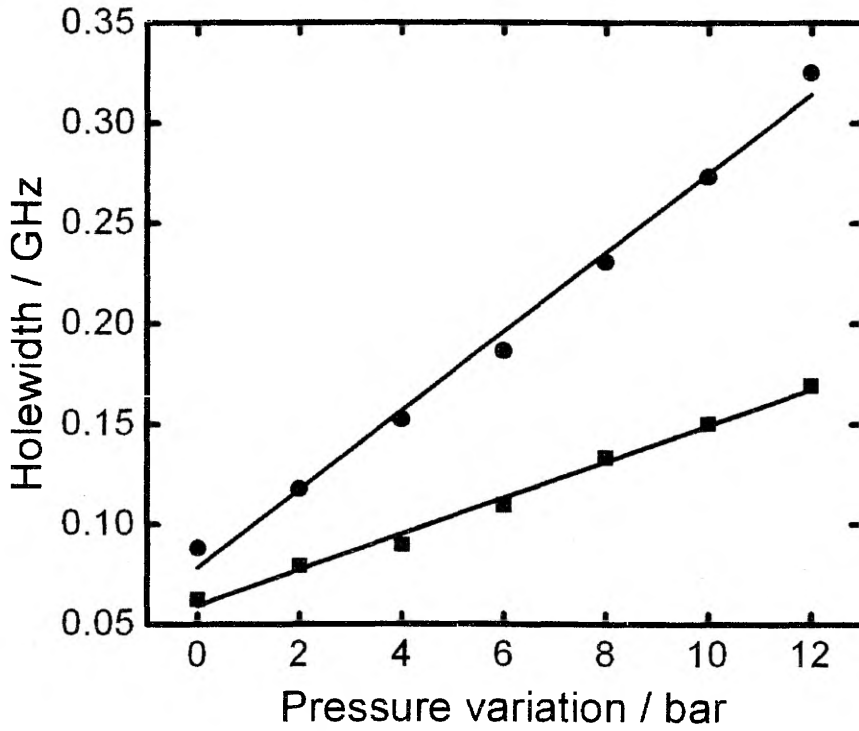
Fig. 1. K. Leiger *et al.*, J. Lumin.
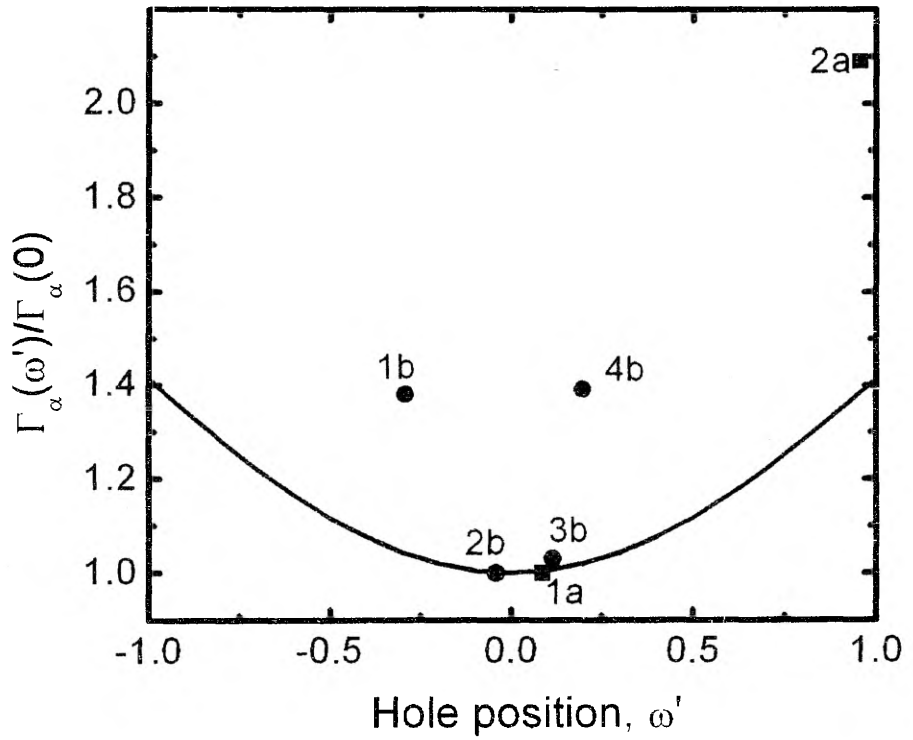
Fig. 2. K. Leiger *et al.*, J. Lumin.

Fig. 3. K. Leiger *et al.*, J. Lumin.

VI

Effect of geometry on storage density in spectral hole burning memories,
J. Kikas, K. Leiger,
Opt. Commun. **94** (1992), 557.

Effect of geometry on storage density in spectral hole burning memories

J. Kikas and K. Leiger

Institute of Physics, Estonian Acad. Sci., EE-2400 Tartu, Estonia

Storage density as a function of a tolerable level of the cross-talking F_m is calculated for different packing geometries in spectral-hole-burning-based frequency-selective 2+1-dimensional (2 spatial + 1 frequency dimension) optical memories. Spatial intercalation of adjacent isofrequency layers is demonstrated to increase the storage density, the highest density obtained for the rhombohedric 3D memory lattice.

1. Introduction

Persistent spectral hole burning [1,2] (see also reviews [3.4] and monographs [5,6]) has been proposed as a method for high-density optical information storage [7,8]. An additional frequency dimension is used to encode the information by burning spectral holes at a set of fixed frequencies within the inhomogeneously broadened impurity absorption band [7]. A rough estimate for the storage density increase, compared with conventional binary optical memories, is given by the ratio of the inhomogeneous width of the impurity absorption band and the minimum tolerable spectral distance between the adjacent holes. The latter in its turn is limited by the tolerable level of cross-talking (mutual influence of holes burnt at different frequencies). A more thorough consideration, however, forces one to take into account the cross-talking in both spectral and spatial dimensions and gives rise to the problem of the optimal storage geometry in a 2+1-dimensional (2 spatial + 1 frequency dimension) recording medium.

2. Model

We suppose that the information is recorded by burning spectral holes at different spatial–spectral locations characterized by the spatial coordinates x, y and the frequency ν. In vector notations for the 3D memory space $r = (x, y, \nu)$. In what follows we propose that the set of all r forms a regular translation lattice: $r = r(i, j, k)$, where i, j, k are integrals. Note that it remains an open question whether the densest packing really lies in this class of packings: to out knowledge the similar question is yet open for the packing of 3D hard spheres where some non-regular packings have been demonstrated to have the same density as the densest regular packing (FCC lattice) has [9]. According to our proposal

$$r(i, j, k) = i\mathbf{a}_1 + j\mathbf{a}_2 + k\mathbf{a}_3 , \tag{1}$$

where the vectors $\mathbf{a}_1$, $\mathbf{a}_2$, $\mathbf{a}_3$ form a basis for the lattice. 3D storage density is then given by

$$\rho = [\det(a_{kl})]^{-1} , \tag{2}$$

where a_{kl} is the matrix of the basis vectors.

The obtainable storage density is limited by the demand that at an arbitrary storage position the influence of all recordings from other positions (cross-talking) does not exceed a given fraction F_m of the signal amplitude. For the maximum value of cross-talking (all positions burnt-in)

$$F \equiv \left(\sum_i \sum_j \sum_k f[0, r(i, j, k)] \right) \Big/ f(0, 0) - 1 \leqslant F_m . \tag{3}$$

In principle, F_m may be of an arbitrary positive value, but for $F_m \geqslant 1$ a complicated non-local decoding algorithm is needed for the read-out. Using N different intensity (signal amplitude) levels for encoding, $F_m < 1/N$ for a simple read-out scheme.

The function of cross-talking, f, was chosen as follows

$$f(r_1, r_2) = \exp\{-[(x_2-x_1)^2+(y_2-y_1)^2]\ln 2/R^2\}$$
$$\times \Gamma^2/[\Gamma^2(\nu_2-\nu_1)^2], \qquad (4)$$

basing on the assumptions of a lorentzian shape of the homogeneous absorption lines and a gaussian spatial intensity distribution of the burning and the recording beams. Note the normalization $f(0, 0) = 1$ and that $2R$ and 2Γ are the fwhm of the corresponding (spatial and spectral) intensity distributions. In what follows, we use R and Γ to scale the corresponding dimensions, i.e. $R = \Gamma = 1$. Note that the 3D density ρ scales as $R^{-2}\Gamma^{-1}$. The behavior of $f(r_1, r_2)$ is essentially different in spatial and frequency dimensions (fig. 1): a fast gaussian cut-off in space and slow a lorentzian tailing in spectrum. This means, particularly, that in numerical calculations a large number of neighboring recordings lying in the "frequency direction" (more than 1000 in our calculations) have to be taken into account, while in "spatial directions" an account of a few neighboring recordings is sufficient. The general problem of optimizing the information packing geometry is a 9D problem of optimizing the matrix a_{kl} to maximize the storage density (2) in case of constraint (3). The dimensionality of the problem is reduced to 8D by taking into account the invariance of eq. (4) on rotations in the (x, y)-plane. Instead of solving this general problem we calculated the dependences of the maximum density on the level of the tolerable cross-talking for some given symmetries of the memory lattice (fig. 2): primitive tetragonal (PT), primitive hexagonal (PH), volume-centered tetragonal (VCT), and rhombohedric (R, fig. 2d). These lattices are characterized by the following basis vectors:
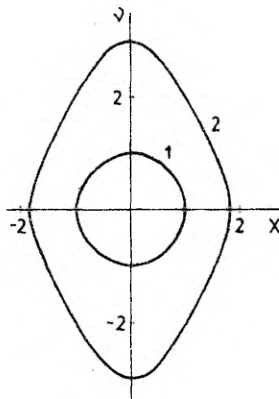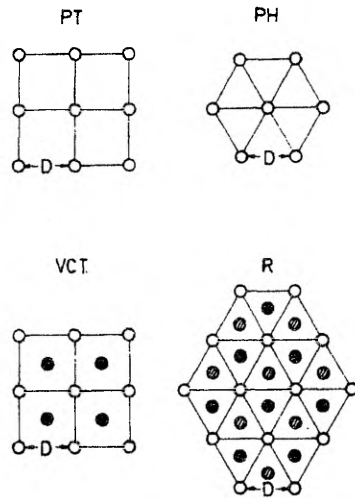

Fig. 2. Memory lattices: primitive tetragonal (PT), primitive hexagonal (PH), volume-centered tetragonal (VCT), and rhombohedric (R). Empty circles denote the recordings in $(x, y, 0)$-plane, dashed circles in (x, y, Δ)-plane, and filled circles in $(x, y, 2\Delta)$-plane. D is the distance between the adjacent recordings in the same spatial plane. The spatial structure for PT and PH lattices is the same for all $(x, y, n\Delta)$-planes, for VCT and R lattices the spatial structure has the frequency period of 2Δ and 3Δ, respectively.

Fig. 1. Isoinfluence curves for a single recording at the origin of space–frequency plane for the values of cross-talking $F = 0.5$ (1) and 0.1 (2).

PT: $a_1 = (D, 0, 0)$, $a_2 = (0, D, 0)$,

       $a_3 = (0, 0, \Delta)$;   (5a)

PH: $a_1 = (D, 0. 0)$, $a_2 = (D/2, \sqrt{3}D/2, 0)$,

       $a_3 = (0, 0, \Delta)$;   (5b)

VCT: $a_1 = (D, 0, 0)$, $a_2 = (0, D, 0)$,

       $a_3 = (D/2, D/2, \Delta)$;   (5c)

R: $a_1 = (D, 0, 0)$, $a_2 = (D/2, \sqrt{3}D/2, 0)$,

       $a_3 = (D/2, \sqrt{3}D/6, \Delta)$.   (5d)

All these bases depend only on two variable parameters that enables us to reduce essentially the dimensionality of the maximization problem.

Note that PT and PH lattices have identical structure for all spatial layers, while in VCT and R lattices the spatial structure of the adjacent isofrequency layers is intercalated and is repeated over ν-periods of 2Δ and 3Δ, respectively.

3. Results and discussion

The maximum packing densities for the lattices (5a–d) were calculated numerically by maximizing eq. (2) at the constraint

$$F = F(D, \Delta) \leqslant F_m .$$

The results are depicted in figs. 3, 4.
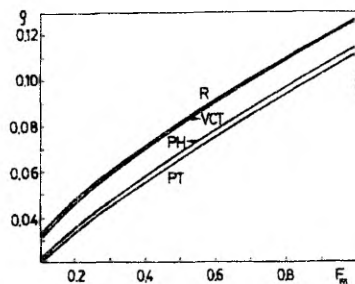
For 1D (spectral or spatial) memories the value

Fig. 3. The dependences of the storage density ρ on the tolerable level of the cross talking F_m for PT, PH, VCT, and R memory lattices (see fig. 2).
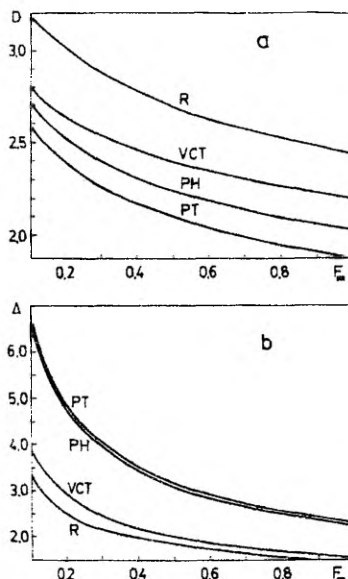

Fig. 4. The dependences of the distance D between the adjacent recordings in the same spatial plane (a) and the spectral distance Δ between the neighboring spatial planes (b) on the tolerable level of the cross-talking F_m for the densest information packing geometries for PT, PH, VCT, and R memory lattices.

of cross-talking from the nearest-neighbor recordings equals 1, when one chooses the unit distance between the adjacent recordings:

$$f(1, 0, 0) + f(-1, 0, 0) = 1 ,$$

$$f(0, 1, 0) + f(0, -1, 0) = 1 ,$$

$$f(0, 0, 1) + f(0, 0, -1) = 1 .$$

The corresponding 1D density is 1. For 3D memory the calculated density (fig. 3) is essentially smaller than the rough estimate by the product of 1D densities. The reason for this is quite obvious: a large number of neighbors in 3D lattice forces on to increase the distances for the same value of cross-talking.

Another interesting observation from the calculation is that the spatial intercalation of the recordings at neighboring frequencies increases, to a cer-

559

tain extent, the maximum storage density. In the considered range of cross-talking $0.1 \leqslant F_m \leqslant 0.9$, $\rho_{PT} < \rho_{PH} < \rho_{VCT} < \rho_R$. The difference of densities for spatially intercalated and non-intercalated cases is essentially larger than that for different spatial geometries (PT and PH lattices). Its relative value increases with decreasing the level of cross-talking: $\rho_R/\rho_{PT} = 1.14$ for $F_m = 0.9$ and $\rho_R/\rho_{PT} = 1.65$ for $F_m = 0.1$. The reason for this is the qualitatively different behavior of f (eq. (3)) in spatial and frequency dimensions. This is also reflected in fig. 4: the decrease of storage density at lower values of cross-talking is related mainly to the increase of the spectral distance Δ.

Acknowledgments

References

[1] A.A. Gorokhovskii, R.K. Kaarli and L.A. Rebane, Pis'ma Zh. Eksp. Teor. Fiz. 20 (1974) 474 (english transl.: JETP Lett. 20 (1974) 216).

[2] B.M. Kharlamov, R.I. Personov and L.A. Bykovskaya, Optics Comm. 12 (1974) 191.

[3] L.A. Rebane, A.A. Gorokhovskii and J.V. Kikas, Appl. Phys. B 29 (1982) 235.

[4] J. Friedrich and D. Haarer, Angew. Chem. Int. Ed. Engl. 23 (1984) 113.

[5] O. Sild and K. Haller, eds., Zero-phonon lines and spectral hole burning, in: Spectroscopy and photochemistry (Springer, Berlin, 1988).

[6] W.E. Moerner, ed., Persistent spectral hole-burning: science and applications, Topics Curr. Phys. Vol. 44 (Springer, Berlin, 1988).

[7] G. Castro, D. Haarer, R.M. Macfarlane and H.P. Trommsdorf, US Patent No. 4101976.

[8] W.E. Moerner and M.D. Levenson, J. Opt. Soc. Am. B 2 (1985) 915.

[9] J.H. Conway and N.J.A. Sloane, Sphere packings, lattices and groups, a series of comprehensive studies, in: Mathematics 290 (Springer, Berlin, 1988).

CURRICULUM VITAE

Kristjan Leiger

Date and place of birth: September 14, 1970, Kärdla, Estonia
Citizenship: Estonian
Family status: Unmarried
Address: Institute of Physics, University of Tartu
                          Riia 142, 51014 Tartu, Estonia
Phone: 372-7-383 034
Fax: 372-7-383 033
E-mail: kristjan@fi.tartu.ee

Education

1977–1985 Kuuste 8-year School
1985–1988 Nõo Secondary School
1988–1992 University of Tartu, B. Sci. in physics
1992–1995 University of Tartu, M. Sci. in physics

Employment

1995–2001 Ph.D. student of Tartu University
1993–1995,
1997–1998,
2001–2002 Laboratory of Laser Spectroscopy, Institute of Physics, engineer
1998   Visiting scientist in Institute of Atomic and Molecular Sciences, Academia Sinica, Taiwan

Scientific work

Main fields of research: Impurity spectra of solids, spectral hole burning, effect of hydrostatic pressure on the impurity spectra and spectral holes, inhomogeneous effects in solids.
Number of publications: 6

CURRICULUM VITAE

Kristjan Leiger

Sünniaeg ja -koht: 14. september 1970, Kärdla
Kodakondsus: Eesti
Perekonaseis: vallaline
Aadress: Tartu Ülikooli Füüsika Instituut
       Riia 142, 51014 Tartu, Eesti
Telefon: 07-383 034
Fax: 07-383 033
E-mail: kristjan@fi.tartu.ee

Haridus

1977–1985 Kuuste 8-kl. Kool
1985–1988 Nõo Keskkool
1988–1992 Tartu Ülikool, B. Sci. füüsikas
1992–1995 Tartu Ülikool, M. Sci. füüsikas

Teenistuskäik

1995–2001 Tartu Ülikooli doktorant
1993–1995,
1997–1998,
2001–2002 Füüsika Instituudi Laserspektroskoopia labori insener
1998   Külalisteadlane Aatomi- ja Molekuliteaduste Instituudis, Academia
     Sinica, Taiwan

Teadustegevus

Peamised uurimissuunad: tahkiste lisandspektroskoopia, spektraal-sälkamine, hüdrostaatilise rõhu mõju lisandspektritele ja spektraal-sälkudele, mittehomogeensed efektid tahkistes.
Publikatsioone: 6

DISSERTATIONES PHYSICAE
UNIVERSITATIS TARTUENSIS

1. Andrus Ausmees. XUV-induced electron emission and electron-phonon interaction in alkali halides. Tartu, 1991.
2. Heiki Sõnajalg. Shaping and recalling of light pulses by optical elements based on spectral hole burning. Tartu, 1991.
3. Sergei Savihhin. Ultrafast dynamics of F-centers and bound excitons from picosecond spectroscopy data. Tartu, 1991.
4. Ergo Nõmmiste. Leelishalogeniidide röntgenelektronemissioon kiiritamisel footonitega energiaga 70–140 eV. Tartu, 1991.
5. Margus Rätsep. Spectral gratings and their relaxation in some low-temperature impurity-doped glasses and chrystals. Tartu, 1991.
6. Tõnu Pullerits. Primary energy transfer in photosynthesis. Model calculations. Tartu, 1991.
7. Olev Saks. Attoampri diapasoonis voolude mõõtmise füüsikalised alused. Tartu, 1991.
8. Andres Virro. AlGaAsSb/GaSb heterostructure injection lasers. Tartu, 1991.
9. Hans Korge. Investigation of negative point discharge in pure nitrogen at atmospheric pressure. Tartu, 1992.
10. Jüri Maksimov. Nonlinear generation of laser VUV radiation for high-resolution spectroscopy. Tartu, 1992.
11. Mark Aizengendler. Photostimulated transformation of aggregate defects and spectral hole burning in a neutron-irradiated sapphire. Tartu, 1992.
12. Hele Siimon. Atomic layer molecular beam epitaxy of A^2B^6 compounds described on the basis of kinetic equations model. Tartu, 1992.
13. Tõnu Reinot. The kinetics of polariton luminescence, energy transfer and relaxation in anthracene. Tartu, 1992.
14. Toomas Rõõm. Paramagnetic H^{2-} and F^+ centers in CaO crystals: spectra, relaxation and recombination luminescence. Tallinn, 1993.
15. Erko Jalviste. Laser spectroscopy of some jet-cooled organic molecules. Tartu, 1993.
16. Alvo Aabloo. Studies of crystalline celluloses using potential energy calculations. Tartu, 1994.
17. Peeter Paris. Initiation of corona pulses. Tartu, 1994.
18. Павел Рубин. Локальные дефектные состояния в CuO_2 плоскостях высокотемпературных сверхпроводников. Тарту, 1994.
19. Olavi Ollikainen. Applications of persistent spectral hole burning in ultrafast optical neural networks, time-resolved spectroscopy and holographic interferometry. Tartu, 1996.
20. Ülo Mets. Methodological aspects of fluorescence correlation spectroscopy. Tartu, 1996.

21. Mikhail Danilkin. Interaction of intrinsic and impurity defects in CaS:Eu luminophors. Tartu, 1997.
22. Ирина Кудрявцева. Создание и стабилизация дефектов в кристаллах KBr, KCl, RbCl при облучении ВУФ-радиацией. Тарту, 1997.
23. Andres Osvet. Photochromic properties of radiation-induced defects in diamond. Tartu, 1998.
24. Jüri Örd. Classical and quantum aspects of geodesic multiplication. Tartu, 1998.
25. Priit Sarv. High resolution solid-state NMR studies of zeolites. Tartu, 1998.
26. Сергей Долгов. Электронные возбуждения и дефектообразование в некоторых оксидах металлов. Тарту, 1998.
27. Kaupo Kukli. Atomic layer deposition of artificially structured dielectric materials. Tartu, 1999.
28. Ivo Heinmaa. Nuclear resonance studies of local structure in $RBa_2Cu_3O_{6+x}$ compounds. Tartu, 1999.
29. Aleksander Shelkan. Hole states in CuO_2 planes of high temperature superconducting materials. Tartu, 1999.
30. Dmitri Nevedrov. Nonlinear effects in quantum lattices. Tartu, 1999.
31. Rein Ruus. Collapse of 3d (4f) orbitals in 2p (3d) excited configurations and its effect on the x-ray and electron spectra. Tartu, 1999.
32. Valter Zazubovich. Local relaxation in incommensurate and glassy solids studied by Spectral Hole Burning. Tartu, 1999.
33. Indrek Reimand. Picosecond dynamics of optical excitations in GaAs and other excitonic systems. Tartu, 2000.
34. Vladimir Babin. Spectroscopy of exciton states in some halide macro- and nanocrystals. Tartu, 2001.
35. Toomas Plank. Positive corona at combined DC and AC voltage. Tartu, 2001.